Supporting Information

BN-Substitution in Dithienylpyrenes Prevents Excimer Formation in Solution and in the Solid State

Yannik Appiarius,[†,§,‡] Philipp J. Gliese,[†,§,‡] Stephan A. W. Segler,[†,§] Pascal Rusch,[ǀ,⊥] Jiangbin Zhang,[ϕ,Δ] Paul J. Gates,[^] Rumpa Pal,[θ] Lorraine A. Malaspina,[Ξ,θ] Kunihisa Sugimoto,[Π] Tim Neudecker,[Γ,§,∨] Nadja C. Bigall,[ǀ,⊥] Simon Grabowsky,[Ξ,θ] Artem A. Bakulin,[◊,Δ] and Anne Staubitz*[,†,§]

[†] Institute for Analytical and Organic Chemistry, University of Bremen, D-28359 Bremen, Germany, E-mail: staubitz@uni-bremen.de.

[§] MAPEX Center for Materials and Processes, University of Bremen, D-28359 Bremen, Germany, Germany.

[ǀ] Institute of Physical Chemistry and Electrochemistry, Leibniz University Hannover, D-30167 Hannover, Germany.

[⊥] Cluster of Excellence PhoenixD (Photonics, Optics, and Engineering-Innovation Across Disciplines), Leibniz University Hannover, D-30167 Hannover, Germany.

[Δ] Cavendish Laboratory, University of Cambridge, CB3 0HE Cambridge, U.K.

[ϕ] College of Advanced Interdisciplinary Studies, National University of Defense Technology, 410073 Changsha, Hunan, China.

[^] School of Chemistry, University of Bristol, BS8 1TS Bristol, U.K.

[θ] Institute of Inorganic Chemistry and Crystallography, University of Bremen, D-28359 Bremen, Germany.

[Ξ] Department of Chemistry, Biochemistry and Pharmaceutical Sciences, University of Bern, CH-3012 Bern, Switzerland.

[Π] Japan Synchrotron Radiation Research Institute (JASRI), Sayo-cho, Hyogo 679-5198, Japan.

[Γ] Institute for Physical and Theoretical Chemistry, University of Bremen, D-28359 Bremen, Germany.

[∨] Bremen Center for Computational Materials Science, University of Bremen, D-28359 Bremen, Germany.

[◊] Department of Chemistry, Imperial College London, SW7 2AZ London, U.K.; Cavendish Laboratory, University of Cambridge, CB3 0HE Cambridge, U.K.

Abstract

Boron–nitrogen substitutions in polycyclic aromatic hydrocarbons (PAHs) have a strong impact on the optical properties of the molecules due to a significantly more heterogeneous electron distribution. However, besides these single-molecule properties, the observed optical properties of PAHs critically depend on the degree of intermolecular interactions such as π–π-stacking, dipolar interactions, or the formation of dimers in the excited state. Pyrene is the most prominent example showing the latter as it exhibits a broadened and strongly bathochromically shifted emission band at high concentrations in solution compared to the respective monomers. In the solid state, the impact of intermolecular interactions is even higher as it determines the crystal packing crucially. In this work, a thiophene-flanked BN-pyrene (**BNP**) was synthesized and compared with its all-carbon analogue (**CCP**) in solution and in the solid state by means of crystallography, NMR spectroscopy, UV–vis spectroscopy, and photoluminescence (PL) spectroscopy. In solution, PL spectroscopy revealed the solvent-dependent presence of excimers of **CCP** at high concentrations. In contrast, no excimers were found in **BNP**. Clear differences were also observed in the single-crystal packing motifs. While **CCP** revealed overlapped pyrene planes with centroid distances in the range of classical π-stacking interactions, the **BNP** scaffolds were displaced and significantly more spatially separated.

Table of Contents

Abbreviations

aq.	Aqueous
ATR	Attenuated total reflection
BNP	BN-substituted pyrene (target molecule)
CCD	Charge coupled device
CCP	CC-substituted pyrene (target molecule)
CI	Chemical ionization
COSY	Correlation spectroscopy
DCM	Dichloromethane
DIPA	*N*,*N*-Di*iso*propylamine
DMSO	Dimethyl sulfoxide
EI	Electron ionization
ESI	Electrospray ionization
FPT	Freeze-pump-thaw
GC	Gas chromatography
HMBC	Heteronuclear multiple-bond correlation spectroscopy
HPLC	High-performance liquid chromatography
HR	High resolution
HSQC	Heteronuclear single-quantum correlation spectroscopy
IR	Infrared spectroscopy
LAH	Lithium aluminum hydride
LDA	Lithium di*iso*propylamide
M	Molar
m (IR) / m (NMR)	Medium intensity (IR) / Multiplet (NMR)
MALDI	Matrix-assisted laser desorption and ionization
MeTHF	2-Methyltetrahydrofuran
m.p.	Melting point
MS	Mass spectrometry
n-BuLi	*n*-Butyllithium
NMR	Nuclear magnetic resonance
$Pd(dppf)_2Cl_2$	[1,1′-Bis(Diphenylphosphino)ferrocene]dichloropalladium(II)
$Pd(PPh_3)_4$	Tetrakis(triphenylphosphine)palladium(0)
$Pd(t\text{-}Bu_3P)_2$	Bis(tri-*tert*-butylphosphine)palladium(0)
qi (NMR)	Quintet
s (IR) / s (NMR)	Strong intensity (IR) / Singlet (NMR)
t (NMR)	Triplet
TCSPC	Time-correlated single photon counting
TEA	Triethylamine
THF	Tetrahydrofuran
TMS	Tetramethylsilane
Tph	Thiophene
t_R	Retention time
w (IR)	Weak intensity

1. General Methods and Materials

Unless stated otherwise, all syntheses were carried out under standard Schlenk conditions under an atmosphere of nitrogen or argon. If necessary, reactions were carried out in a nitrogen flushed glovebox from Inert Innovative Technology Inc. or reagents were prepared and stored there. All used glassware was heated under a vacuum below 0.1 mbar and flushed with inert gas at least three times prior to use. Syringes were flushed with inert gas at least three times before use. NMR tubes were dried in an oven at 110 °C for at least 2 h before use.

1.1. NMR Spectroscopy

^{1}H NMR, ^{13}C{^{1}H} NMR, ^{11}B{^{1}H} NMR, ^{29}Si{^{1}H} and ^{119}Sn{^{1}H} NMR spectra were recorded at 300 K. The respective spectrometers and the frequencies are given in the left table below. The chemical shifts (δ) are given in ppm.

Nucleus	Spectrometer frequency
^{1}H	500 MHz (Bruker DRX 500)
	600 MHZ (Bruker AVANCE 600)
	601 MHz (Bruker AVANCE NEO)
^{13}C{^{1}H}	126 MHz (Bruker DRX 500)

Nucleus	Spectrometer frequency
^{13}C{^{1}H}	151 MHz (Bruker AVANCE 600)
	151 MHz (Bruker AVANCE NEO)
^{11}B{^{1}H}	160 MHz (Bruker DRX 500)
^{29}Si{^{1}H}	99 MHz (Bruker DRX 500)
^{119}Sn	187 MHz (Bruker DRX 500)

^{1}H and ^{13}C{^{1}H} NMR spectra were referenced against the residual solvent signals ($CDCl_3$: 7.26 ppm / 77.16 ppm, C_6D_6: 7.16 ppm / 128.06 ppm). The reference for the ^{119}Sn NMR spectra was calculated based on the ^{1}H NMR signal of TMS. ^{29}Si{^{1}H} NMR spectra were referenced against TMS. ^{11}B{^{1}H} NMR spectra were referenced against $BF_3 \cdot OEt_2$. The signals were identified by using two dimensional methods such as ^{1}H - ^{1}H COSY, ^{1}H - ^{13}C{^{1}H} HSQC and ^{1}H - ^{13}C HMBC experiments when possible. The positions of hydrogen and carbon atoms are labelled with letters to simplify their assignment.

1.2. Microwave Syntheses

Microwave experiments were performed in a Biotage Initiator+ SP Wave microwave synthesizer. The reactions were performed in 20 mL microwave vials, sealed with an aluminum / Teflon crimp top with a maximal exposure temperature of 250 °C and a maximum internal pressure of 20 bar. The temperature was measured with an external IR sensor during microwave heating.

1.3. Mass Spectrometry

High resolution EI spectra were recorded on a VG Autospec EI instrument, operating at 70 eV. High resolution ESI spectra were recorded on a Bruker Daltonics MicrOTof II.

1.4. IR Spectroscopy

IR spectra were recorded on a Perkin Elmer Paragon 1000 FT-IR spectrometer with a A531-G Golden-Gate-ATR-unit or on a Thermo Scientific Nicolet FT-IR Spectrometer System spectrometer with an ATR unit, equipped with a diamond window. The resolution was 4 cm^{-1}. The absorption bands are reported in cm^{-1}.

1.5. Differential Scanning Calorimetry and Thermal Analysis

Differential scanning calorimetry was measured on a DSC 3+ STAR and thermal analysis on a TGA/DSC 3+ by Mettler Toledo.

1.6. Melting Points

Melting points were recorded on a LG1586 Electrothermal IA6304 capillary melting point apparatus.

1.7. Chemicals

Unless noted otherwise, all reagents were used as supplied without further purification. If a chemical was degassed by three freeze pump thaw cycles, this is denoted as FPT.

Chemical	Supplier	Purity	Notes
Ammonium chloride	Grüssing Inc.	99.5%	
Acetic acid	Grüssing Inc.	99%	Glacial
Benzophenone	Acros Inc.	99%	
Boron trichloride solution	Acros Inc.		1.0 M in DCM
2-Bromothiophene	VWR / Alfa Aesar	98%	FPT
Copper(I) chloride	VWR / Alfa Aesar	99.999%	
Copper(I) iodide	VWR / Alfa Aesar	99.999%	
1,3-Dibromobenzene	Alfa Aesar	98%	
2,6-Dibromopyridine	Sigma-Aldrich	98%	
Ethyl bromide	VWR / Merck Millipore	98.0%	FPT
Iodine	abcr	99.8%	
Lithium aluminum hydride	Acros Inc.	95%	
Magnesium sulfate	Grüssing Inc.	99%	
Molecular sieves, 3 Å	Merck Inc.		
Molecular sieves, 4 Å	Merck Inc.		
N,*N*-Di*iso*propylamine	Fischer Scientific	99%	Distilled over $CaCl_2$
Di-*n*-butyltin dichloride	Acros Inc.	97%	
n-Butyllithium	Acros Inc.		2.5 M in hexane
$Pd(dppf)_2Cl_2$	Sigma Aldrich	>98%	
$Pd(PPh_3)_4$	abcr	99%	
$Pd(t\text{-}Bu_3P)_2$	Strem	>98%	
Phenylboronic acid	VWR / Alfa Aesar	98%	
Platinum(II) chloride	Strem	99.9%	
Potassium hydroxide	Grüssing Inc.	85%	
Propargyl bromide	Acros Inc.		80% w/w solution in toluene
Sodium	Merck Inc.	≥99%	
Sodium carbonate	Grüssing Inc.	98%	
Sodium chloride	Grüssing Inc.	98%	
Sodium hydroxide	Grüssing Inc.	98%	
Sodium thiosulfate	Grüssing Inc.	97%	
Sodium borohydride	Abcr	98%	
Sodium hydrogen carbonate	Grüssing Inc.	98%	
Triethylamine	Sigma Aldrich	99.5%	FPT
Trimethylsilylacetylene	abcr	98%	FPT
Trimethyltin chloride	TCI	98.0%	
Triphenylmethane	Sigma Aldrich	99%	

1.8. Solvents

Unless stated otherwise, all solvents used in the reactions and purifications were freshly distilled before use. Benzophenone was used as indicator in distillations over sodium and triphenylmethane in distillations over LAH. If solvents were degassed by three freeze-pump-thaw cycles, this is denoted as FPT. All dried solvents were stored under a nitrogen atmosphere in the presence of molecular sieves (3 Å).

Solvent	Supplier	Notes
Benzene-d_6	Deutero 99.5%	Distilled over sodium, FPT
Cyclohexane	VWR	
Chloroform	VWR	

Chloroform-d_1	Deutero 99.8%,	Used as received
Dichloromethane	VWR	Purified by solvent purification system, FPT
Diethyl ether	VWR	Distilled over sodium, FPT
DMSO	Sigma Aldrich, ≥99.5%	Used as received
n-Hexane	VWR	
Methanol	VWR	
2-Methyl THF	VWR	Distilled over LAH, FPT
n-Pentane	VWR	
THF	VWR	Distilled over sodium, FPT
Toluene	VWR	Distilled over sodium, FPT
Water		Deionized

1.9. Chromatography

For the filtrations over silica, silica gel from Grüssing Inc. with a grain size of 0.040 – 0.063 mm was used. Thin layer chromatography was performed using pre-coated plates from Macherey-Nagel Inc., ALUGRAM® Xtra SIL G/UV254. Column chromatography was performed on an Interchim Puriflash 430 column machine. The cartridges were used depending on the amount of substance (15 g – 120 g; supplied from Interchim GmbH; grain size: 50 μm).

1.10. UV-Vis Spectroscopy

UV/vis spectra were recorded with a resolution of 0.1 nm on a Shimadzu UV-2700 spectrometer with double monochromator.

1.11. Photoluminescence

PL measurements of **BNP** and **CCP** solutions were performed with the FLS 980 (90° detection angle) or FLS 1000 (45° detection angle) spectrometers by Edinburgh Instruments. The sub-ns pulsed laser diode source at 407 nm (PicoQuant) could be triggered at an internal frequency (2.5-40.0 MHz) or from an alternative source by the trigger box / power supply unit (PDL 800-B, PicoQuant). The light was focused onto the sample and the collected PL was measured with a spectrograph (SpectraPro2500i, Princeton Instrument) and a thermoelectrically cooled CCD camera (PIXIS 100-F, Princeton Instruments), which were both integrated into WinSpec (Princeton Instruments) software. A long-pass filter at 420 nm (Schott) was used to filter the residual excitation light. Measurements in solution were performed in Quartz Cuvettes with 10 mm path length by Hellma Analytics.

Time-resolved photoluminescence was also measured using intensified CCD (iCCD) setup. The excitation light at 710 nm comes from a NOPA (non colinear optical parametric amplifier) seeded with a Ti:Sapphire ultrafast laser at a 1 kHz repetition rate. BBO crystal was then used to double the light frequency, yielding UV light at 355 nm. Proper filters were used to filter out other unwanted wavelengths. The collected PL was focused onto the slits of the spectrograph (Shamrock 303i, Andor) coupled to an iCCD (iStar DH740, Andor).

Time correlated single photon counting (TCSPC) was measured in a one box detector (Lifespec-ps, Edinburgh Instruments), which contains the multi-channel plate photomultiplier tube (R3809U-50, Hamamatsu) detector synchronized with the triggering box. The detector switched on at the appropriate time to receive the produced emission and the signal was sent to the software via a VTC900 PCI card, which was controlled and visualized by the software (F900, Edinburgh Instruments). Furthermore, TCSPC measurements were performed using a fast response MCP-PMT detector on the FLS 1000 and a 376 nm Edinburgh EPL Laser as excitation source with 10 – 20 MHz repetition rate and 80 ps pulse width.

Absolute quantum yields were measured using an Edinburgh integrating sphere. The error of the used measurement setup was estimated by repeated measurements of a reference sample (Rhodamin 6G in EtOH) over the course of 2 weeks to be around an absolute ±0.05.

2. Syntheses

2.1. Trimethyl(penta-1,4-diyn-1-yl)silane (9)[1]

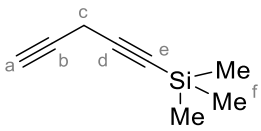

Preparation of ethylmagnesium bromide: Under rapid stirring, ethyl bromide (26.2 g, 17.9 mL, 240 mmol, 1.00 eq.) was added to magnesium (5.84 g, 240 mmol, 1.00 eq.) in THF (120 mL) over the course of 15 min with occasional ice cooling. After continuing stirring at 19 °C for 16 h, a black mixture was obtained.

To this solution of ethylmagnesium bromide, trimethylsilylacetylene (34.4 mL, 240 mmol, 1.00 eq.) was added dropwise over the course of 15 min while cooling the solution in an ice bath. It was stirred for 30 min at 21 °C and then for 60 min at 50 °C. The flask was transferred into a glove box, where copper(I) chloride (1.82 g, 18.2 mmol, 7.5 mol%) and propargyl bromide (40.4 mL, 460 mmol, 2.00 eq.) were added (very exothermic reaction). The mixture was heated to reflux for 4 h. During this time, the color changed from dark orange to green and a light green precipitate was formed. The reaction mixture was allowed to cool to 25 °C and stirred for 2 d at this temperature. The solvent was removed in vacuo and the product was distilled under inert conditions (60 °C, 8 mbar) to yield the product as a colorless liquid (32.2 g, 51%, Lit.: 55%[1]), which was stored under inert conditions at –30 °C.

^{1}H NMR (500 MHz, C_6D_6): δ = 2.80 (d, ^{4}J = 2.8 Hz, 2H, c), 1.70 (t, ^{4}J = 2.8 Hz, 1H, a), 0.11 (s, 9H, f) ppm.

^{13}C{^{1}H} NMR (126 MHz, C_6D_6): δ = 99.9 (b/d), 85.6 (e), 77.8 (b/d), 69.5 (a), 10.6 (c), -0.1 (f) ppm.

^{29}Si NMR (99 MHz, C_6D_6): δ = –18.4 ppm.

HRMS (EI, 70 eV): *m/z* calcd. for $C_7H_9{}^{28}Si$ 121.0474 $[M]^+$, found 121.0479 $[M]^+$.

MS (EI, 70 eV): *m/z* (% relative intensity) 121 (85) $[M]^+$, 84 (100) $[CH_2Cl_2$ (solvent)$]^+$.

* An IR spectrum could not be recorded due to the air sensitive nature of the compound.

2.2. Di(*n*-butyl)stannane (10)[2]

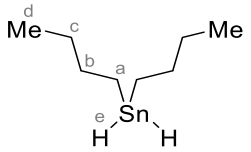

The solvents used in this reaction were previously degassed by flushing them with nitrogen for 60 min without previous drying. $NaBH_4$ (66.4 g, 1.76 mol, 5.35 eq.) was dissolved in water (600 mL) at 0 °C. A solution of *n*-Bu_2SnCl_2 (100 g, 329 mmol, 1.00 eq.) in Et_2O (600 mL) was slowly added over the course of 60 min and the solution was stirred for another 60 min at this temperature. The organic layer was separated, washed with water (3 x 200 mL) and dried over $MgSO_4$. It was filtered and after removing the solvent in vacuo, the residue was distilled (100 °C, 8 mbar) to give the product as a colorless oil (61.7 g, 80%, Lit.: 85%[2]), which was stored under inert conditions at –30 °C.

^{1}H NMR (500 MHz, C_6D_6): δ = 4.76 (qi, ^{3}J = 2.1 Hz, 2H, e), 1.53 – 1.46 (m, 4H, a), 1.33 – 1.23 (m, 4H, b), 0.97 – 0.91 (m, 4H, c), 0.86 (t, ^{3}J = 7.3 Hz, 6H, d) ppm.

^{13}C{^{1}H} NMR (126 MHz, C_6D_6): δ = 30.7 (a), 27.2 (t, $^{1}J_{^{119}Sn\text{-}^{1}H}$ = 817 Hz, b), 13.8 (c), 7.1 (d) ppm.

^{119}Sn NMR (187 MHz, C_6D_6): δ = –203.6 (t, $^{1}J_{^{119}Sn\text{-}^{1}H}$ = 1669 Hz) ppm.

HRMS (EI, 70 eV): *m/z* calcd. for $C_8H_{19}{}^{120}Sn$ 235.0509 $[M]^+$, found 235.0504 $[M]^+$.

MS (EI, 70 eV): *m/z* (% relative intensity) 235 (43) $[M]^+$, 57 (100) $[C_4H_9]^+$.

* An IR spectrum could not be recorded due to the air sensitive nature of the compound. In the literature, no IR spectra are presented.

2.3. (1,1-Di(*n*-butyl)-1,4-dihydrostannin-2-yl)trimethylsilane (11)[3]

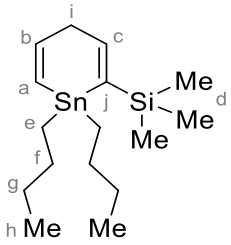

Trimethyl(penta-1,4-diyn-1-yl)silane (**9**, 10.9 g, 80.0 mmol, 1.00 eq.) and di(*n*-butyl)stannane (**10**, 18.8 g, 80.0 mmol, 1.00 eq.) were dissolved in toluene (50 mL) and the solution was heated to reflux for 16 h. After cooling to 25 °C, the solvent was removed in vacuo and the residue was distilled (140 °C, 0.14 mbar) to yield the product as a colorless oil (17.6 g, 47%, Lit.: 66%[3]), which was stored under inert conditions at –30 °C.

^{1}H NMR (500 MHz, C_6D_6): δ = 6.85 (tt, ^{3}J = 3.8 Hz, ^{5}J = 1.1 Hz, 1H, c), 6.56 (dtd, ^{3}J = 14.0 Hz, ^{3}J = 3.9 Hz, ^{5}J = 1.3 Hz, 1H, b), 6.32 (dtd, ^{3}J = 14.0 Hz, ^{4}J = 1.9 Hz, ^{5}J = 0.8 Hz, 1H, a), 2.97 (td, ^{3}J = 3.9 Hz, ^{4}J = 1.9 Hz, 2H, i), 1.70 – 1.50 (m, 4H, e), 1.42 – 1.30 (m, 4 H, f), 1.11 – 0.97 (m, 4H, g), 0.91 (t, ^{3}J = 7.3 Hz, 6H, h), 0.17 (s, 9H, d) ppm.

^{13}C{^{1}H} NMR (126 MHz, C_6D_6): δ = 151.8 (b), 145.1 (c), 140.5 (j), 126.4 (a), 38.7 (i), 29.7 (e), 27.5 (f), 13.9 (g), 11.6 (h), –0.4 (d) ppm.

^{119}Sn NMR (187 MHz, C_6D_6): δ = –151.3 ppm.

^{29}Si{^{1}H} NMR (99 MHz, C_6D_6): δ = –4.2 ppm.

HRMS (EI, 70 eV): *m/z* calcd. for $C_{16}H_{31}{}^{120}Sn^{28}Si$ 371.1217 $[M]^+$, found 371.1212 $[M]^+$.

MS (EI, 70 eV): *m/z* (% relative intensity) 371 (12) $[M]^+$, 315 (79) $[M\text{-}C_4H_8]^+$, 84 (100) $[CH_2Cl_2$ (solvent)$]^+$.

* An IR spectrum could not be recorded due to the air sensitive nature of the compound.

2.4. (1-Chloro-1,4-dihydroborinin-2-yl)trimethylsilane (8)[3]

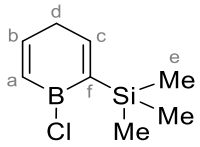

BCl_3 (60.0 mL, 60.0 mmol, 1.27 eq., 1.0 M in DCM) was added dropwise over the course of 6 min to (1,1-di(*n*-butyl)-1,4-dihydrostannin-2-yl)trimethylsilane (**11**, 17.5 g, 47.1 mmol, 1.00 eq.) in DCM (90 mL) at -78 ˚C. After stirring for 30 min at –78 ˚C, the temperature was allowed to rise to 22 ˚C over the course of 12 h, leading to a color change to light brown. The resulting solution was evaporated in vacuo to dryness and the product was distilled under inert conditions (80 ˚C, 0.09 mbar) to yield the product as a slightly yellow liquid (8.54 g, 98%, Lit.: 54%[3]), which was stored under inert conditions at –30 °C.

^{1}H NMR (500 MHz, C_6D_6): δ = 7.24 (m, 1H, c), 6.79 (m, 1H, b), 6.60 (dt, ^{3}J = 11.9 Hz, ^{4}J = 1.6 Hz, 1H, a), 2.48 (td, ^{3}J = 3.0, 1.6 Hz, 2H, d), 0.31 (s, 9 H, e) ppm.

^{13}C{^{1}H} NMR* (126 MHz, C_6D_6): δ = 164.3 (b/c), 155.6 (b/c), 144.3 (f), 134.6 (a), 38.1 (d), -0.6 (e) ppm.

^{11}B{^{1}H} NMR (160 MHz, $CDCl_3$): δ = 53.8 ppm.

^{29}Si{^{1}H} NMR (99 MHz, $CDCl_3$): δ = –3.2 ppm.

* Carbon f was not observed due to the quadrupolar relaxation of the boron nucleus.

** IR and MS spectra could not be collected due to the air sensitive nature of the compound.

2.5. Trimethyl(thiophen-2-ylethynyl)silane (16)[4]

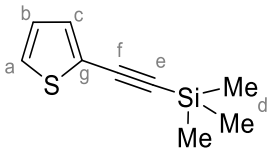

2-Bromothiophene (41.3 g, 253 mmol, 1.00 eq.), TEA (100 mL), $Pd(PPh_3)_4$ (1.00 g, 865 µmol, 0.3 mol%), CuI (800 mg, 4.20 mmol, 1.0 mol%), and trimethylsilylacetylene (53.1 mL, 376 mmol, 1.49 eq.) were suspended in THF (280 mL). The reaction mixture was stirred for 5 d at 22 °C, filtered through filter paper, diluted with Et_2O (30 mL) and washed with a sat. aq. sol. of NH_4Cl (3 x 70 mL). The organic layer was dried over $MgSO_4$, filtered and the solvent was removed in vacuo. The crude product was filtered over silica (eluent: cyclohexane) and the solvent was removed in vacuo to afford the product (52.2 g, 99%, Lit.: 96%[4]) as a yellow liquid.

^{1}H NMR (500 MHz, $CDCl_3$): δ = 7.24 – 7.22 (m, 2H, a,c), 6.95 (dd, ^{3}J = 5.1, 3.7 Hz, 1H, b), 0.26 (s, 9H, d) ppm.

^{13}C{^{1}H} NMR (126 MHz, $CDCl_3$): δ = 132.8 (c), 127.4 (a), 127.0 (b), 123.4 (g), 98.9 (e), 97.7 (f), 0.0 (d) ppm.

^{29}Si{^{1}H} NMR (99 MHz, $CDCl_3$): δ = –17.3 ppm.

IR (ATR): $\tilde{\nu}$ = 3106 (w), 2958 (w), 2898 (w), 2145 (m), 2066 (w), 2012 (w), 1948 (w), 1656 (w), 1513 (w), 1420 (w), 1349 (w), 1248 (m), 1163 (m), 1139 (w), 1076 (w), 1042 (w), 835 (s), 757 (s), 695 (s), 640 (m), 572 (w), 558 (w), 541 (w), 514 (w), 486 (w), 456 (w) cm^{-1}.

HRMS (EI, 70 eV): *m/z* calcd. for $C_9H_{12}S^{28}Si$ 180.0429 $[M]^+$, found 180.0424 $[M]^+$.

MS (EI, 70 eV): *m/z* (% relative intensity) 180 (38) $[M]^+$, 165 (100) $[M\text{-}CH_3]^+$.

2.6. 2-Ethynylthiophene (6)[5]

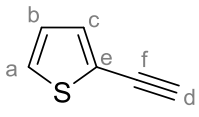

This reaction was not performed under inert conditions.

Trimethyl(thiophen-2-ylethynyl)silane (**16**, 45.0 g, 250 mmol, 1.00 eq.) was dissolved in Et_2O (500 mL) and NaOH (60.0 g, 1.50 mol, 5.00 eq.) in MeOH (500 mL) was added. The reaction mixture was stirred for 18 h at 21 °C, diluted with Et_2O (200 mL) and brine (200 mL) and the organic phase was separated. The aqueous phase was extracted with DCM (3 x 200 mL) and the combined organic fractions were dried over $MgSO_4$. It was filtered and then water (100 mL) was added to the crude product, which was then extracted with *n*-pentane (3 × 100 mL) to remove remaining methanol. After drying over $MgSO_4$ and filtration, the solvent was removed in vacuo to afford the product (26.7 g, 99%, Lit.: 99%[5]) as a light yellow liquid.

^{1}H NMR (500 MHz, $CDCl_3$): δ = 7.28 (dd, ^3J = 3.6 Hz, ^4J = 1.1 Hz, 1H, c), 7.26 (dd, ^3J = 5.2 Hz, ^4J = 1.1 Hz, 1H, a), 6.97 (dd, ^3J = 5.2, 3.6 Hz, 1H, b), 3.33 (s, 1H, d) ppm.

^{13}C{^{1}H} NMR (126 MHz, $CDCl_3$): δ = 133.2 (c), 127.6 (a), 127.0 (b), 122.2 (e), 81.4 (f), 77.1 (d) ppm.

IR (ATR): $\tilde{\nu}$ = 3000 (w), 2102 (m), 1570 (m), 1204 (m), 406 (m), 124 (s) cm^{-1}.

HRMS* (EI, 70 eV): *m/z* calcd. for $C_{12}H_8S_2$ 216.0067 $[M]_2^+$, found 216.0061 $[M]_2^+$.

MS (EI, 70 eV): *m/z* (% relative intensity) 216 (100) $[M]_2^+$, 84 (68) $[CH_2Cl_2$ (solvent)$]^+$.

* The dimer was likely formed during the ionization during MS analysis.

2.7. 2,6-bis(Thiophen-2-ylethynyl)pyridine (7)

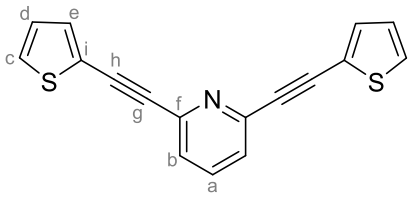

2-Ethynylthiophene (**6**, 17.1 g, 158 mmol, 2.70 eq.), $Pd(PPh_3)_4$ (200 mg, 173 µmol, 0.3 mol%), CuI (60.0 mg, 315 µmol, 0.5 mol%), DIPA (60 mL) and 2,6-dibromopyridine (**5**, 13.8 g, 58.5 mmol, 1.00 eq.) were suspended in toluene (100 mL) and stirred for 6 d at 22 °C. The mixture was filtered through filter paper and extracted with a sat. aq. sol. of NH_4Cl (4 x 100 mL). The solvent was removed in vacuo and the crude product was filtered over silica (eluents: 50% DCM in cyclohexane). The solvents were removed in vacuo to yield the product as a yellow solid (9.01 g, 53%).

^{1}H NMR (500 MHz, $CDCl_3$): δ = 7.67 (t, ^3J = 7.8 Hz, 1H, a), 7.44 (d, ^3J = 7.8 Hz, 2H, b), 7.40 (dd, ^3J = 3.6 Hz, ^4J = 1.1 Hz, 2H, e), 7.36 (dd, ^3J = 5.1 Hz, ^4J = 1.1 Hz, 2H, c), 7.03 (dd, ^3J = 5.1, 3.6 Hz, 2H, d) ppm.

^{13}C{^{1}H} NMR (126 MHz, $CDCl_3$): δ = 143.8 (f), 136.6 (a), 133.7 (e), 128.8 (c), 127.4 (d), 126.1 (b), 122.2 (i), 92.1 (g), 83.4 (h) ppm.

IR (ATR): $\tilde{\nu}$ = 3104 (w), 3075 (w), 2198 (w), 1552 (m), 1424 (m), 1399 (m), 1203 (m), 1135 (m), 761 (s), 684 (s), 566 (m), 468 (m) cm^{-1}.

HRMS (EI, 70 eV): *m/z* calcd. for $C_{17}H_9NS_2$ 291.0176 $[M]^+$, found 291.0180 $[M]^+$.

MS (EI, 70 eV): *m/z* (% relative intensity) 291 (100) $[M]^+$.

m.p.: 146 °C.

2.8. 5,9-Di(thiophen-2-yl)-10a-aza-10b-borapyrene (BNP)

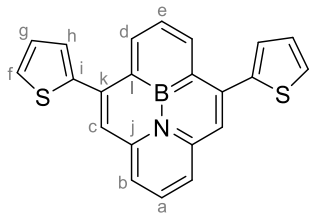

(1-Chloro-1,4-dihydroborinin-2-yl)trimethylsilane (**8**, 174 mg, 943 µmol, 1.00 eq.) was added to 2,6-bis(Thiophen-2-ylethynyl)pyridine (**7**, 519 mg, 1.78 mmol, 1.89 eq.) in toluene (35 mL) and $PtCl_2$ (12.0 mg, 45.1 µmol, 5.0 mol%). The mixture was stirred for 15 h at 115 °C under microwave irradiation[12]. After cooling, the mixture was purified *via* flash column chromatography using 5% Et_2O in cyclohexane. The product was obtained as a yellow crystalline solid (393 mg, 60%).

^{1}H NMR (601 MHz, $CDCl_3$): δ = 9.11 (d, ^3J = 7.7 Hz, 2H, d), 8.44 (d, ^3J = 7.7 Hz, 2H, b), 8.35 (dd, ^3J = 8.4, 7.2 Hz, 1H, a), 8.22 (s, 2H, c), 8.09 (dd, ^3J = 7.7 Hz, 1H, e), 7.79 (dd, ^3J = 3.5 Hz, ^4J = 1.1 Hz, 2H, h), 7.59 (dd, ^3J = 5.1 Hz, ^4J = 1.1 Hz, 2H, f), 7.35 (dd, ^3J = 5.1, 3.5 Hz, 2H, g) ppm.

^{13}C{^{1}H} NMR (151 MHz, $CDCl_3$): δ = 142.6 (k), 142.2 (i), 138.9 (j), 128.7 (d), 128.5 (a), 128.0 (h), 127.9 (g), 126.5 (f), 123.0 (e), 121.0 (b), 117.8 (c) ppm.

^{11}B NMR (160 MHz, C_6D_6): δ = 23.5 ppm.

IR (ATR): $\tilde{\nu}$ = 2921 (s), 2851 (s), 2360 (w), 1709 (w), 1659 (w), 1632 (w), 1522 (m), 1462 (m), 1377 (w), 1350 (m), 1259 (m), 1081 (m), 1018 (s), 797 (s), 741 (m), 701 (m) cm^{-1}.

HRMS (EI, 70 eV): *m/z* calcd. for $C_{22}H_{14}NS_2{}^{11}B$ 367.0661 $[M]^+$, found 367.0667 $[M]^+$.

MS (EI, 70 eV): *m/z* (% relative intensity) 367 (100) $[M]^+$.

m.p.** (DSC): 176 °C.

* Carbon l was not observed due to the quadrupolar relaxation of the boron nucleus.

** The melting point was determined for a crystalline sample after three heating-cooling cycles between 25 °C and 200 °C as the onset temperature.

2.9. 1,3-Dibromo-2-iodobenzene (12)[6]

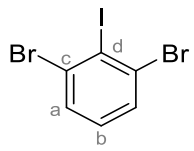

LDA was prepared by adding *n*-BuLi (21.4 mL, 52.5 mmol, 1.05 eq., 2.45 M in hexanes) over the course of 9 min to DIPA (7.73 mL, 55.0 mmol, 1.10 eq.) in THF (125 mL) at 0 °C. The solution was stirred for 1 h at 0 °C. 1,3-Dibromobenzene (11.8 g, 50.0 mmol, 1.00 eq.) was added dropwise over the course of 3 min at -78 °C and the reaction mixture was stirred for 3 h at this temperature. Iodine (13.3 g, 52.5 mmol, 1.05 eq.) in THF (45 mL) was added dropwise over the course of 2 min and the solution was stirred for 15 min at -78 °C. An aq. sol. of sodium thiosulfate (50 mL, 0.63 M) and THF (100 mL) were added and the aqueous phase was extracted with Et_2O (3 × 75 mL). The combined organic layers were dried over $MgSO_4$, filtered and concentrated in vacuo. The residue was filtered over silica, using cyclohexane as eluent to yield the product as a colorless solid (17.9 g, 99%, Lit.: 91%[6]).

^{1}H NMR (500 MHz, $CDCl_3$): δ = 7.56 (d, ^3J = 8.0 Hz, 2H, a), 7.07 (t, ^3J = 8.0 Hz, 1H, b) ppm.

^{13}C{^{1}H} NMR* (126 MHz, $CDCl_3$): δ = 131.5 (c), 131.2 (a), 130.5 (b) ppm.

IR (ATR): $\tilde{\nu}$ = 3056 (w), 1929 (w), 1862 (w), 1796 (w), 1669 (w), 1551 (w), 1426 (m), 1397 (m), 1343 (m), 1277 (w), 1251 (w), 1204 (m), 1184 (m), 1140 (m), 1072 (m), 1029 (w), 999 (m), 970 (w), 897 (w), 767 (s), 724 (s), 697 (m), 688 (s), 559 (w), 491 (w), 466 (m) cm^{-1}.

HRMS (EI, 70 eV): *m/z* calcd. for $C_6H_3{}^{79}Br_2I$ 359.7646 $[M]^+$, found 359.7649 $[M]^+$.

MS (EI, 70 eV): *m/z* (% relative intensity) 362 (58) $[M]^+$, 84 (100) $[CH_2Cl_2\ (solvent)]^+$.

m.p.: 97 °C (Lit.: 99 – 100 °C).

* Carbon d was not observed.

[1] Two separate approaches due to a limited volume of the microwave vials.
[2] The conversion was monitored via ^{1}H NMR. If no complete conversion was detected, another 5 mol% of catalyst was added and the reaction mixture was heated for another 15 h at 115 °C under microwave conditions.

2.10. 2,6-Dibromo-1,1'-biphenyl (13)[7]

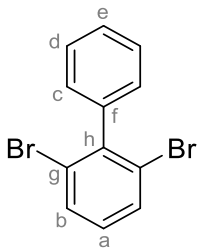

2,6-Dibromoiodobenzene (**12**, 3.62 g, 10.0 mmol, 1.00 eq.), phenylboronic acid (1.22 g, 10.0 mmol, 1.00 eq.), Pd(dppf)Cl_2 (400 mg, 490 µmol, 5.0 mol%) and Na_2CO_3 (4.24 g, 40.0 mmol, 4.00 eq.) were dissolved in DMSO (40 mL) and water (10 mL). The mixture was stirred in a chemglass pressure flask at 110 °C for 3 d. A sat. aq. sol. of $NaHCO_3$ (50 mL) was added and the mixture was extracted with DCM (3 x 50 mL). The extract was dried over $MgSO_4$ and filtered over silica (350 mL, eluent: *n*-pentane). After the solvent was removed in vacuo, the product was afforded as a colorless solid (1.84 g, 59%, Lit.: 62%[7]).

^{1}H NMR (500 MHz, $CDCl_3$): δ = 7.64 (d, ^3J = 8.0 Hz, 2H, b), 7.50 – 7.41 (m, 3H, d,e), 7.25 – 7.21 (m, 2H, c), 7.08 (t, ^3J = 8.0 Hz, 1H, a) ppm.

^{13}C{^{1}H} NMR (126 MHz, $CDCl_3$): δ = 143.2 (h), 141.3 (f), 132.0 (b), 130.0 (a), 129.3 (d), 128.3 (c), 128.2 (e), 124.7 (g) ppm.

IR (ATR): $\tilde{\nu}$ = 3056 (w), 2344 (w), 1929 (w), 1862 (w), 1669 (w), 1599 (w), 1577 (m), 1546 (m), 1497 (m), 1439 (w), 1420 (s), 1405 (m), 1386 (m), 1343 (m), 1277 (w), 1251 (m), 1204 (m), 1185 (m), 1141 (m), 1071 (m), 1028 (m), 999 (m), 970 (m), 898 (m), 766 (s), 717 (s), 696 (s), 688 (s), 648 (m), 627 (m), 574 (m), 558 (m), 509 (m), 466 (m), 179 (m) cm^{-1}.

HRMS (EI, 70 eV): *m/z* calcd. for $C_{12}H_8{}^{79}Br_2$ 309.8993 $[M]^+$, found 309.8997 $[M]^+$.

MS (EI, 70 eV): *m/z* (% relative intensity) 312 (67) $[M]^+$, 152 (84) $[M\text{-}Br_2]^+$ 84 (100) $[CH_2Cl_2$ (solvent)$]^+$.

m.p.: 38 °C.

2.11. Trimethyl(thiophen-2-ylethynyl)stannane (14)[8]

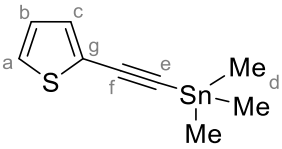

n-BuLi (23.2 mL, 56.8 mmol, 1.02 eq., 2.45 M in hexanes) was added to 2-ethynylthiophene (**6**, 6.00 g, 55.5 mmol, 1.00 eq.) in MeTHF (50 mL) over the course of 6 min at –78 °C and the solution was stirred for 50 min at this temperature. A solution of Me_3SnCl (13.1 g, 65.7 mmol, 1.18 eq.) in MeTHF (10 mL) was added at -78 °C and the mixture was stirred for another 16 h while being allowed to warm to 20 °C. The solvent was removed in vacuo and the crude product was distilled under inert conditions (100 °C, 0.2 mbar) to yield the product as a colorless liquid (6.68 g, 45%, Lit.: 93%[8]), which was stored in an air sealed flask.

^{1}H NMR (500 MHz, C_6D_6): δ = 7.13 (d, ^3J = 3.6 Hz, 1H, c), 6.60 (d, ^3J = 5.1 Hz, 1H, a), 6.49 (dd, ^3J = 5.1, 3.6 Hz, 1H, b), 0.15 (s, 9H, d) ppm.

^{13}C{^{1}H} NMR (126 MHz, C_6D_6): δ = 132.2 (c), 127.0 (b), 126.7 (a), 124.7 (g), 102.0 (f), 98.8 (e), -8.14 (d) ppm.

^{119}Sn NMR (187 MHz, C_6D_6): δ = –65.4 (s) ppm.

HRMS (EI, 70 eV): *m/z* calcd. for $C_9H_{12}{}^{119}SnS$ 271.9682 $[M]^+$, found 271.9691 $[M]^+$.

MS (EI, 70 eV): *m/z* (% relative intensity) 272 (7) $[M]^+$, 257 (35) $[M\text{-}CH_3]^+$, 84 (100) $[CH_2Cl_2$ (solvent)$]^+$.

* An IR spectrum could not be recorded due to the air sensitive nature of the compound.

2.12. 2,6-bis(Thiophen-2-ylethynyl)-1,1'-biphenyl (15)

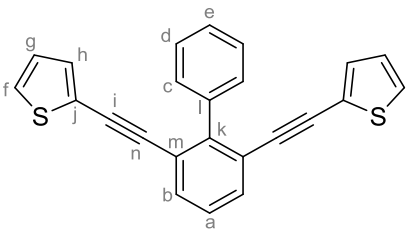

2,6-Dibromo-1,1'-biphenyl (**13**, 378 mg, 1.21 mmol, 1.00 eq.), Pd(*t*-$Bu_3P)_2$ (22.0 mg, 43.0 µmol, 3.5 mol%) and trimethyl(thiophen-2-ylethynyl)stannane (**14**, 710 mg, 2.62 mmol, 2.16 eq.) were dissolved in THF (10 mL). The reaction mixture was stirred for 1 d at 85 °C. It was washed with brine (2 × 10 mL), dried over $MgSO_4$, filtered and the solvent was removed in vacuo. The residue was filtered over silica (eluent: *n*-pentane). The solvent was removed in vacuo to afford the product as a viscous yellow oil (310 mg, 99%).

^{1}H NMR (500 MHz, $CDCl_3$): δ = 7.60 (d, ^3J = 7.5 Hz, 2H, c), 7.57 (d, ^3J = 7.8 Hz, 2H, b), 7.48 (t, ^3J = 7.5 Hz, 2H, d), 7.42 (t, ^3J = 7.5 Hz, 1H, e), 7.31 (t, ^3J = 7.8 Hz, 1H, a), 7.22 (dd, ^3J = 5.1, ^4J = 0.9 Hz, 2H, f), 7.01 (dd, ^3J = 3.7 Hz, ^4J = 0.9 Hz, 2H, h), 6.93 (dd, ^3J = 5.1, 3.7 Hz, 2H, g) ppm.

^{13}C{^{1}H} NMR (126 MHz, $CDCl_3$): δ = 145.7 (k), 138.6 (l), 131.8 (b), 131.8 (h), 130.2 (c), 127.7 (e), 127.5 (d), 127.4 (f), 127.1 (a), 127.0 (g), 123.2 (j), 123.0 (m), 92.5 (n), 86.3 (i) ppm.

IR (ATR): $\tilde{\nu}$ = 2251 (w), 1258 (s), 755 (s), 308 (s) cm^{-1}.

HRMS (MALDI): *m/z* calcd. for $C_{24}H_{14}S_2$ 366.0531 $[M]^+$, found 366.0541 $[M]^+$.

2.13. 4,10-Di(thiophen-2-yl)pyrene (CCP)

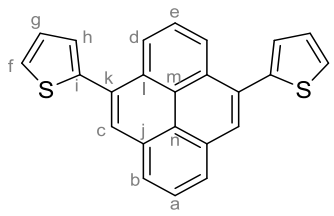

2,6-Bis(Thiophen-2-ylethynyl)-1,1'-biphenyl (**15**, 30.5 mg, 83.2 µmol) and $PtCl_2$ (5.0 mg, 18.8 µmol, 22 mol%) were suspended in toluene (4 mL) and the mixture was stirred at 120 °C for 2 d. After removing the solvent under reduced pressure, the crude product was subjected to column chromatography (silica, eluents: 8% DCM in *n*-pentane → 13% DCM in *n*-pentane). Pure fractions were collected. Impure fractions were crystallized (DCM/acetonitrile, 1:2) to afford the product as a colorless solid (11.0 mg, 36%).

^{1}H NMR (500 MHz, $CDCl_3$): δ = 8.59 (d, ^3J = 7.9 Hz, 2H, d), 8.22 (d, ^3J = 7.7 Hz, 2H, b), 8.21 (s, 2H, c), 8.05 (t, ^3J = 7.7 Hz, 1H, a), 8.01 (t, ^3J = 7.9 Hz, 1H, e), 7.52 (dd, ^3J = 5.2 Hz, ^4J = 1.2 Hz, 2H, f), 7.45 (dd, ^3J = 3.5 Hz, ^4J = 1.2 Hz, 2H, h), 7.28 (dd, ^3J = 5.2, 3.5 Hz, 2H, g) ppm.

^{13}C{^{1}H} NMR (126 MHz, $CDCl_3$): δ = 142.0 (i), 132.2 (k), 130.8 (l), 130.5 (j), 129.4 (c), 127.9 (h), 127.5 (g), 126.7 (a), 126.1 (e), 125.8 (b), 125.8 (f), 125.6 (m), 124.3 (d), 124.1 (n) ppm.

IR (ATR): $\tilde{\nu}$ = 3067 (w), 2953 (w), 2953 (w), 2928 (w), 2856 (w), 1605 /w), 1590 (w), 1573 (w), 1482 (m), 1428 (w), 1365 (w), 1253 (w), 1211 (m), 1070 (w), 1042 (w), 930 (m), 888 (m), 851 (m), 790 (m), 721 (s), 680 (s) cm^{-1}.

HRMS (EI, 70 eV): *m/z* calcd. for $C_{24}H_{14}S_2$ 366.0537 $[M]^+$, found 366.0544 $[M]^+$.

MS (EI, 70 eV): *m/z* (% relative intensity) 366 (62) $[M]^+$, 84 (100) $[CH_2Cl_2$ (solvent)$]^+$.

m.p.: 190 °C.

3. NMR Spectra

3.1. Trimethyl(penta-1,4-diyn-1-yl)silane (9)

^{1}H NMR (500 MHz, C_6D_6)

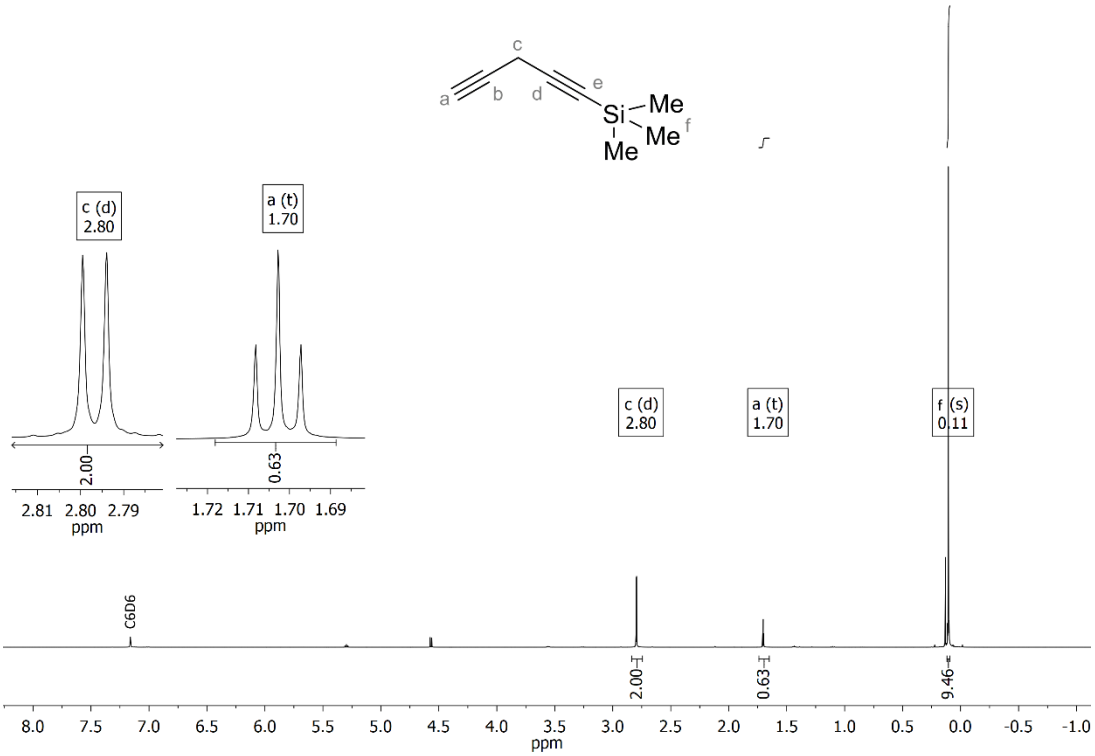

^{13}C{^{1}H} NMR (126 MHz, C_6D_6)

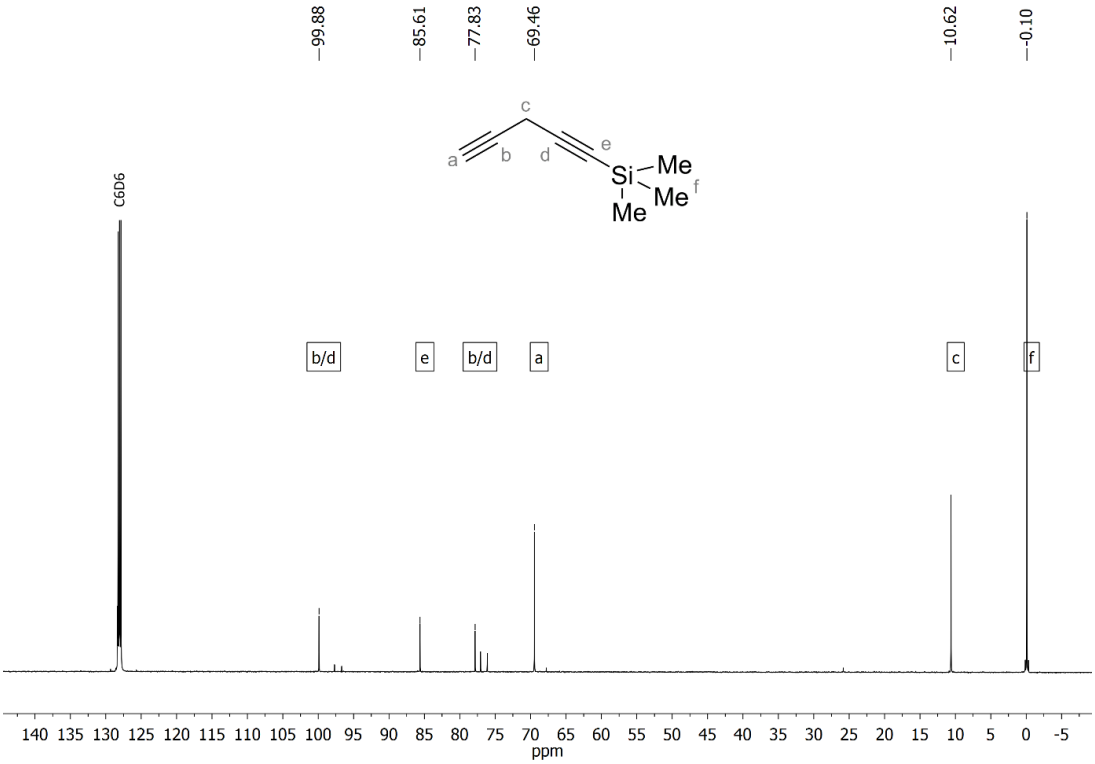

^{29}Si NMR (99 MHz, C_6D_6)

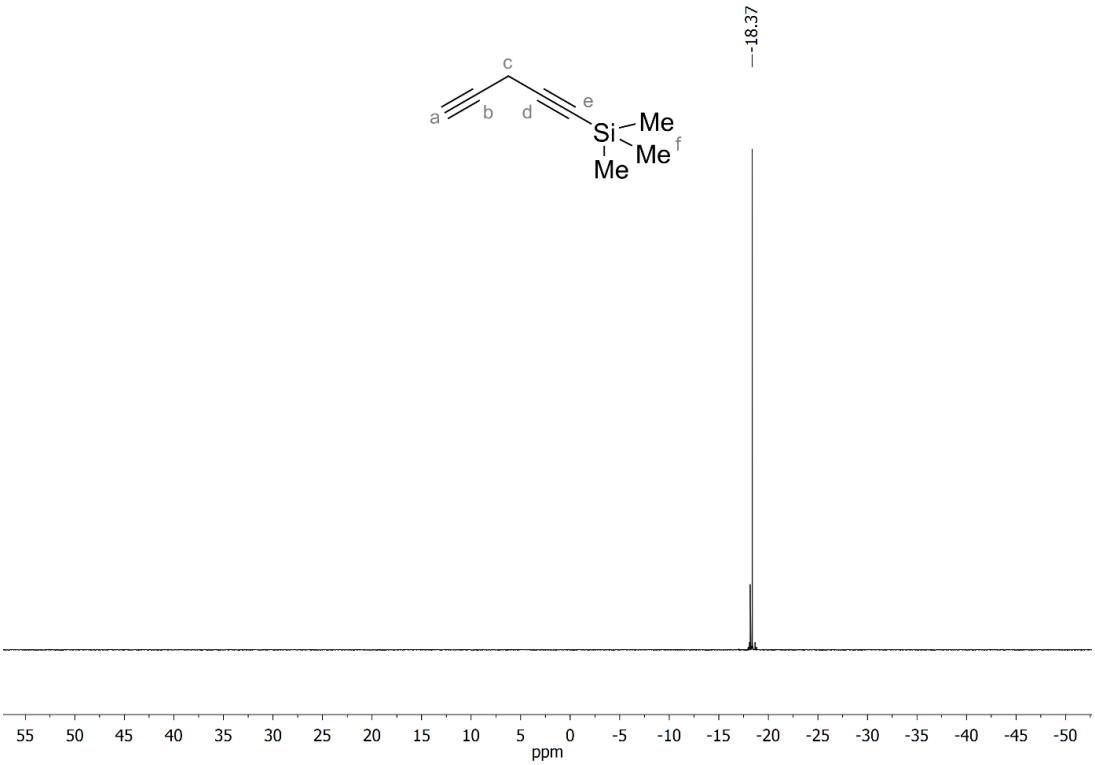

3.2. Di(*n*-butyl)stannane (10)

^{1}H NMR (500 MHz, C_6D_6)

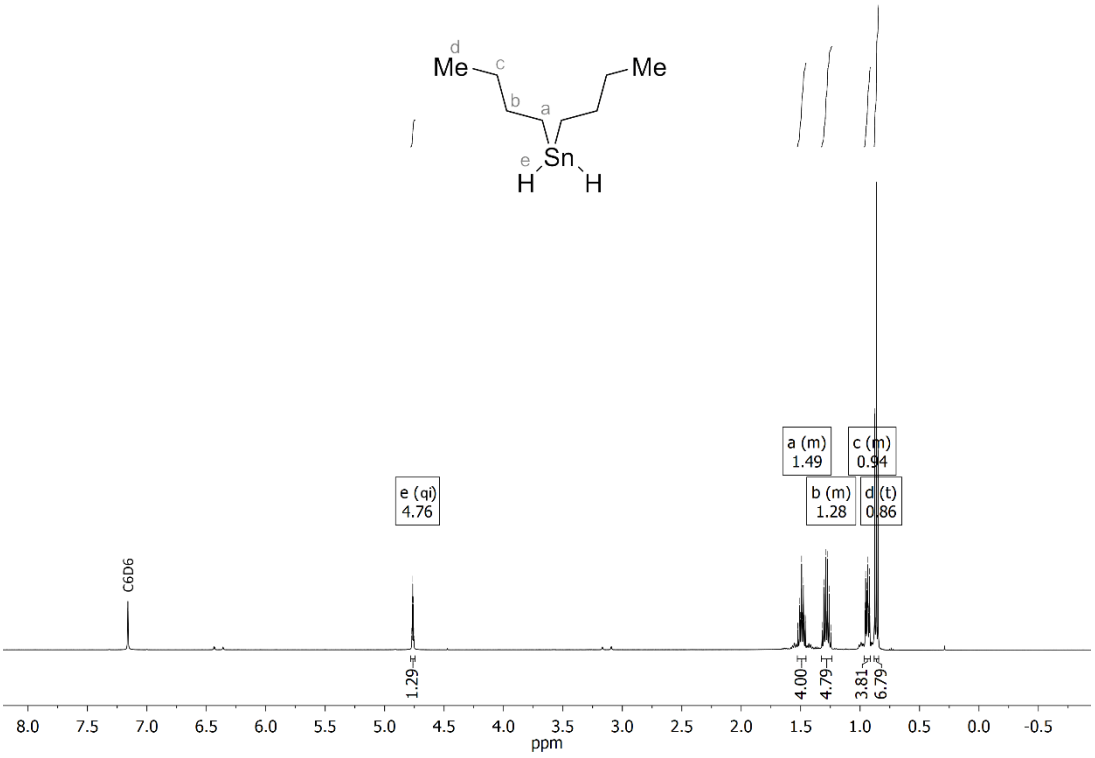

$^{13}C\{^{1}H\}$ NMR (126 MHz, C_6D_6)

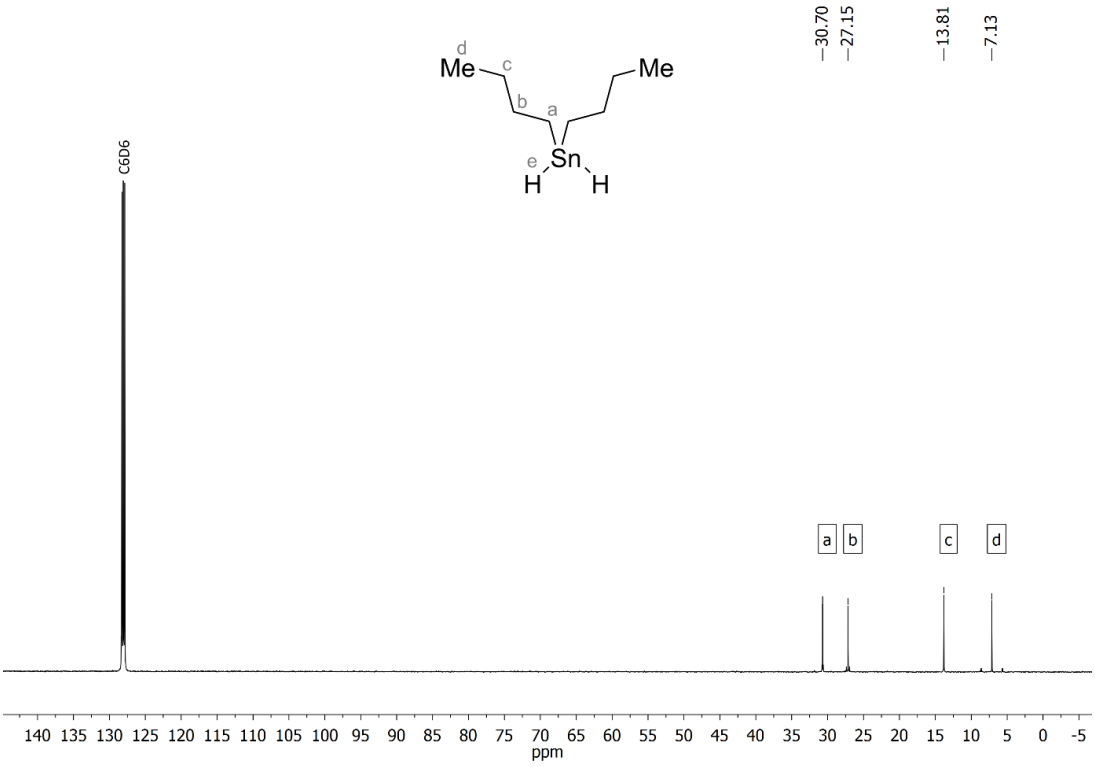

^{119}Sn NMR (187 MHz, C_6D_6)

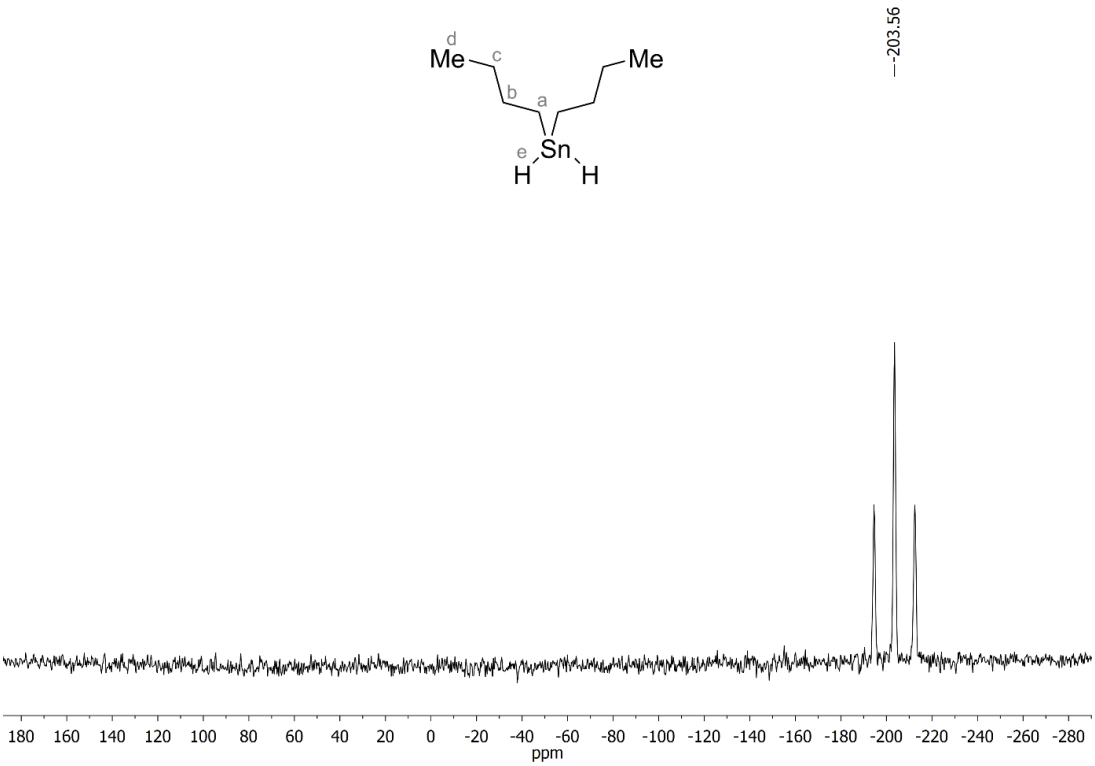

3.3. (1,1-Di(*n*-butyl)-1,4-dihydrostannin-2-yl)trimethylsilane (11)

^{1}H NMR (500 MHz, C_6D_6)

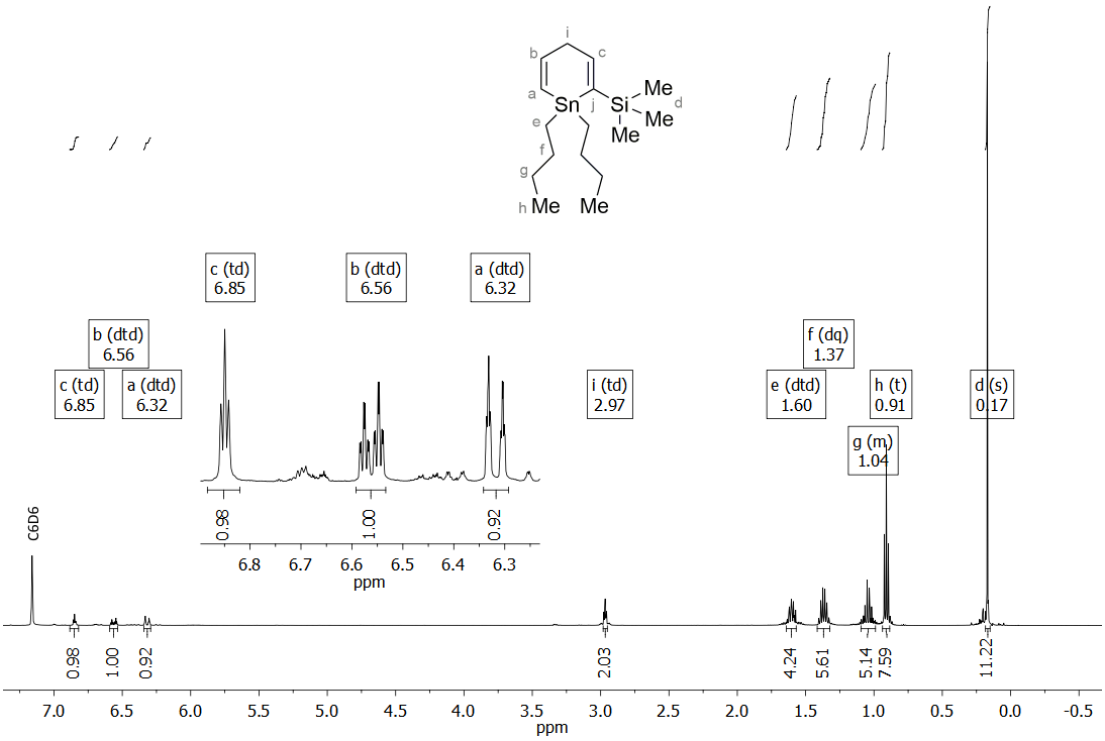

^{13}C{^{1}H} NMR (126 MHz, C_6D_6)

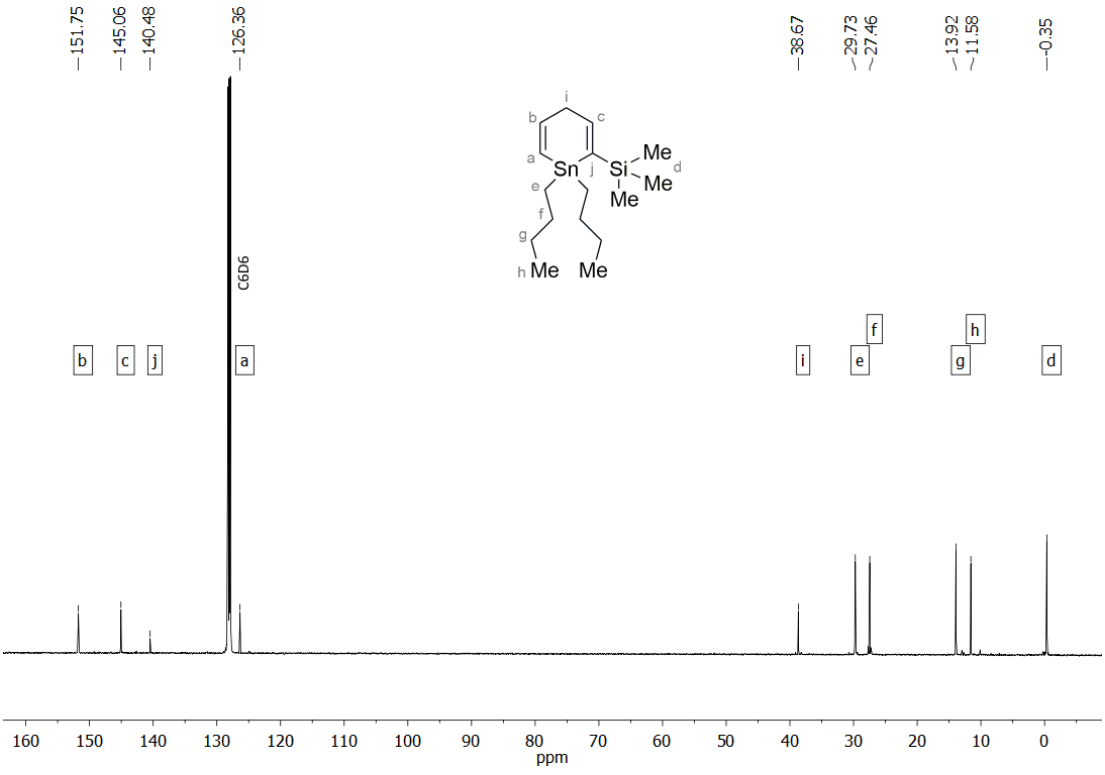

$^{29}Si\{^{1}H\}$ NMR (99 MHz, C_6D_6)

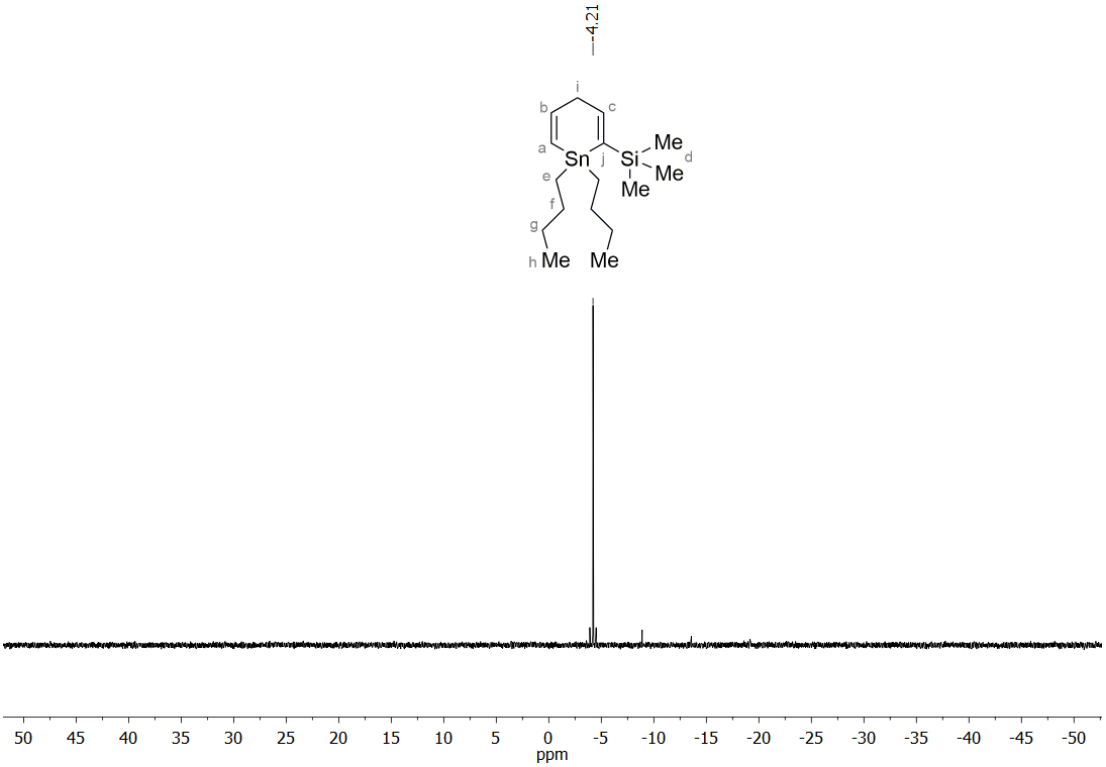

^{119}Sn NMR (187 MHz, C_6D_6)

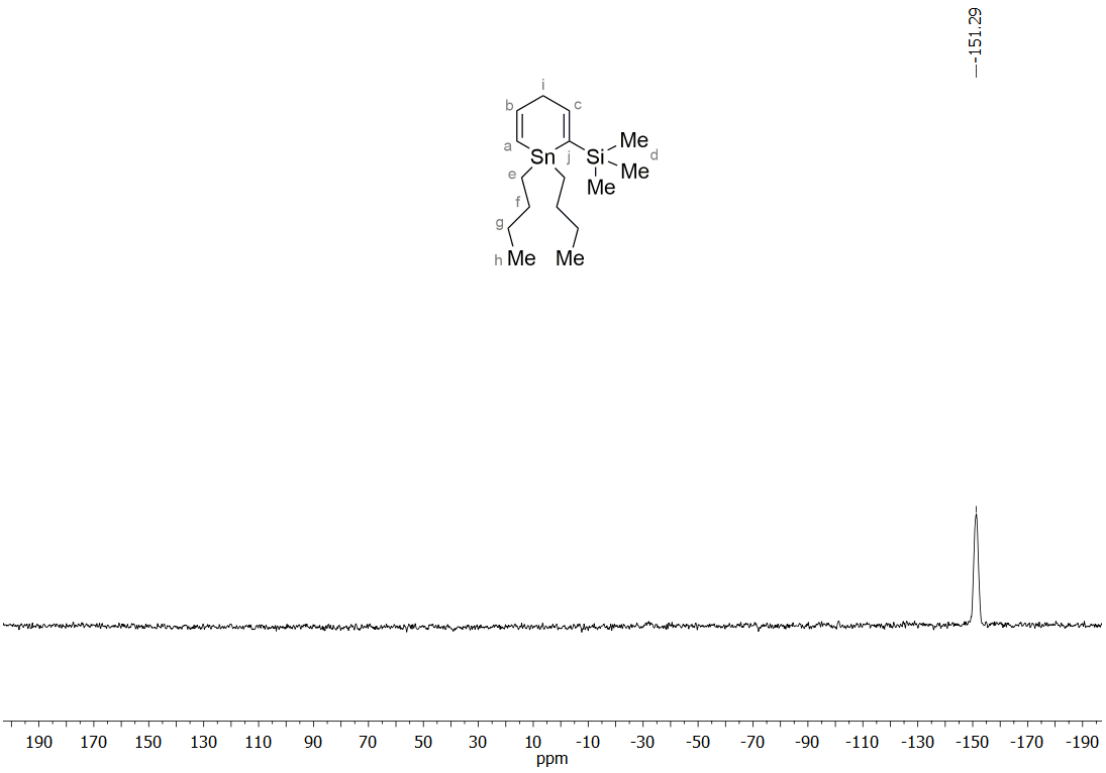

3.4. (1-Chloro-1,4-dihydroborinin-2-yl)trimethylsilane (8)

^{1}H NMR (500 MHz, C_6D_6)

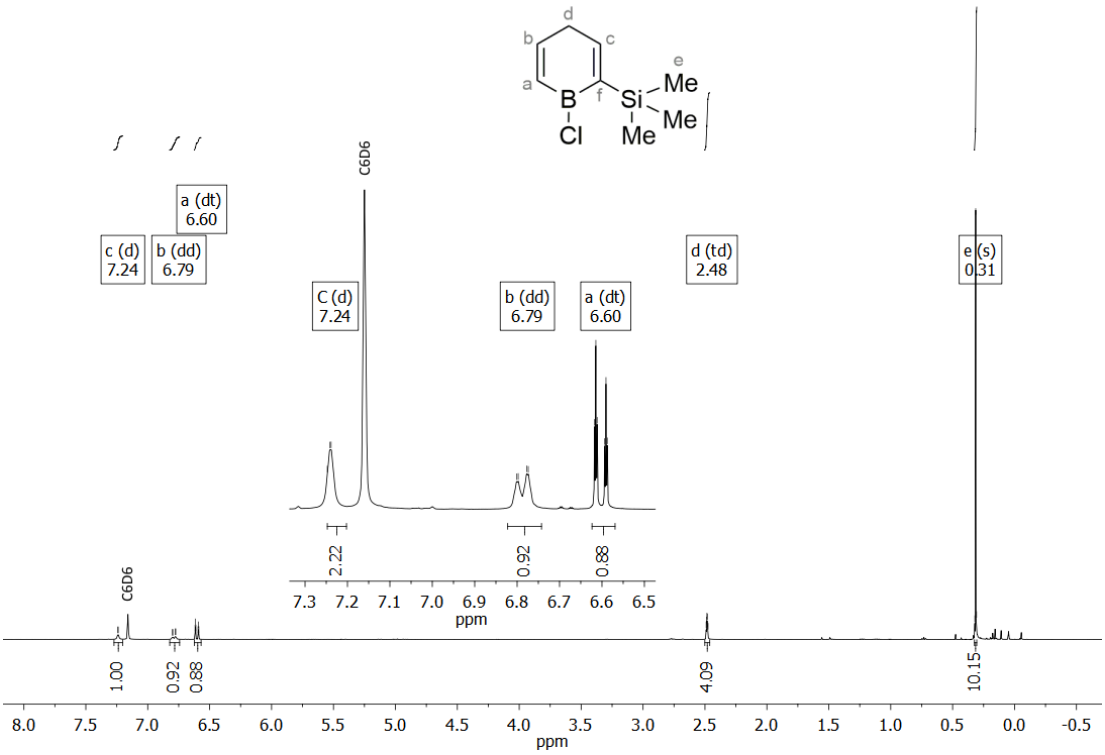

^{13}C{^{1}H} NMR (126 MHz, C_6D_6)

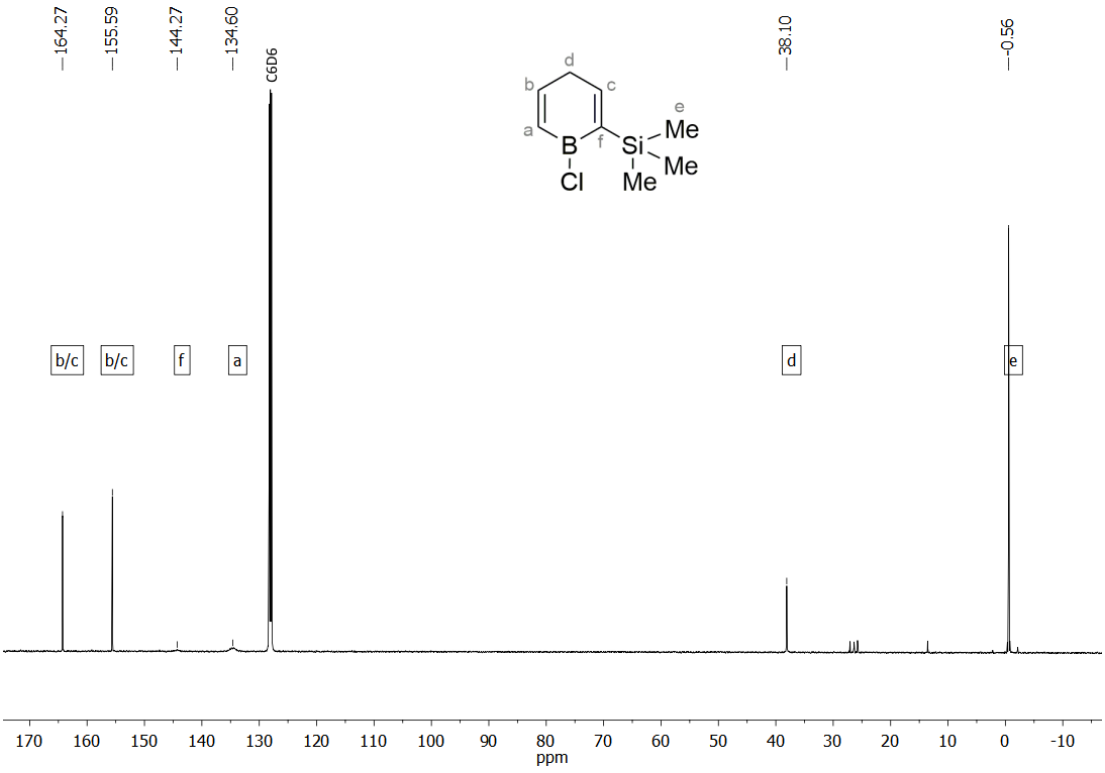

$^{11}B\{^{1}H\}$ NMR (160 MHz, $CDCl_3$)

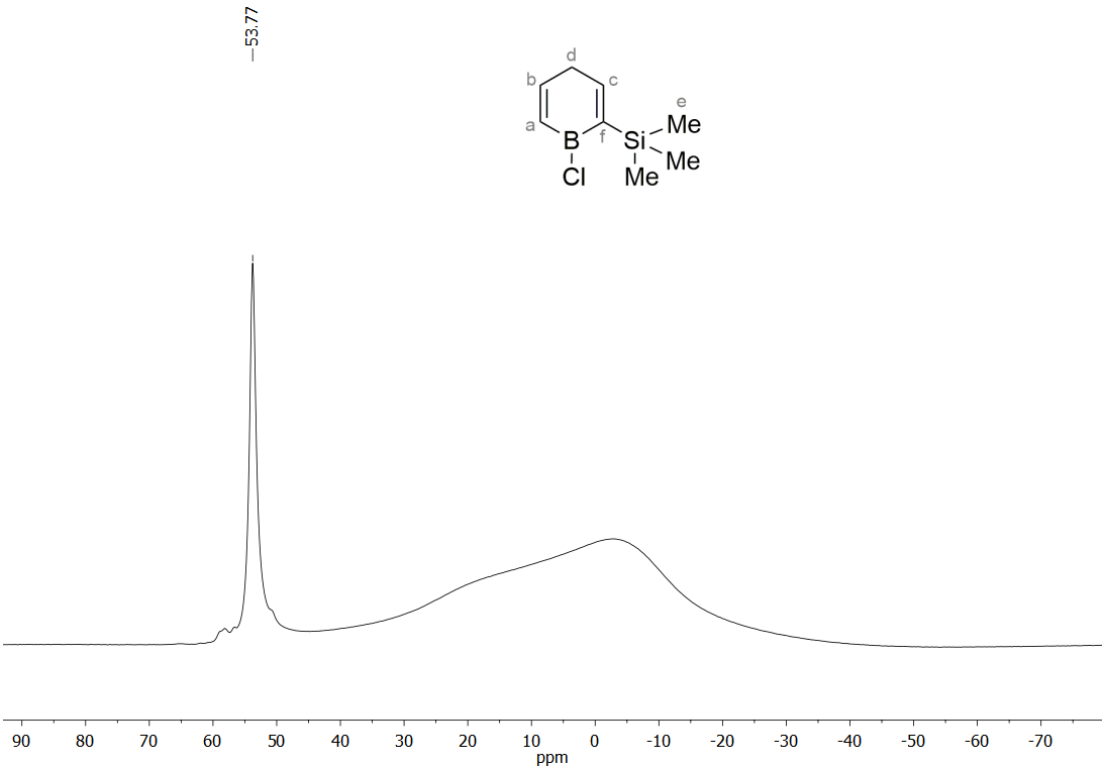

$^{29}Si\{^{1}H\}$ NMR (99 MHz, $CDCl_3$)

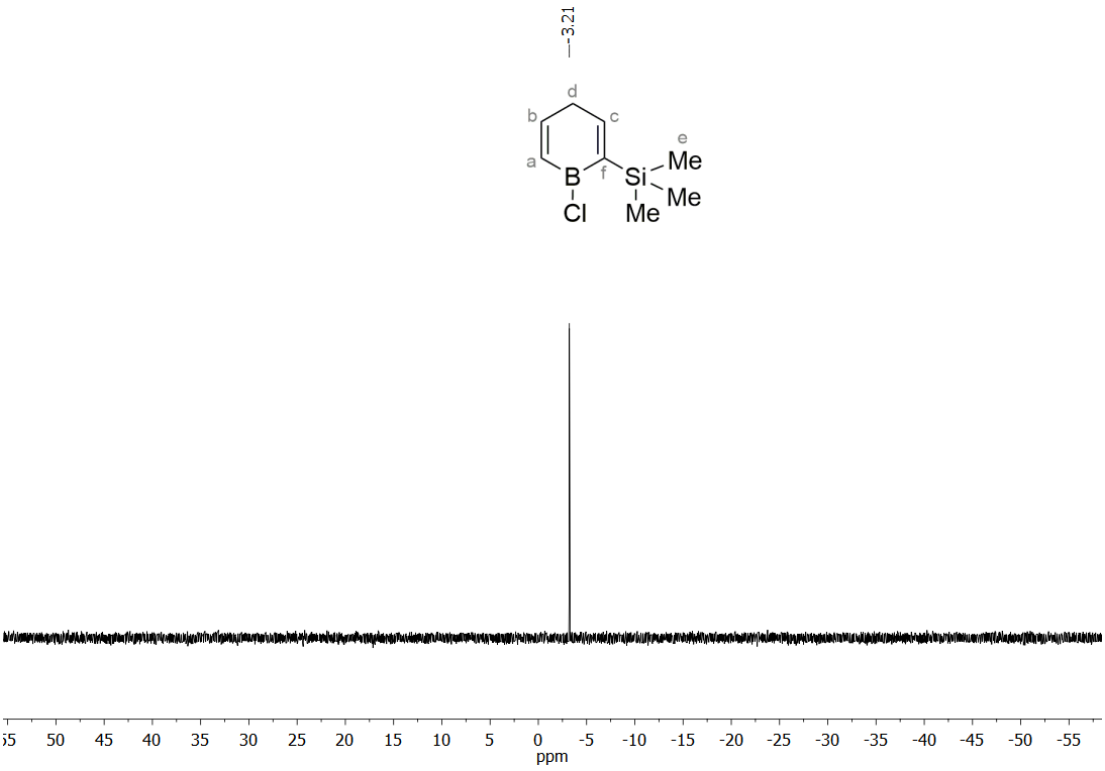

3.5. Trimethyl(thiophen-2-ylethynyl)silane (16)

^{1}H NMR (500 MHz, $CDCl_3$)

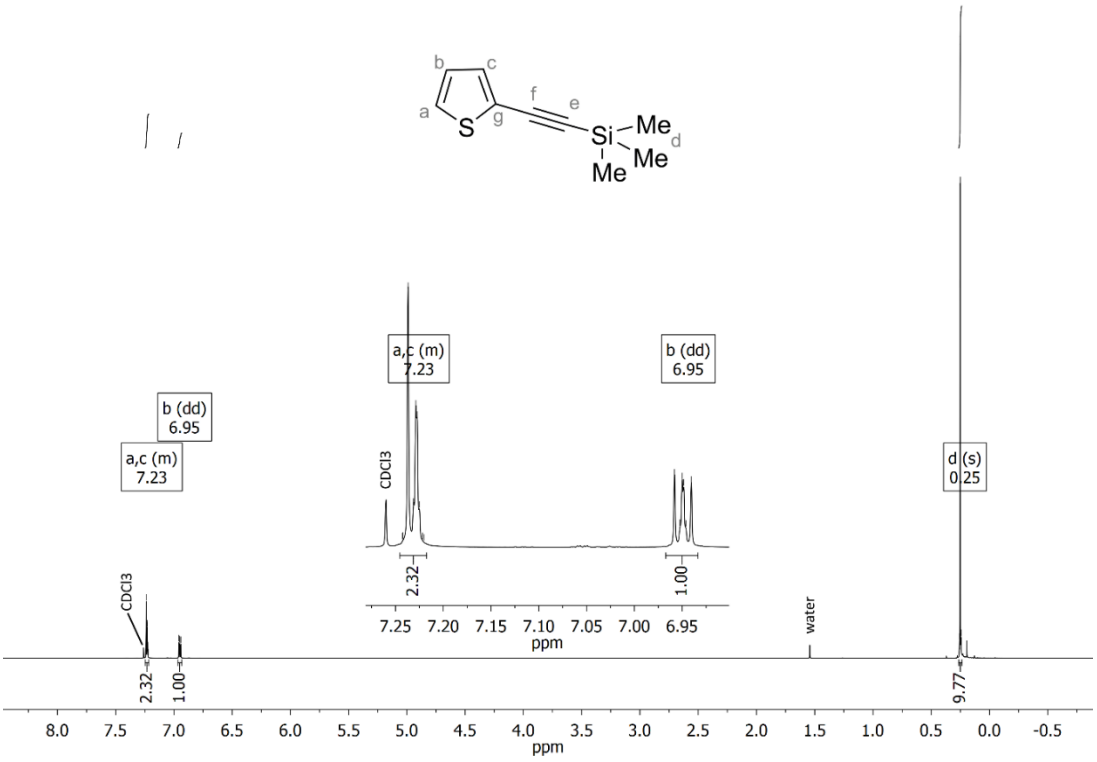

^{13}C{^{1}H} NMR (126 MHz, $CDCl_3$)

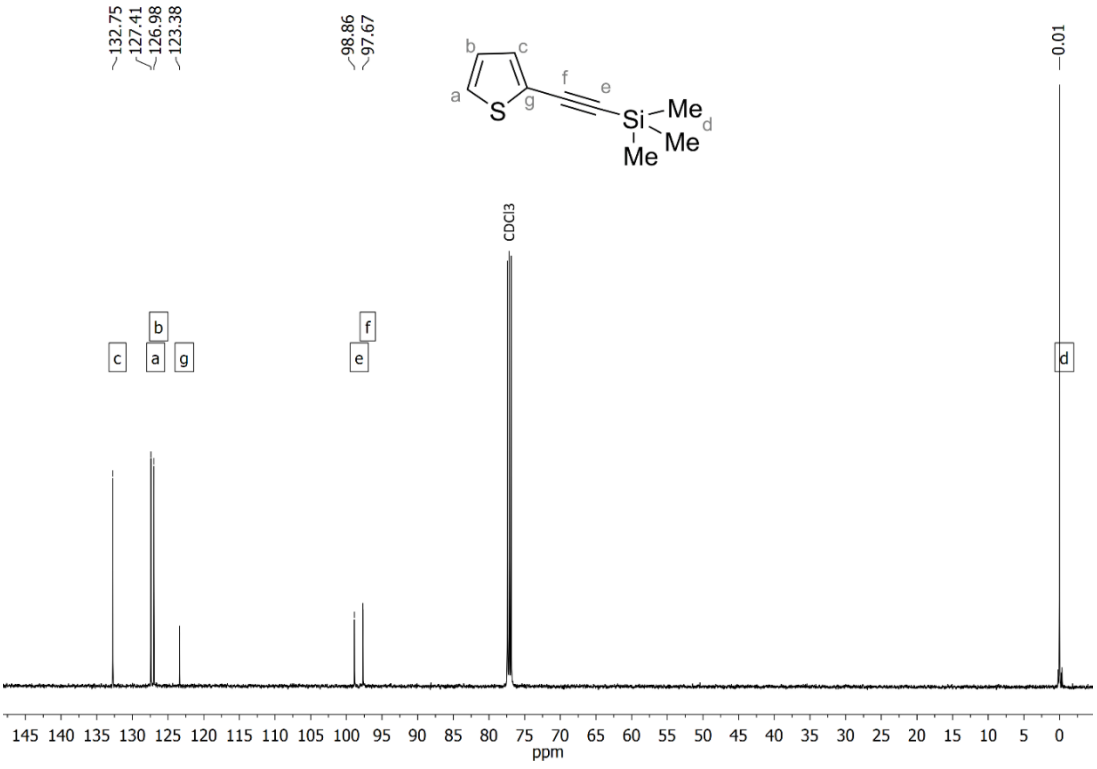

$^{29}Si\{^{1}H\}$ NMR (99 MHz, $CDCl_3$)

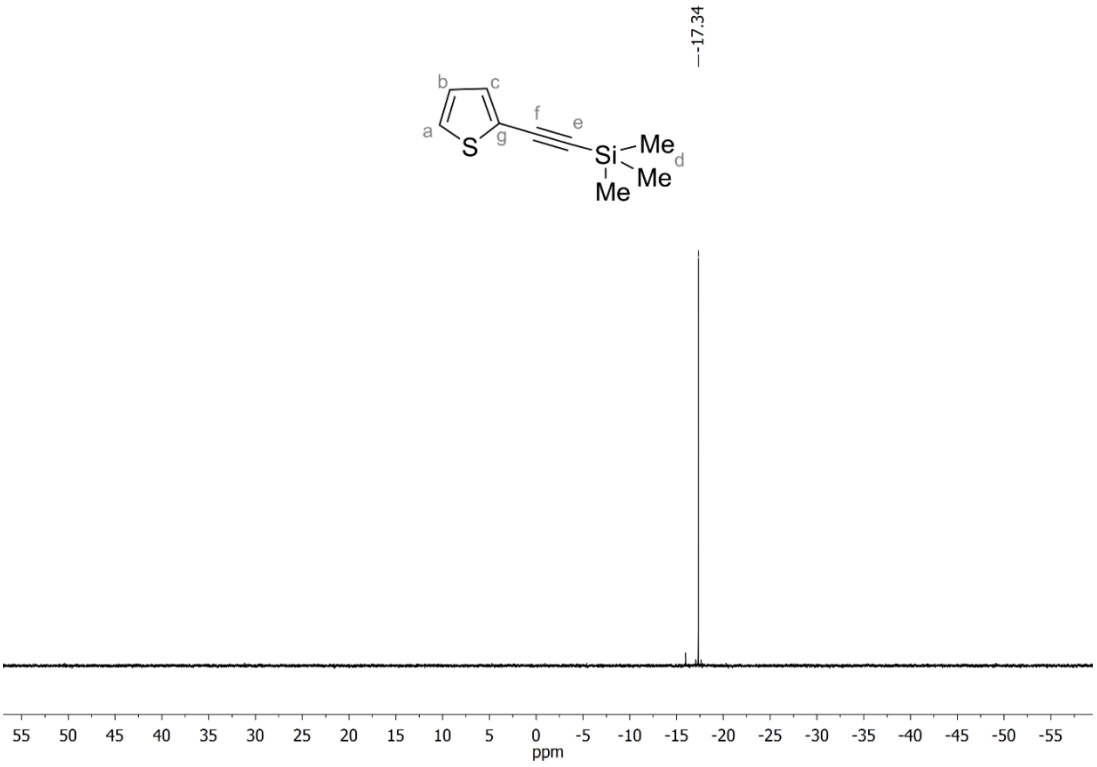

3.6. 2-Ethynylthiophene (6)

^{1}H NMR (500 MHz, $CDCl_3$)

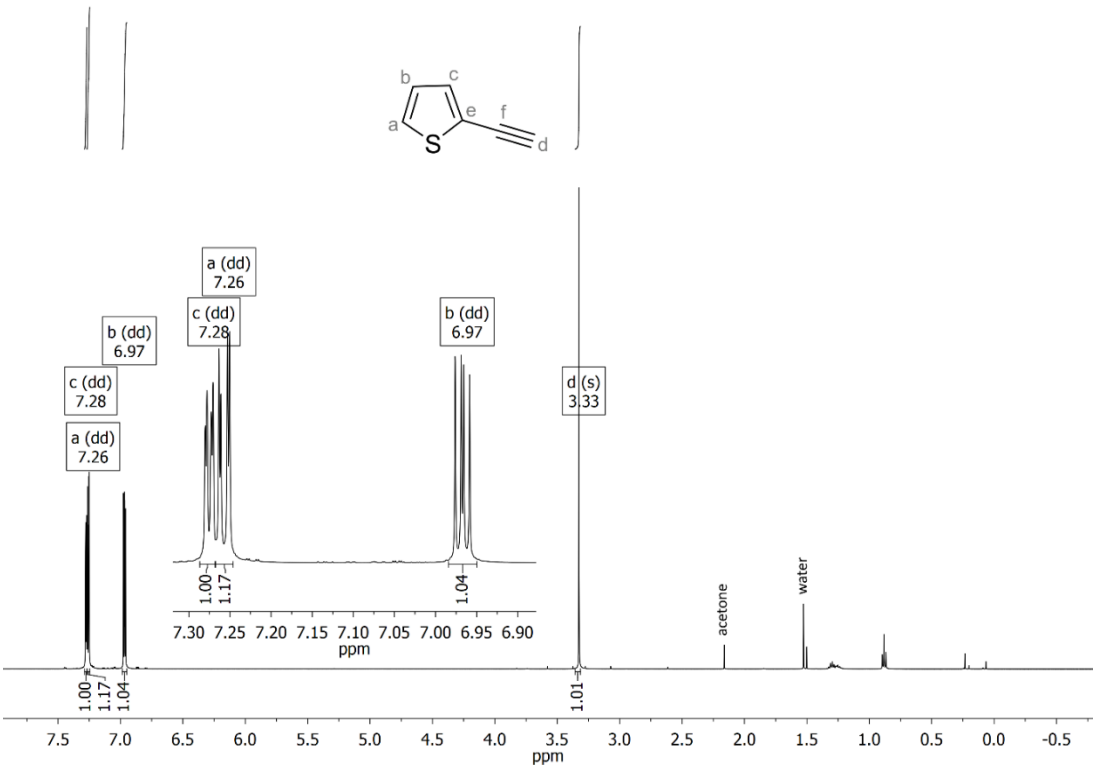

$^{13}C\{^{1}H\}$ NMR (126 MHz, $CDCl_3$)

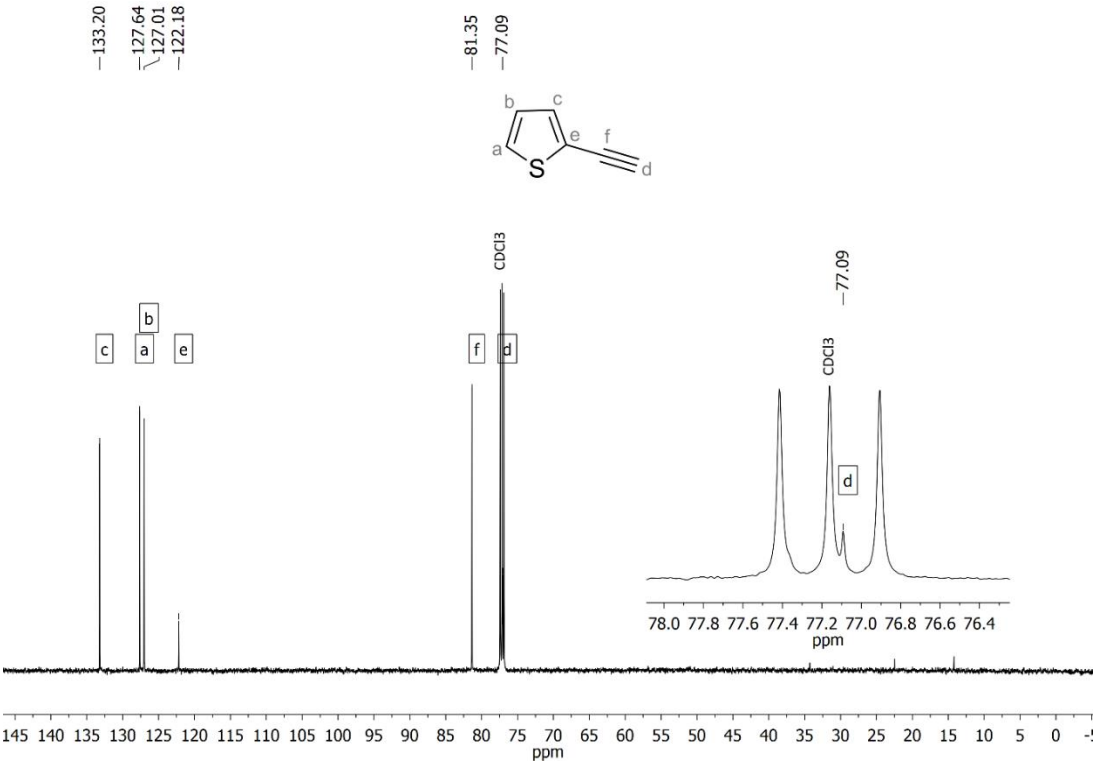

3.7. 2,6-bis(Thiophen-2-ylethynyl)pyridine (7)

^{1}H NMR (500 MHz, $CDCl_3$)

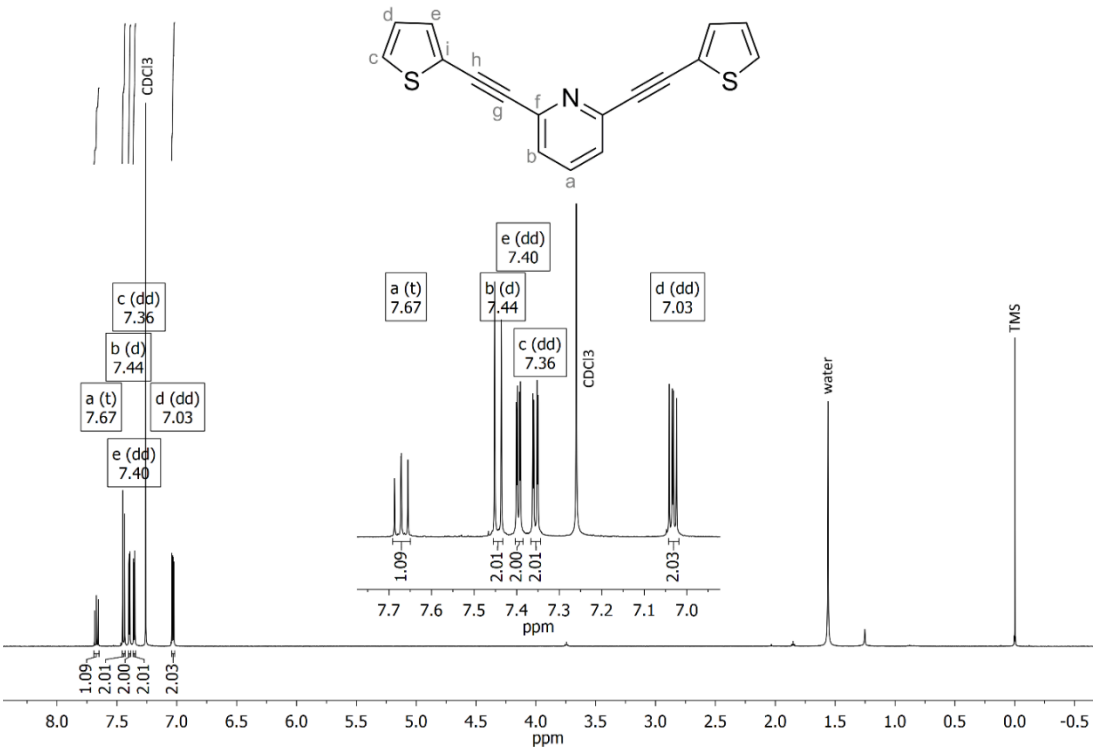

$^{13}C\{^{1}H\}$ NMR (126 MHz, $CDCl_3$)

3.8. 5,9-Di(thiophen-2-yl)-10a-aza-10b-borapyrene (BNP)

^{1}H NMR (601 MHz, $CDCl_3$)

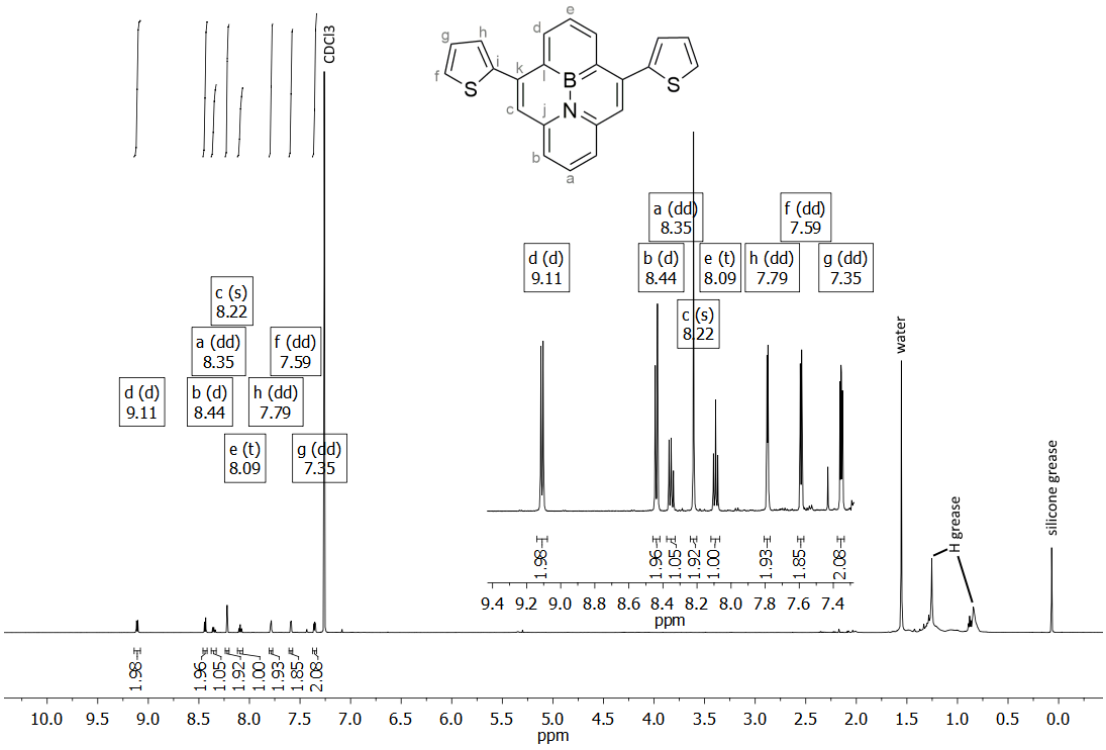

$^{13}C\{^{1}H\}$ NMR (151 MHz, $CDCl_3$)

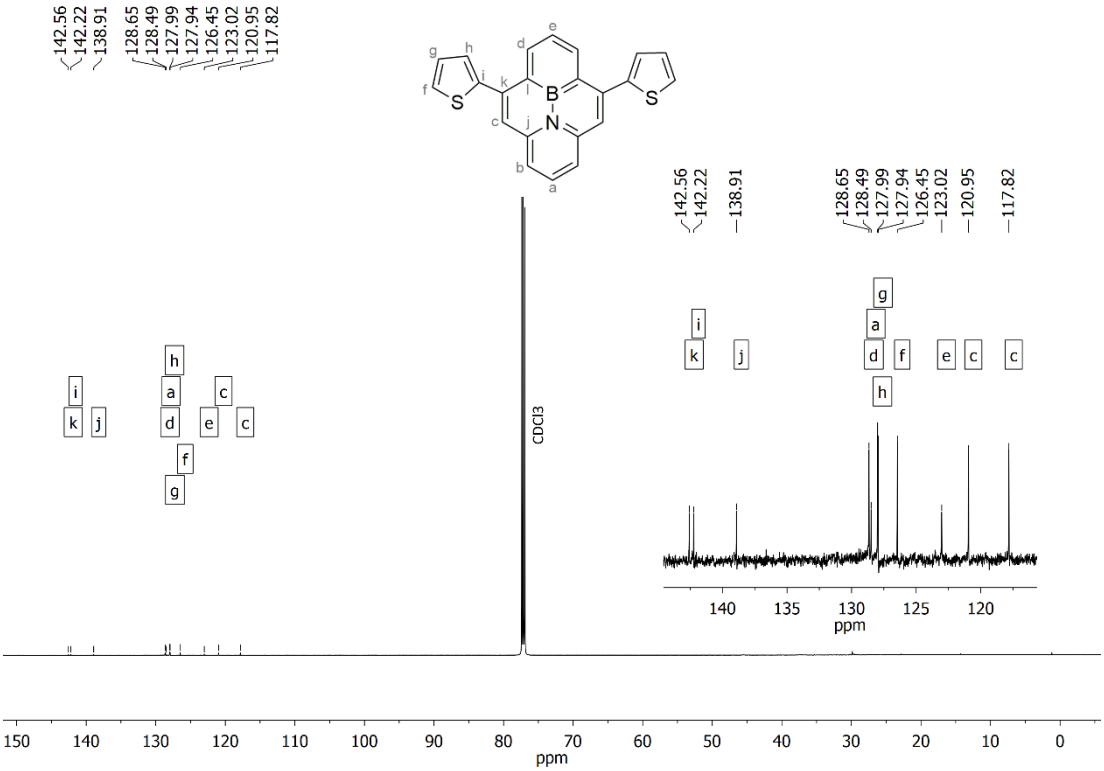

$^{11}B\{^{1}H\}$ NMR (160 MHz, C_6D_6)

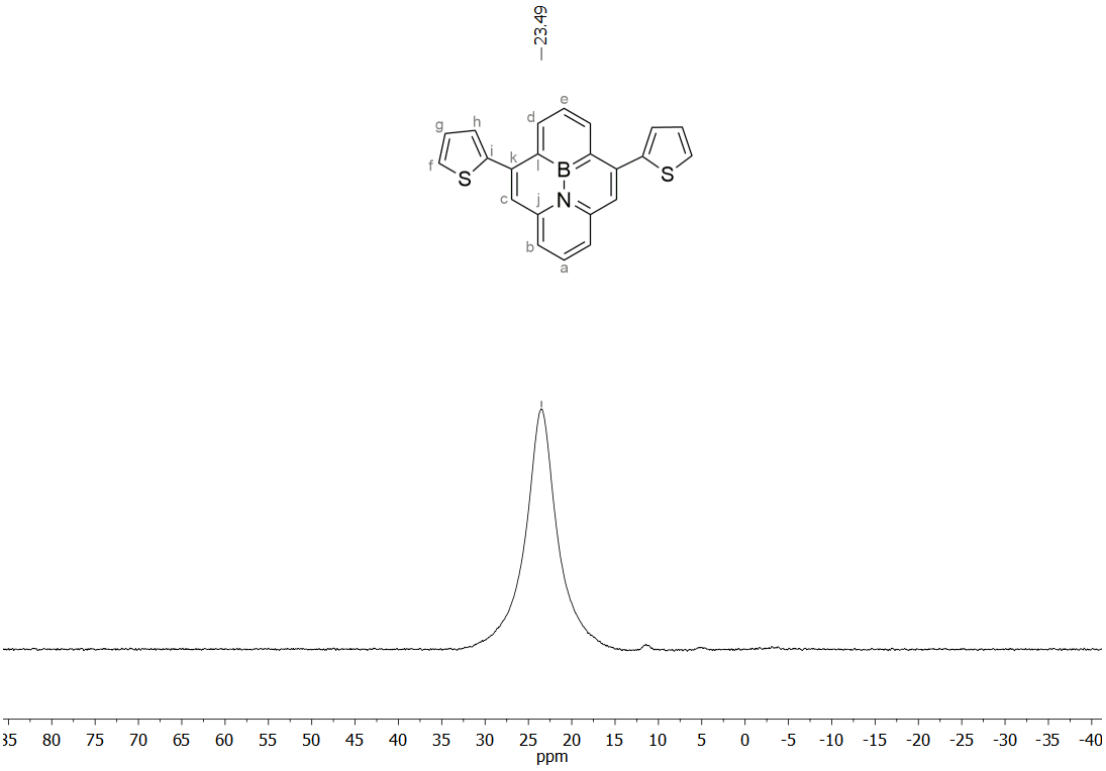

3.9. 1,3-Dibromo-2-iodobenzene (12)

^{1}H NMR (500 MHz, $CDCl_3$)

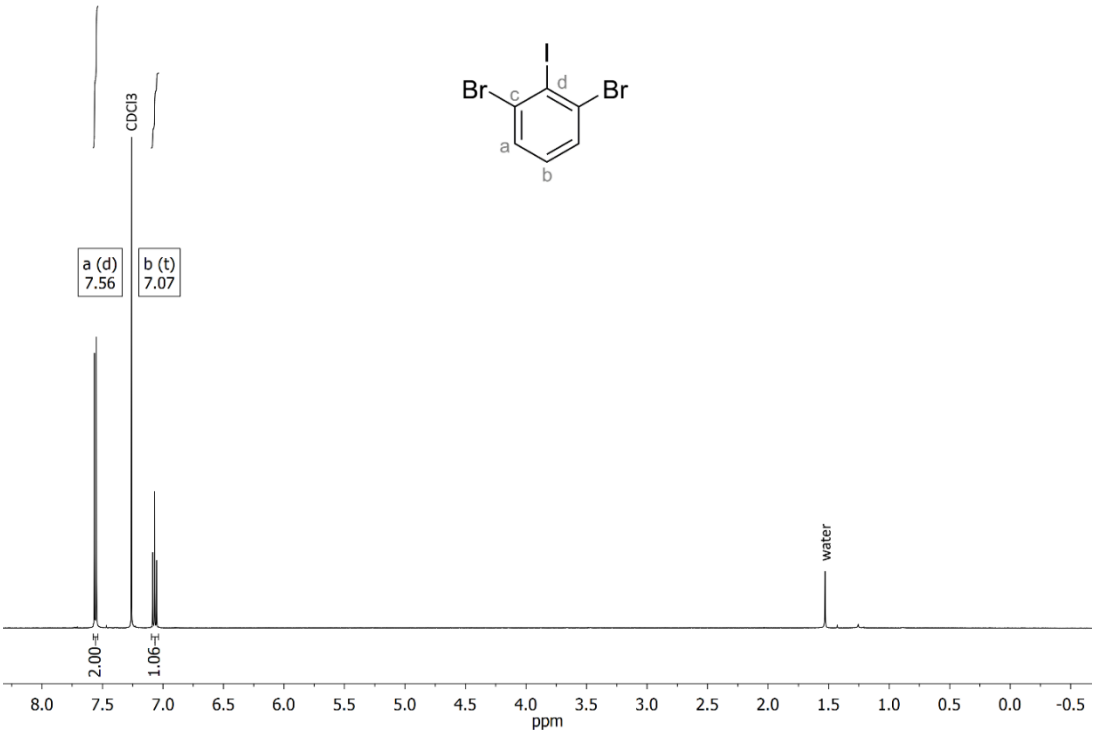

^{13}C{^{1}H} NMR (126 MHz, $CDCl_3$)

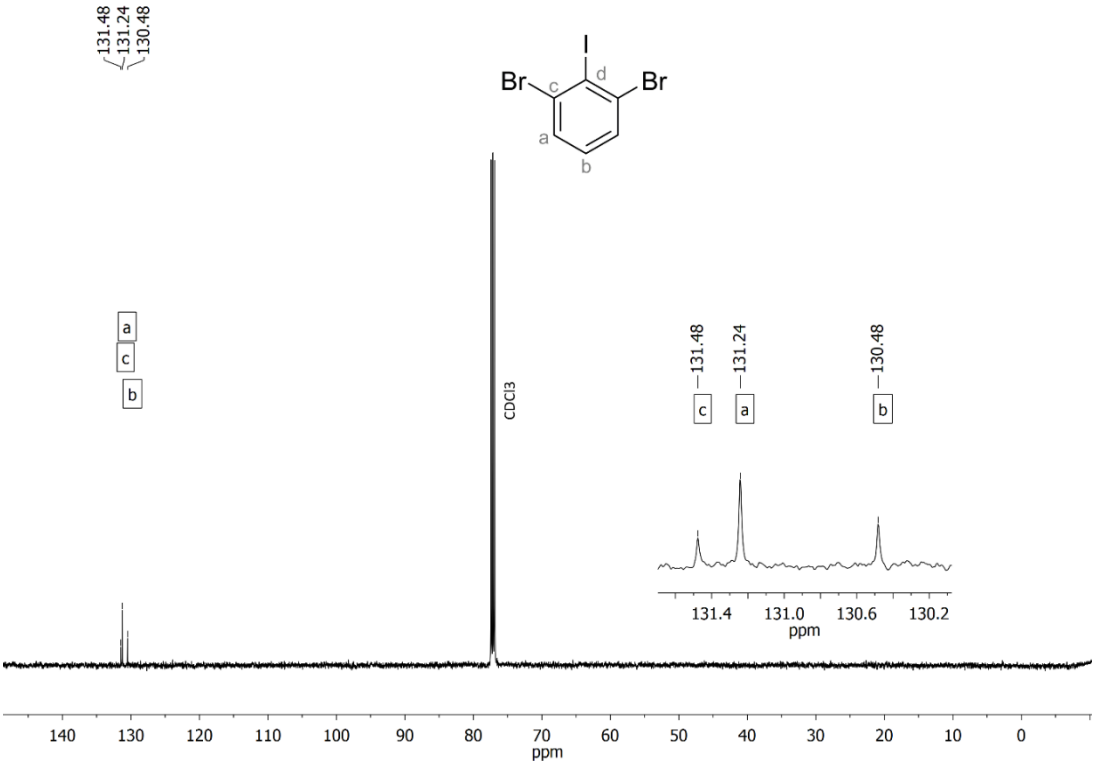

3.10. 2,6-Dibromo-1,1'-biphenyl (13)

^{1}H NMR (500 MHz, $CDCl_3$)

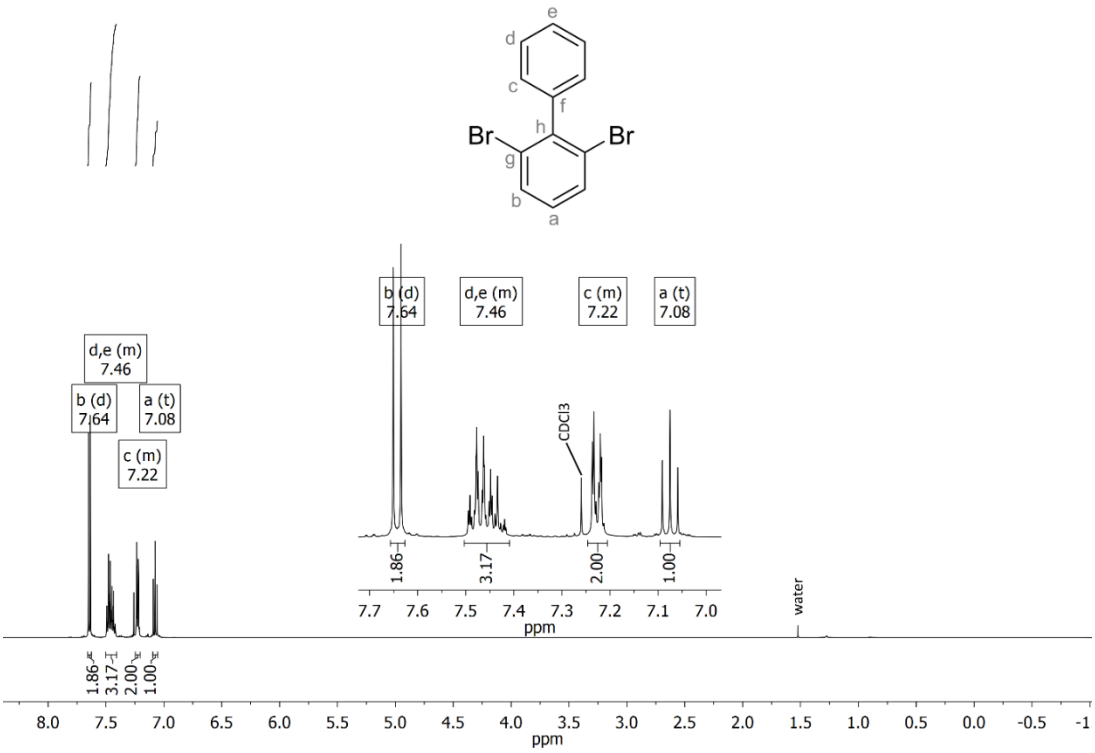

^{13}C{^{1}H} NMR (126 MHz, $CDCl_3$)

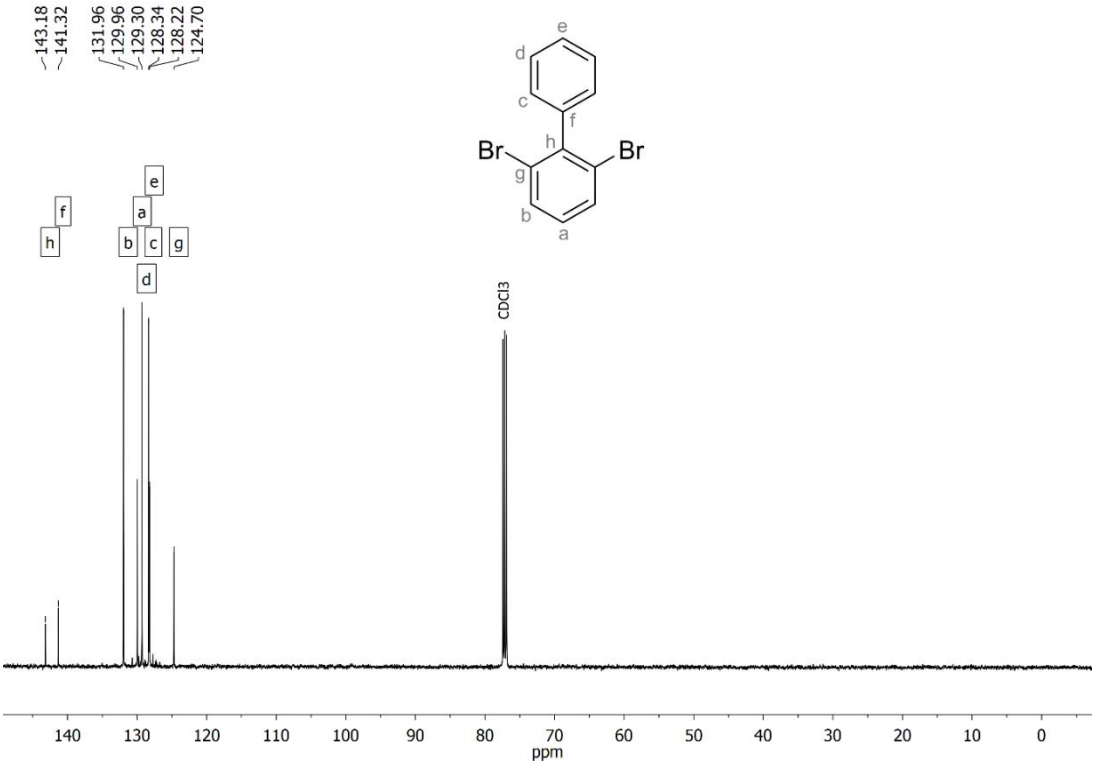

3.11. Trimethyl(thiophen-2-ylethynyl)stannane (14)

^{1}H NMR (500 MHz, C_6D_6)

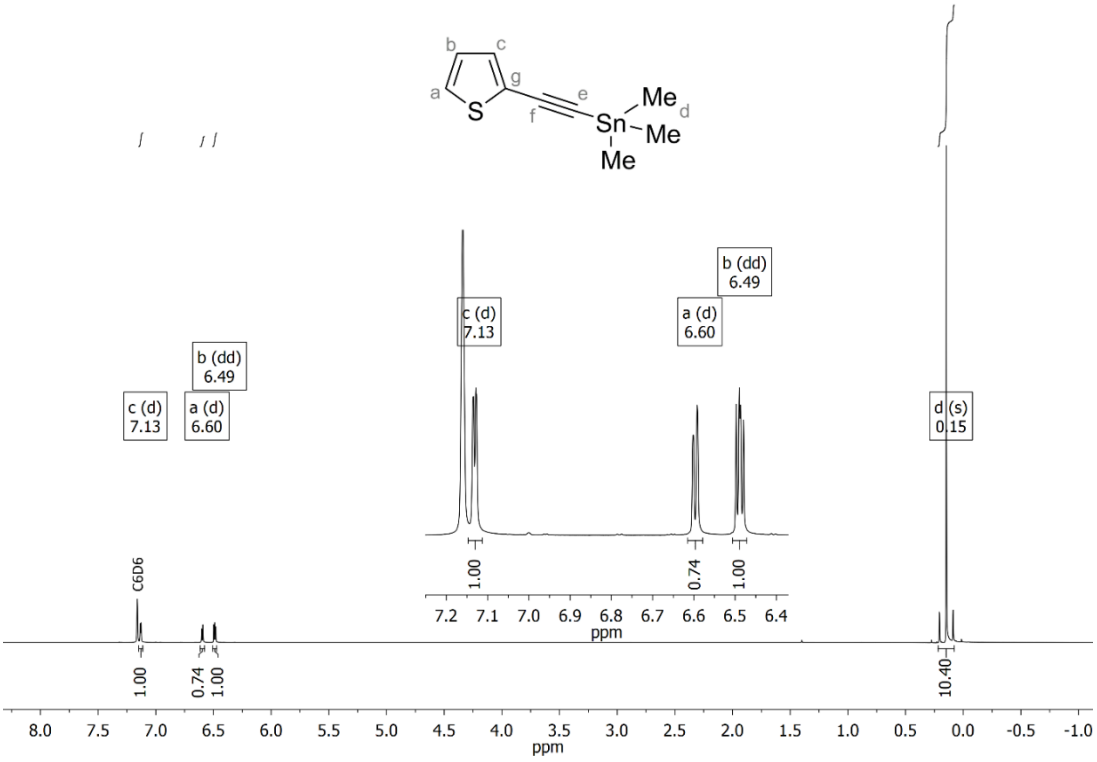

^{13}C{^{1}H} NMR (126 MHz, C_6D_6)

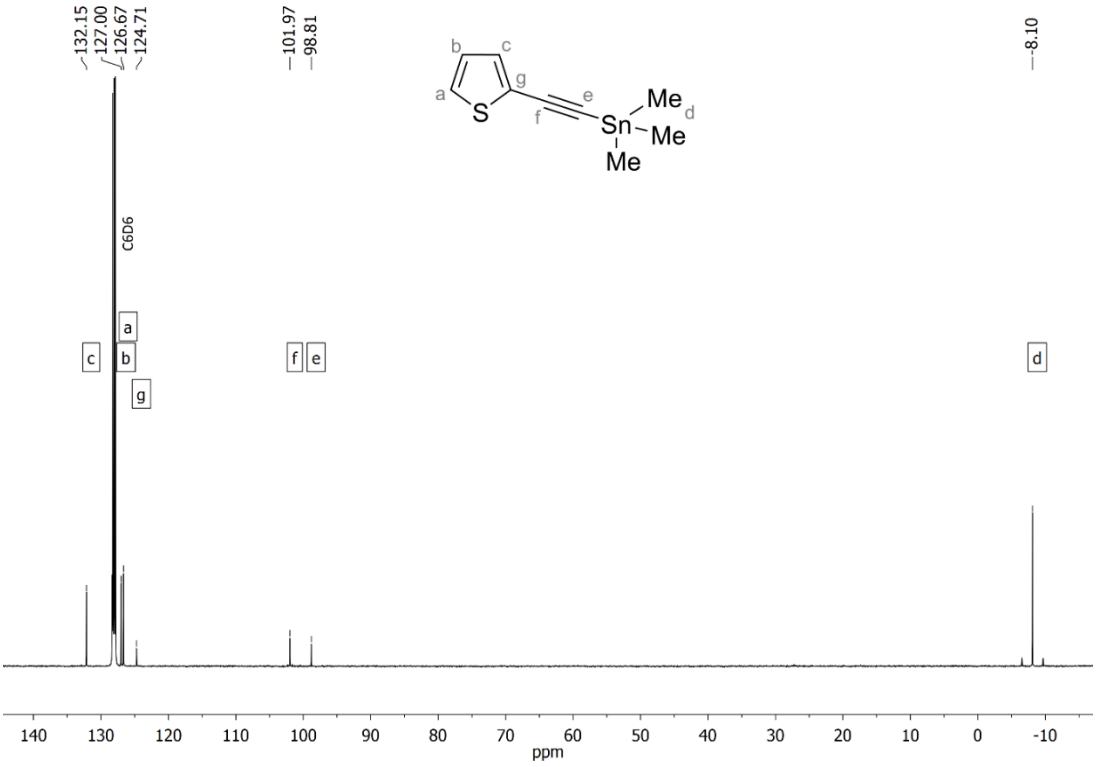

^{119}Sn NMR (187 MHz, C_6D_6)

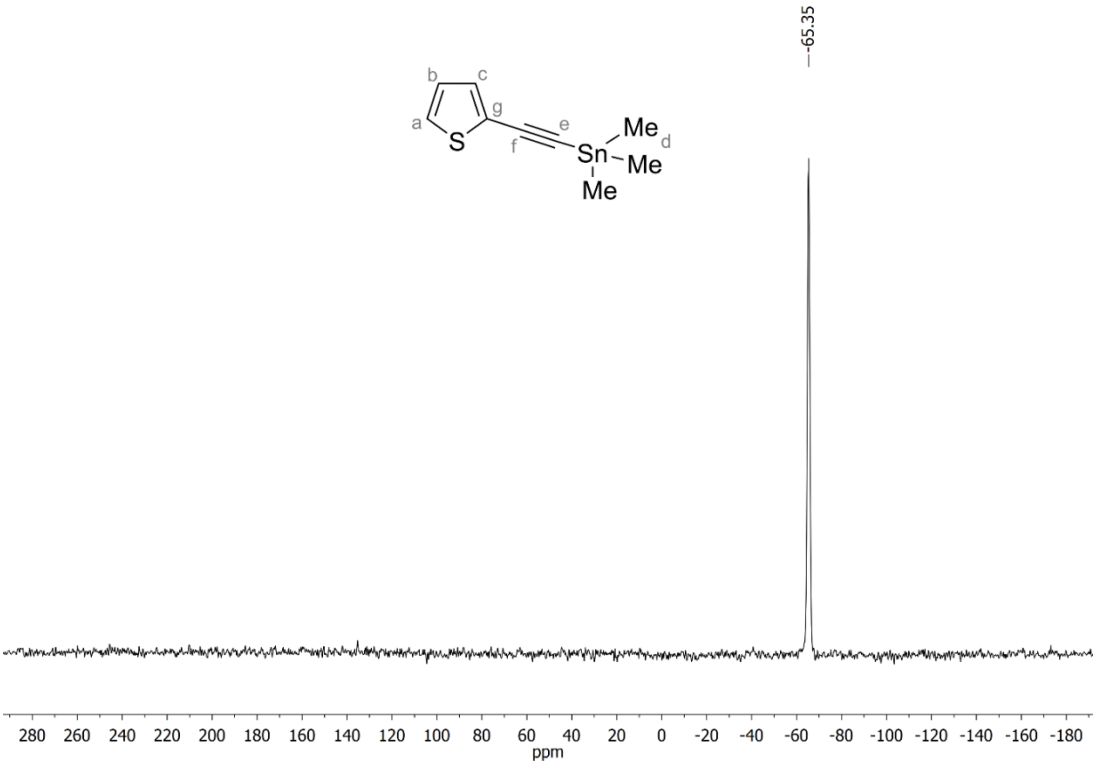

3.12. 2,6-bis(Thiophen-2-ylethynyl)-1,1'-biphenyl (15)

^{1}H NMR (500 MHz, $CDCl_3$)

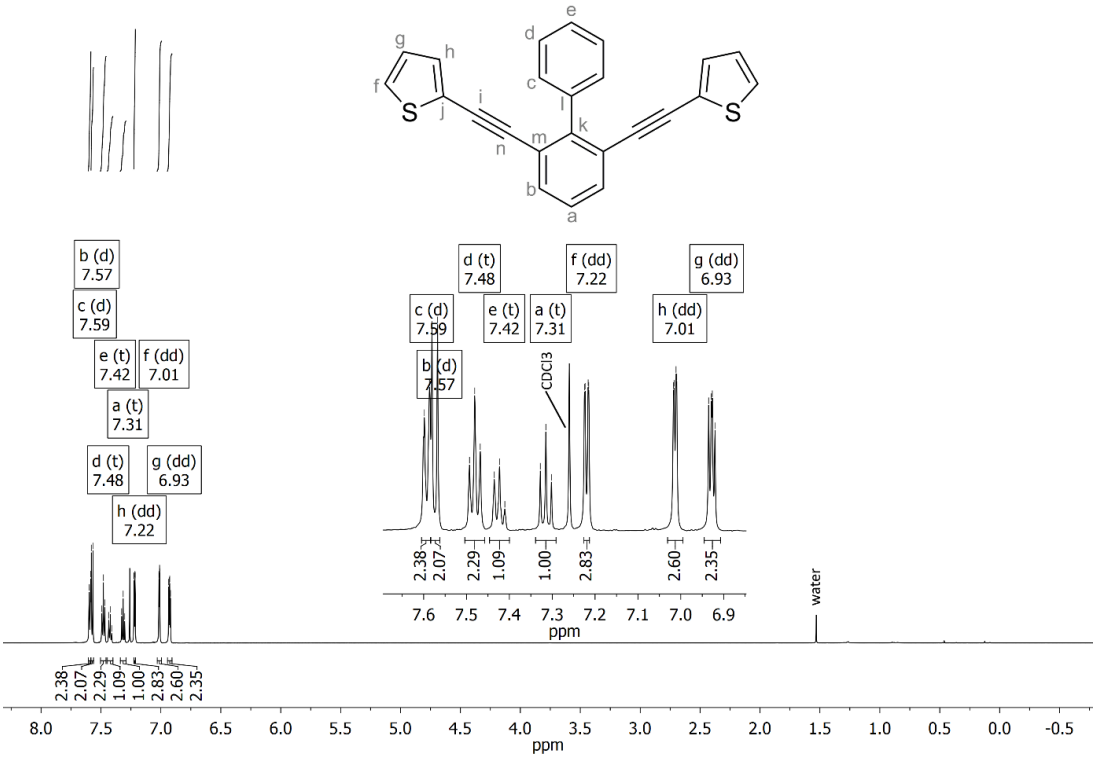

$^{13}C\{^{1}H\}$ NMR (126 MHz, $CDCl_3$)

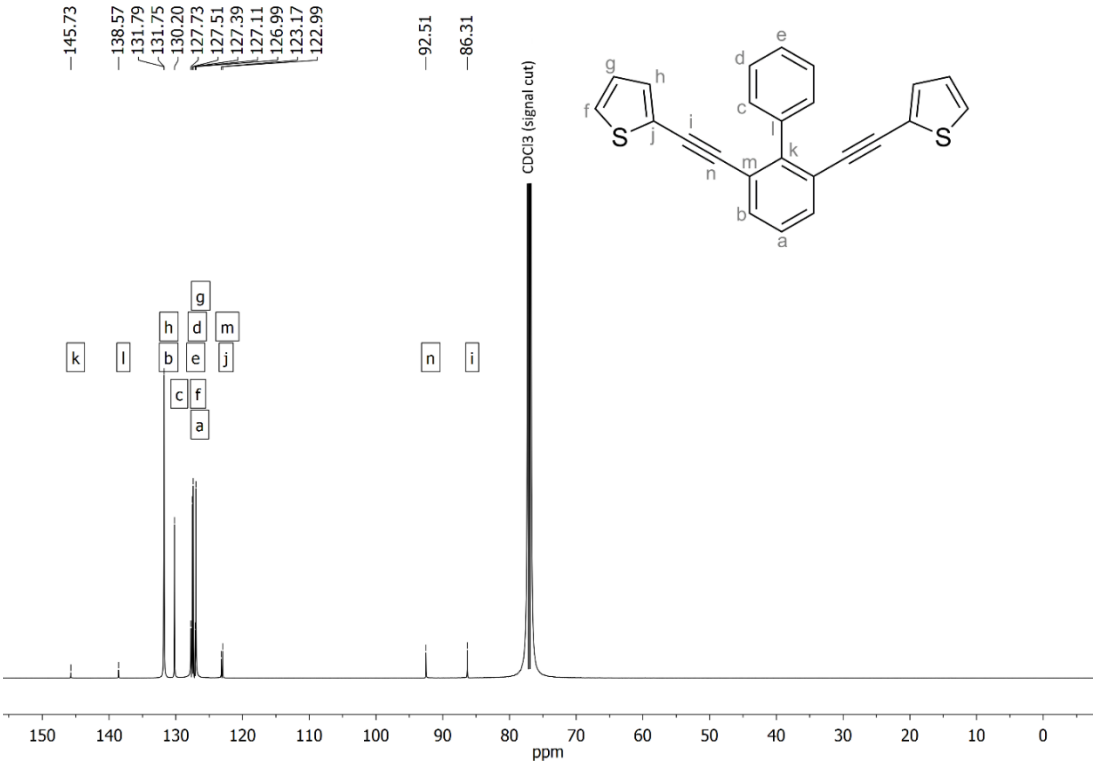

3.13. 4,10-Di(thiophen-2-yl)pyrene (CCP)

^{1}H NMR (500 MHz, $CDCl_3$)

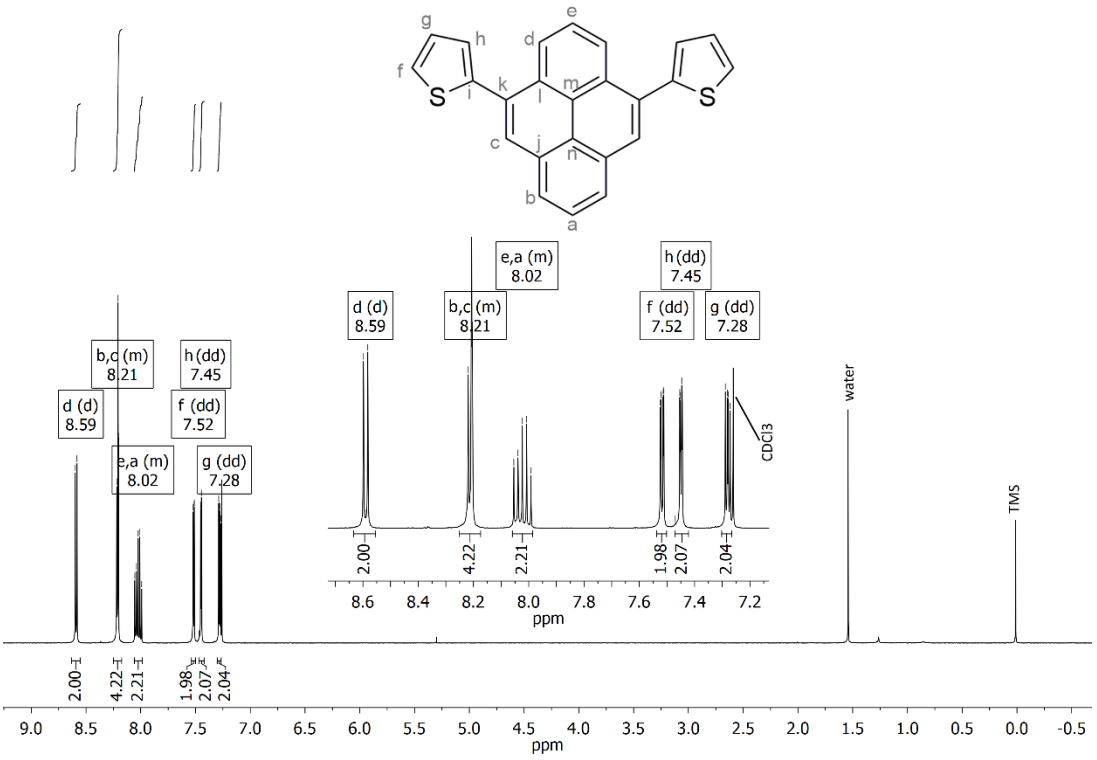

$^{13}C\{^{1}H\}$ NMR (126 MHz, $CDCl_3$)

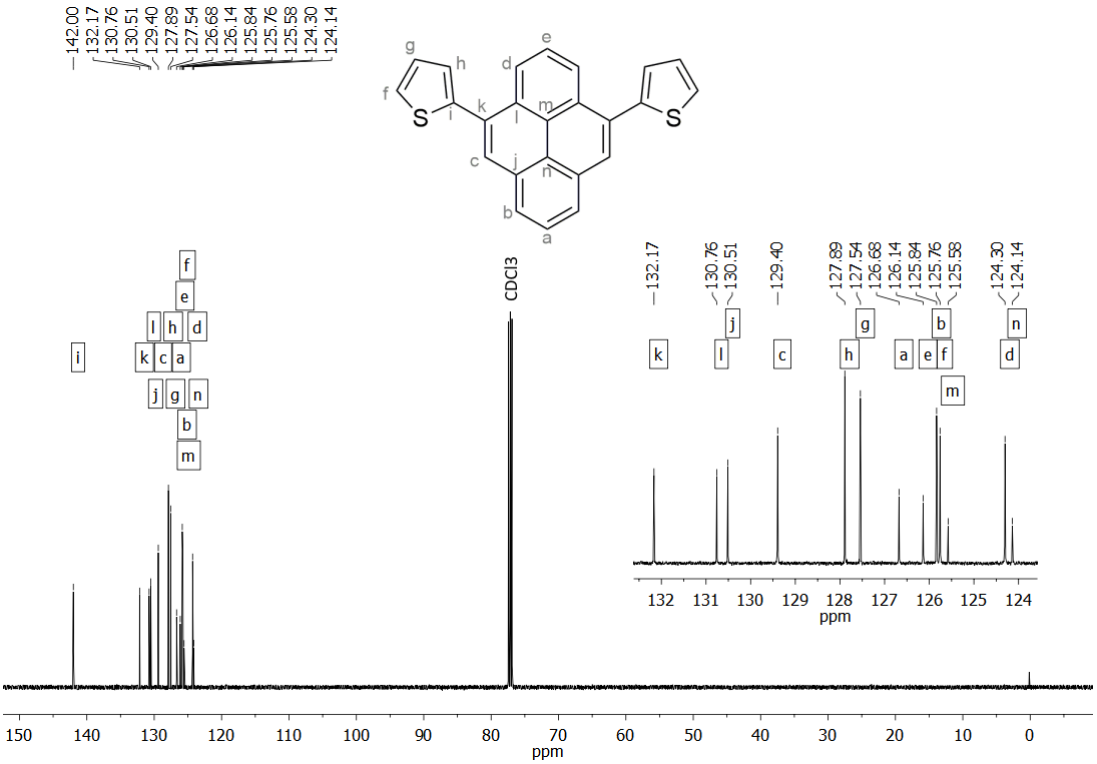

3.14. NMR Comparison in Deuterated Chloroform

Figure S1 shows a comparison of the proton resonances of **BNP** (top) and **CCP** (bottom) in $CDCl_3$ solution measured at 601 MHz.

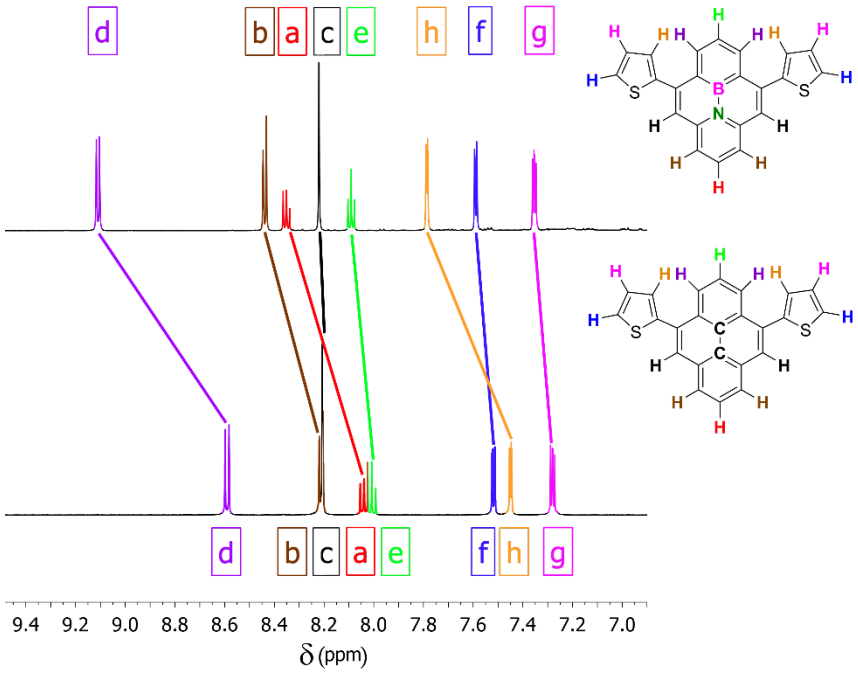

Figure S1. Comparison of the proton resonances in the respective ^{1}H-NMR spectra of **BNP** (top) and **CCP** (bottom). For better perceptibility, the signals of the solvent ($CDCl_3$) were removed.

3.15. Diffusion Ordered Spectroscopy (DOSY)

We performed diffusion ordered spectroscopy (DOSY) NMR measurements in C_6D_6 in order to answer the question whether different kinds of aggregations of **BNP** are present at different concentrations (Figure S2 and Figure S3). However, for both measured concentrations, the diffusion coefficients were very similar, indicating that only one species predominates. Observable shifts of the diffusion coefficients are due to artifacts of the measurement and do not refer to the detection of different aggregated species.

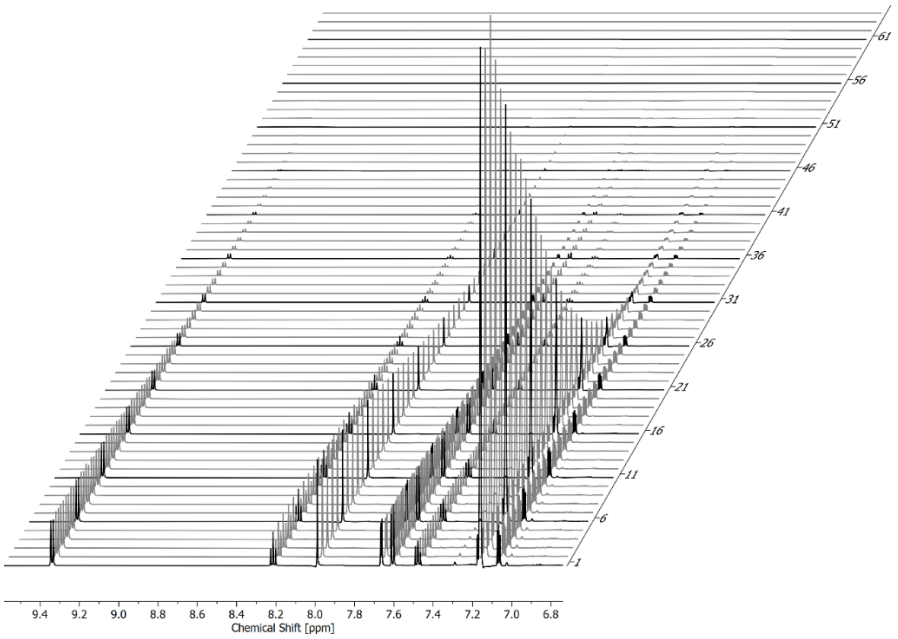

Figure S2. 3D DOSY plot of **BNP**, displaying the chemical shifts and intensities as a function of gradient strength.

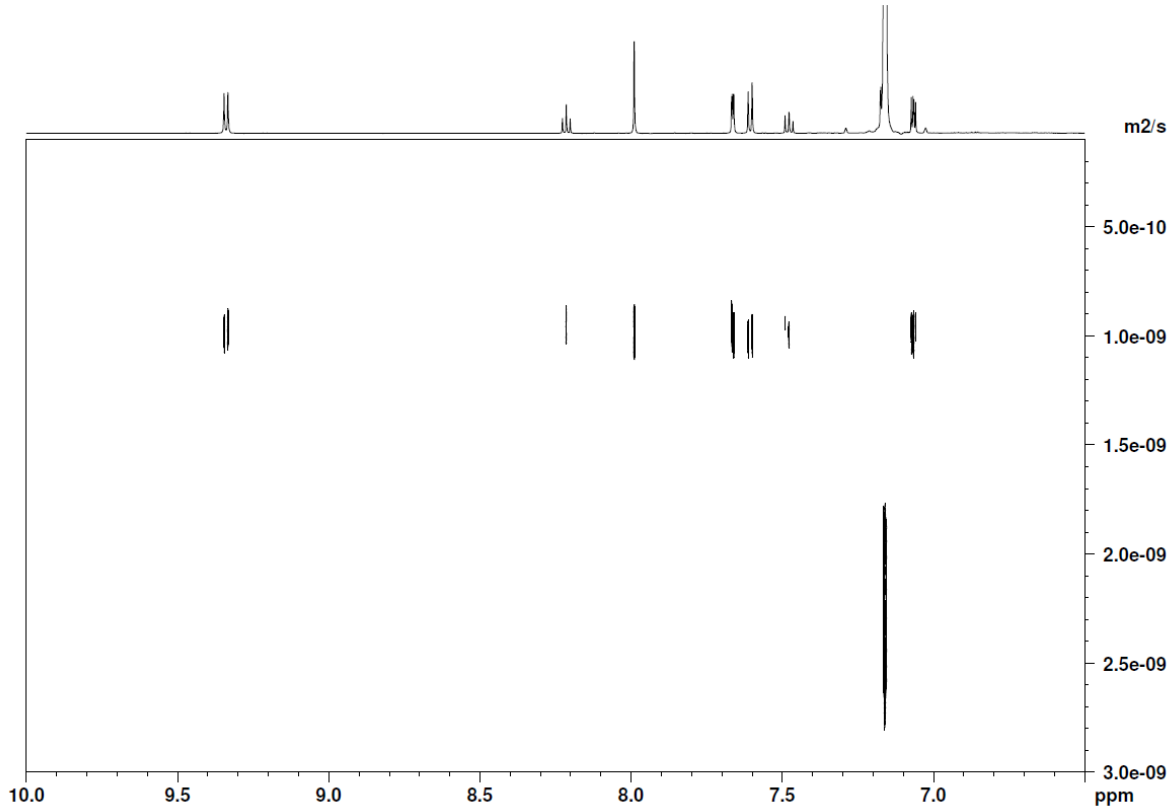

Figure S3. 2D DOSY plot of **BNP**, displaying the chemical shifts and diffusion coefficients.

The DOSY spectrum was first analyzed within the T1T2 relaxation module of Bruker TopSpin software. The experimentally obtained values for the signal intensity at the corresponding gradient strength, with exception of outlier in the data points, were exported with the report function and imported into Origin software. The signal intensity was plotted against the gradient strength. The experimental data were fitted with the following fit function "vargrad".

$$I = I(0)\exp\left(-D4\pi^2\gamma^2 LD^2 G^2\left(\frac{BD - LD}{3}\right) * 1 \cdot 10^4\right)$$

The specific values of the variables of the fit function are summarized in Table S1.

Table S1. Variables for the fit function "vargrad" (1) and their respective values for the fit function for the concentrated sample.

Variable	Value	Function
I		signal intensity
I(0)	0.1	signal intensity at gradient strength 0
D	1.0E^{-10} (D_{start})	diffusion coefficient / $\frac{m^2}{s}$
γ	4257.7	gyromagnetic ratio of the measured nucleus / $\frac{Hz}{G}$
G		gradient strength / $\frac{G}{cm}$
BD	1.4593E^{-1}	Big Delta (diffusion delay time) ($\approx d20$) / s
LD	2.6E^{-3}	Little Delta (gradient pulse width) ($2 * p30$) / s

Table S2. Fit results of the analyzed signals in the DOSY spectrum for both the concentrated sample (left) and the diluted sample (right) at T = 300 K.

Peak	**δ / ppm**	**Concentrated sample (c = 9.33 mg mL^{-1})**				**Diluted sample (c = 0.15 mg mL^{-1})**			
		number of outlier data points	**number of fitted data points**	**I(0) / 10^{-3} (± std. err.)**	**D / 10^{-10} $\frac{m^2}{s}$ (± std. err.)**	**number of outlier data points**	**number of fitted data points**	**I(0) / 10^{-3} (± std. err.)**	**D / 10^{-10} $\frac{m^2}{s}$ (± std. err.)**
1	9.333	1	63	98.44 (±6.058·10^{-5})	9.652 (±1.192·10^{-2})	0	64	9.68 (±6.921·10^{-5})	10.190 (±15.139·10^{-2})
2	8.214	2	62	53.04 (±4.019·10^{-5})	9.677 (±1.426·10^{-2})	0	64	4.84 (±7.136·10^{-5})	10.147 (±31.202·10^{-2})
3	7.990	5	59	96.56 (±1.038·10^{-4})	9.481 (±1.763·10^{-2})	0	64	9.04 (±5.585·10^{-5})	9.779 (±12.588·10^{-2})
4	7.660	4	60	95.49 (±1.310·10^{-4})	9.772 (±2.354·10^{-2})	0	64	9.16 (±6.078·10^{-5})	10.011 (±13.945·10^{-2})
5	7.600	2	62	107.52 (±1.200·10^{-4})	9.974 (±2.140·10^{-2})	0	64	9.76 (±5.393·10^{-5})	10.212 (±11.726·10^{-2})
6	7.477	3	61	53.35 (±6.299·10^{-5})	9.671 (±2.140·10^{-2})	1	63	4.17 (±7.918·10^{-5})	9.693 (±36.921·10^{-2})
7	7.160 (solvent)	1	63	1032.15 (±2.460·10^{-3})	21.61 (±9.584·10^{-2})	1	63	1040.4 (±1.040·10^{-3})	23.605 (±4.360·10^{-2})
8	7.068	1	63	87.66 (±1.413·10^{-4})	10.000 (±3.222·10^{-2})	3	61	9.55 (±9.807·10^{-5})	10.180 (±19.160·10^{-2})
				weighted mean	**9.691 (±6.695·10^{-3})**			weighted mean	**10.053 (±6.022·10^{-2})**

4. Crystallography and Hirshfeld Surface Analysis

The crystal structure of **BNP** was measured in-house using a Bruker Venture D8 diffractometer with a shutterless Photon100 detector at 100 K. Monochromatic Mo-K_α radiation was provided by a IμS microfocus source. The crystal structure of **CCP** was obtained from a synchrotron X-ray diffraction experiment at beamline BL02B1 of SPring-8. The measurement was carried out at 20 K using a helium open-flow gas stream device. BL02B1 is equipped with a large cylindrical imaging plate and a kappa-geometry diffractometer. Using Olex2[9], the structures were solved with the ShelXT[10] structure solution program using intrinsic phasing and were refined with the ShelXL[11] software package using full-matrix least squares minimization. Conformational disorder of the thiophene groups was treated using partially refined and partially fixed site occupation factors. Hydrogen atoms were inserted in geometrically calculated positions. Pertinent crystallographic, measurement and refinement details are given in Table S3. The Hirshfeld surface analysis as well as the model energy calculations were carried out with the program CrystalExplorer 3.3.[12] Molecular wavefunctions for the model-energy analysis were calculated with Gaussian09[13] as interfaced with CrystalExplorer at the B3LYP/6-31G(d,p) level of theory.

Table S3. Crystallographic measurement and refinement details.

	BNP	**CCP**
Empirical formula	$C_{22}H_{14}S_2BN$	$C_{24}H_{14}S_2$
Formula weight	367.27	366.47
Crystal size (mm)	0.40x0.06x0.06	0.14x0.05x0.02
Crystal system	Monoclinic	Monoclinic
Space group	$P2_1/c$	$P2_1/n$
a(Å)	10.9900(4)	15.7326(6)
b(Å)	16.1376(7)	3.95640(10)
c(Å)	9.5771(3)	26.6349(10)
β(°)	90.931(3)	96.369(7)
Volume (Å^3),Z	1698.30(11),4	1647.64(10),4
Calculated density (g cm^{-3})	1.44	1.477
F(0 0 0)	760	760
λ (Å)	0.71073	0.4015
μ (mm^{-1})	0.318	0.082
Temperature (K)	100(1)	20(1)
θ range (°)	1.853- 26.005	1.394- 26.359
R_{int}	0.0257	0.0655
Measured reflections	12484	14984
Unique reflections	3310	4060
Completeness (%)	99.2	99.30
$R(F^2)$ / $wR(F^2)$ (all data)	0.0455/ 0.0940	0.0698/0.1525
$R(F^2)$ / $wR(F^2)$ ($I> 2\sigma(I)$)	0.0358/ 0.0894	0.0475/ 0.1327
Goodness of fit	1.057	1.111
$\Delta\rho_{min}$, $\Delta\rho_{max}$ (eÅ^{-3})	-0.201, 0.359	-0.275, 0.608
CCDC number	2040669	2040670

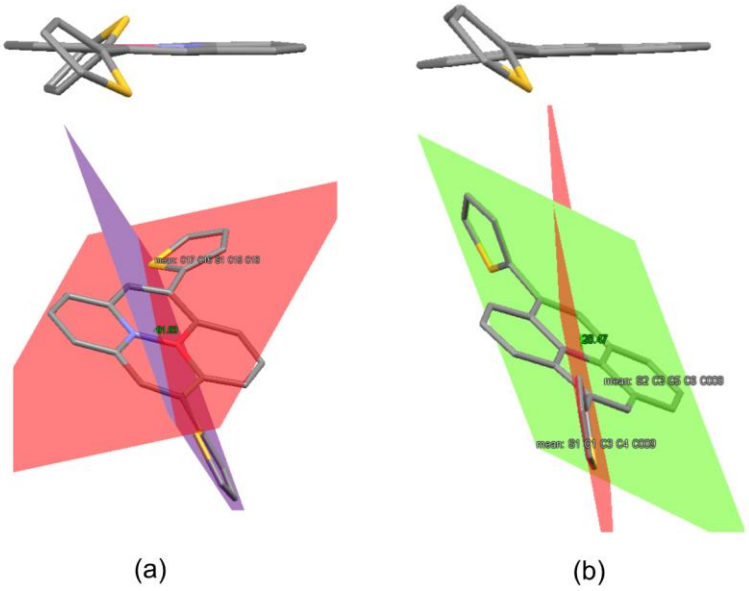

Figure S4. Relative orientation of the two thiophene rings in (a) **BNP** and (b) **CCP**. In the figure, the two planes across the thiophene rings that constitute the dihedral angle are shown. The angles are 81.83° for **BNP** and 28.47° for **CCP**.

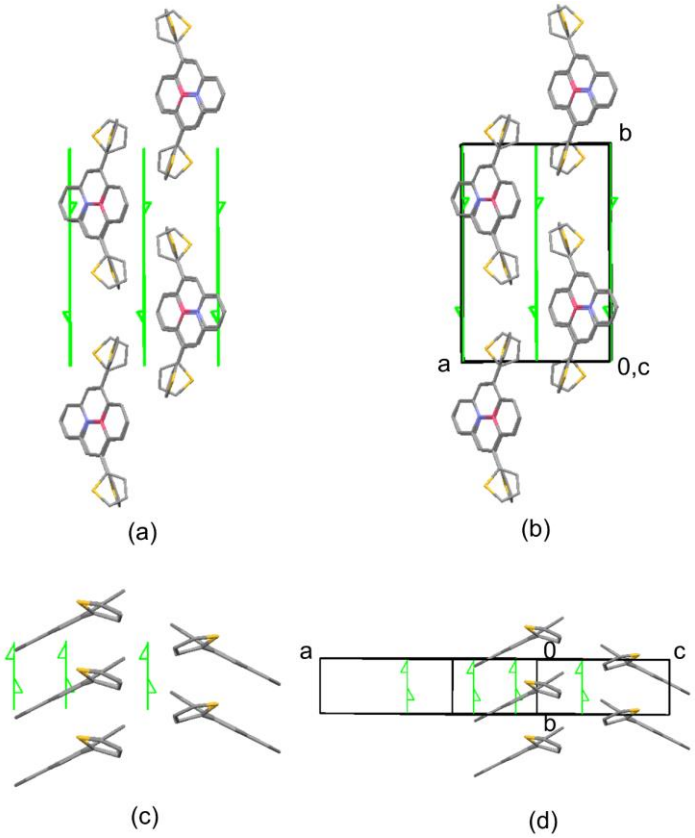

Figure S5. Comparison of crystal packing along the 2_1 screw axis in **BNP** (a,b) and **CCP** (c,d).

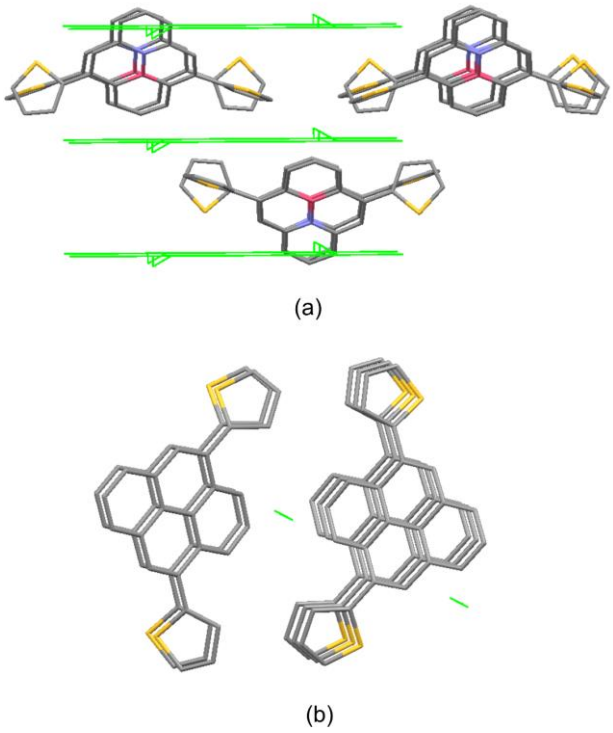

Figure S6. View of the differences in packing of (a) **BNP** and (b) **CCP** that highlights that the orientation of the thiophene rings in consecutive molecules is significantly different.

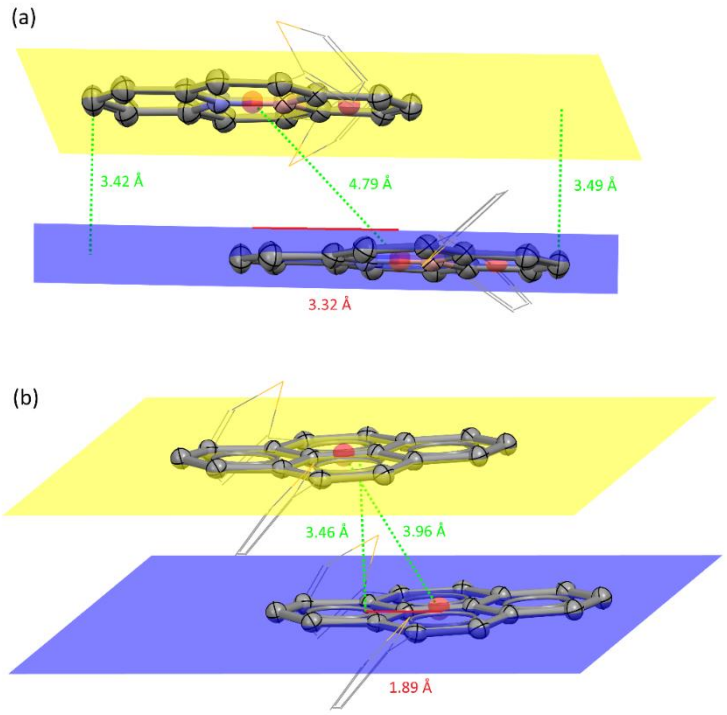

Figure S7. Centroid-centroid distances and plane distances of **BNP** (a) and **CCP** (b).

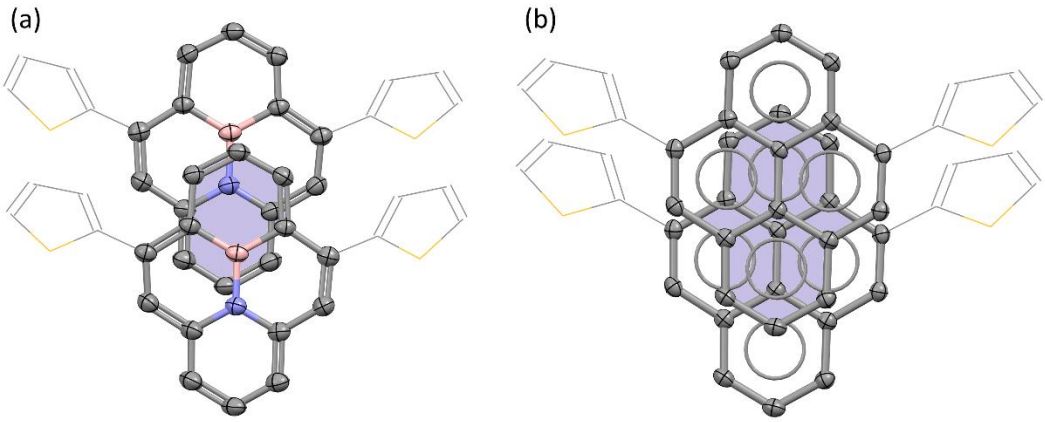

Figure S8. The overlap of the respective, neighboring π-planes in **BNP** (a) and **CCP** (b).

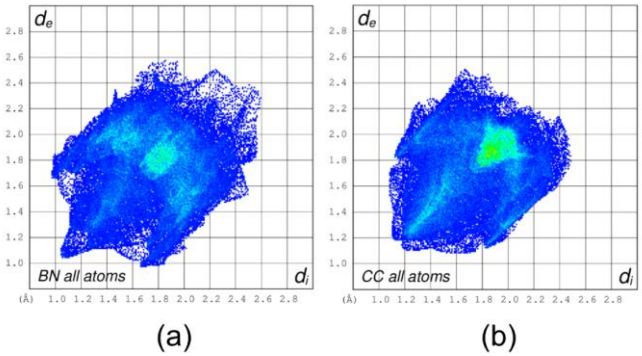

Figure S9. Hirshfeld surface (HS) fingerprint plots for (a) **BNP** and (b) **CCP**. d_e is the distance of any surface point to the closest atom outside the HS, d_i inside the HS. The color represents the density of data points.

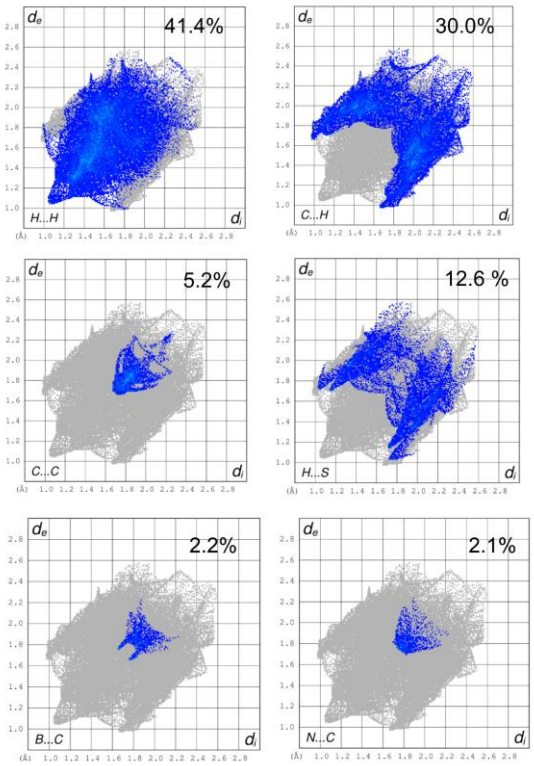

Figure S10. Fingerprint plot breakdown plots corresponding to individual atom-atom contacts in **BNP**.

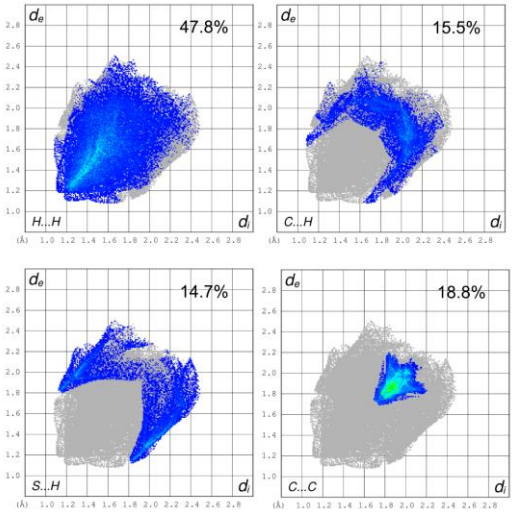

Figure S11. Fingerprint plot breakdown plots corresponding to individual atom-atom contacts in **CCP**.

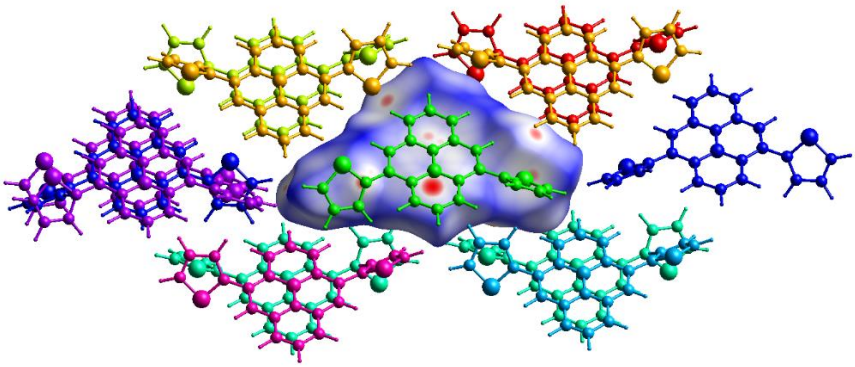

Figure S12. First coordination sphere around the asymmetric unit of **BNP**, enclosed in a Hirshfeld surface mapped with d_{norm}. The color codes of the surrounding molecules correspond to the CE-B3LYP model energy calculations in Table S4.

Table S4. CrystalExplorer model energies (in kJ mol^{-1}) for **BNP**. The electrostatic (E_ele), polarization (E_pol), dispersion (E_dis) and repulsion (E_rep) energy terms are not scaled, whereas the total energy term (E_tot) is the sum of the scaled components. Scale factors depend on the level of theory (here B3LYP/6-31G(d,p)).[14]

	Symop	R	Electron Density	E_ele	E_pol	E_dis	E_rep	E_tot
	-x, -y, -z	10.54	B3LYP/6-31G(d,p)	-6.1	-1.3	-22.2	24.4	-11.6
	-x, y+1/2, -z+1/2	9.51	B3LYP/6-31G(d,p)	-6.7	-0.9	-25.7	22.0	-16.4
	-x, -y, -z	10.34	B3LYP/6-31G(d,p)	-4.8	-1.2	-21.3	16.1	-14.4
	x, -y+1/2, z+1/2	4.79	B3LYP/6-31G(d,p)	-18.3	-3.8	-102.1	76.5	-62.9
	-x, y+1/2, -z+1/2	10.05	B3LYP/6-31G(d,p)	-9.9	-1.4	-30.6	23.2	-23.5
	-x, -y, -z	11.34	B3LYP/6-31G(d,p)	-2.3	-0.4	-16.6	8.2	-11.8
	x, y, z	16.14	B3LYP/6-31G(d,p)	-2.0	-0.5	-7.9	8.6	-4.1
	-x, -y, -z	11.15	B3LYP/6-31G(d,p)	-4.4	-0.5	-19.8	11.7	-14.8
	Total:			-54.5	-10.0	-246.2	190.7	-159.5

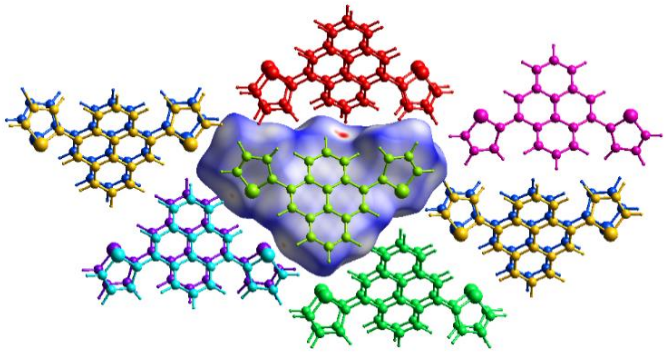

Figure S13. First coordination sphere around the asymmetric unit of **CCP**, enclosed in a Hirshfeld surface mapped with d_{norm}. The color codes of the surrounding molecules correspond to the CE-B3LYP model energy calculations in Table S5.

Table S5. CrystalExplorer model energies (in kJ mol^{-1}) for **CCP**. The electrostatic (E_ele), polarization (E_pol), dispersion (E_dis) and repulsion (E_rep) energy terms are not scaled, whereas the total energy term (E_tot) is the sum of the scaled components. Scale factors depend on the level of theory (here B3LYP/6-31G(d,p)).[14]

	Symop	R	Electron Density	E_ele	E_pol	E_dis	E_rep	E_tot
	-x+1/2, y+1/2, -z+1/2	7.80	B3LYP/6-31G(d,p)	-9.2	-1.1	-36.8	29.6	-24.0
	x+1/2, -y+1/2, z+1/2	14.74	B3LYP/6-31G(d,p)	-1.9	-0.3	-7.4	4.9	-5.5
	x, y, z	3.96	B3LYP/6-31G(d,p)	-9.0	-4.3	-126.8	84.8	-69.2
	-x+1/2, y+1/2, -z+1/2	9.67	B3LYP/6-31G(d,p)	-3.8	-0.5	-18.4	14.6	-11.3
	-x, -y, -z	10.79	B3LYP/6-31G(d,p)	-6.4	-0.6	-21.0	22.6	-11.6
	x+1/2, -y+1/2, z+1/2	14.98	B3LYP/6-31G(d,p)	-1.3	-0.4	-8.3	6.6	-4.8
	-x, -y, -z	10.39	B3LYP/6-31G(d,p)	-7.9	-0.8	-25.4	24.0	-16.1
	-x, -y, -z	16.46	B3LYP/6-31G(d,p)	1.0	-0.4	-6.2	2.8	-2.8
	Total:			-38.5	-8.4	-250.3	189.9	-145.3

5. Optical Spectroscopy

5.1. Molar Extinction Coefficients

For the determination of the molar extinction coefficients, dilution series in chloroform were prepared. Linear fittings of the resulting maximum absorptions according to the Lambert Beer law were applied to obtain the molar extinction coefficients (Figure S14 and Figure S15).

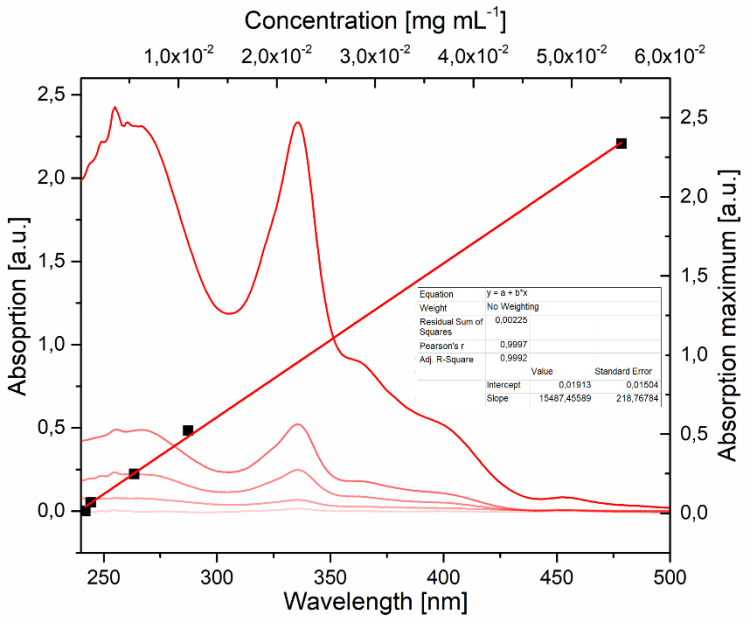

Figure S14. Absorption spectra of **BNP** at different concentrations ($5.5 \cdot 10^{-4}$ to $5.5 \cdot 10^{-2}$ mg mL^{-1}) and linear fitting of the respective maxima at λ_{abs} = 281 nm according to the Lambert Beer law.

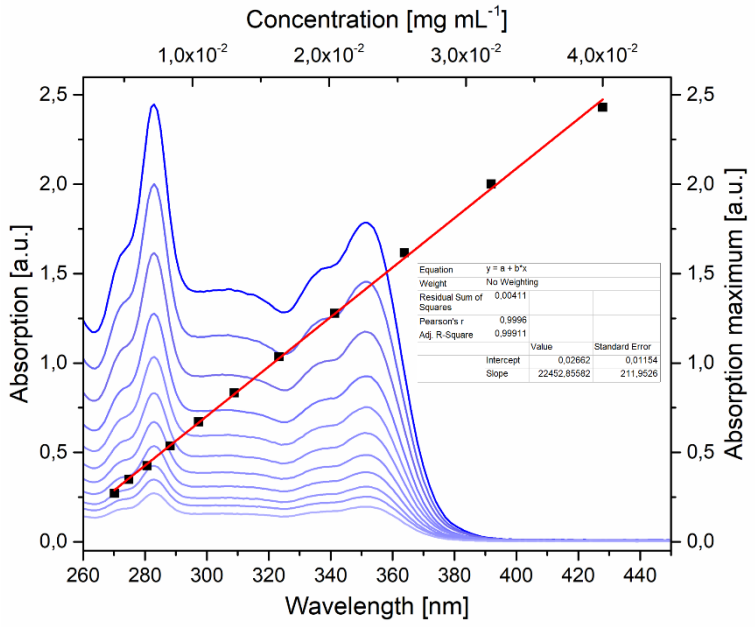

Figure S15. Absorption spectra of **CCP** at different concentrations ($4.3 \cdot 10^{-4}$ to $4.0 \cdot 10^{-2}$ mg mL^{-1}) and linear fitting of the respective maxima at λ_{abs} = 336 nm according to the Lambert Beer law.

5.2. Concentration- and Solvent-Dependent PL Spectra

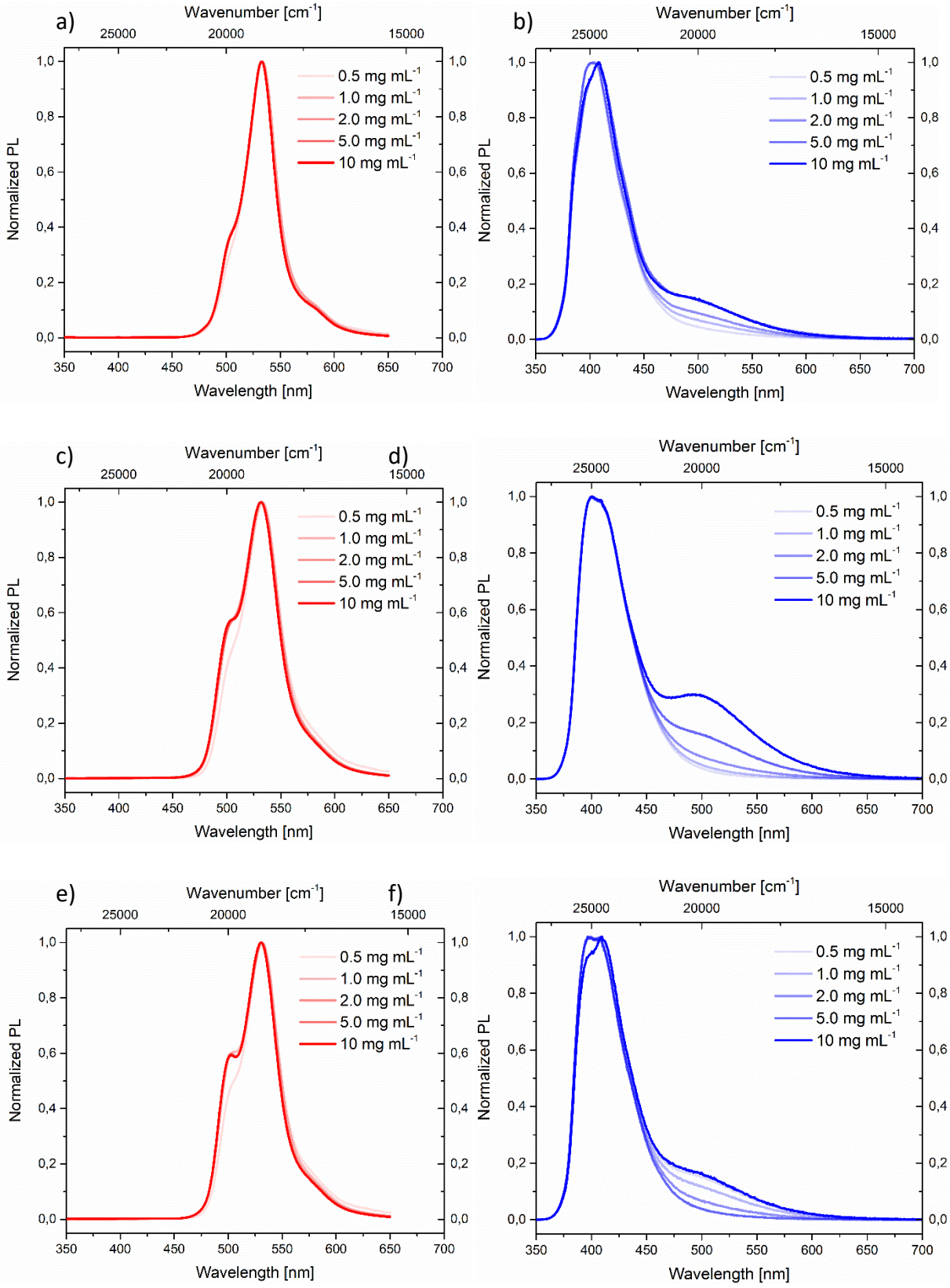

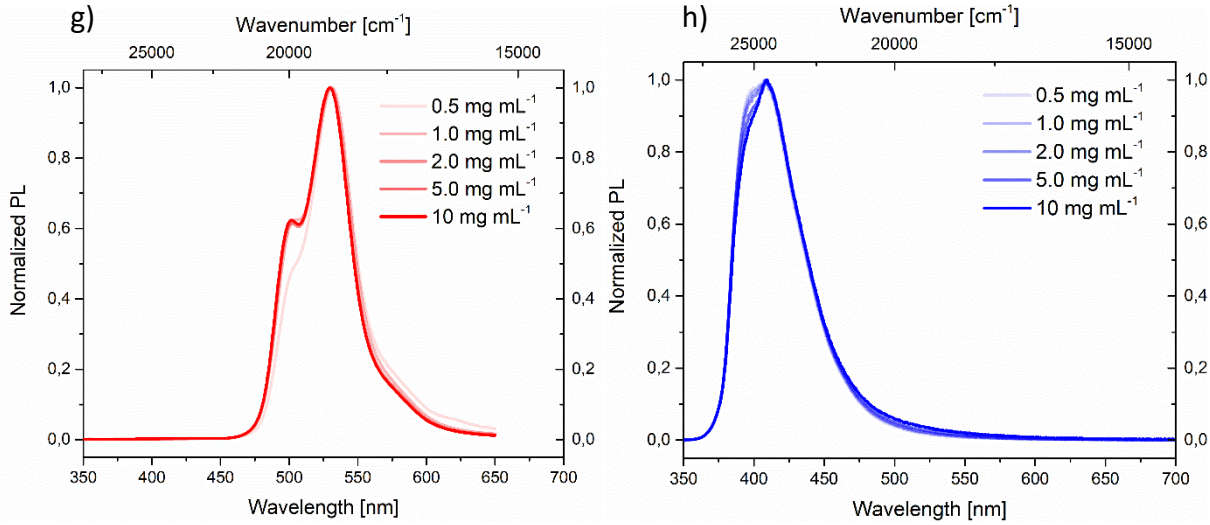

Figure S16. Normalized, concentration dependent PL spectra of **BNP** (red) and **CCP** (blue) in cyclohexane (a,b), DCM (c,d), ethyl acetate (e,f) and methanol (g,h).

5.3. PL Lifetime Measurements

Figure S17 and Figure S18 show the results from PL lifetime measurements of **BNP** and **CCP** in non-degassed and degassed DCM.

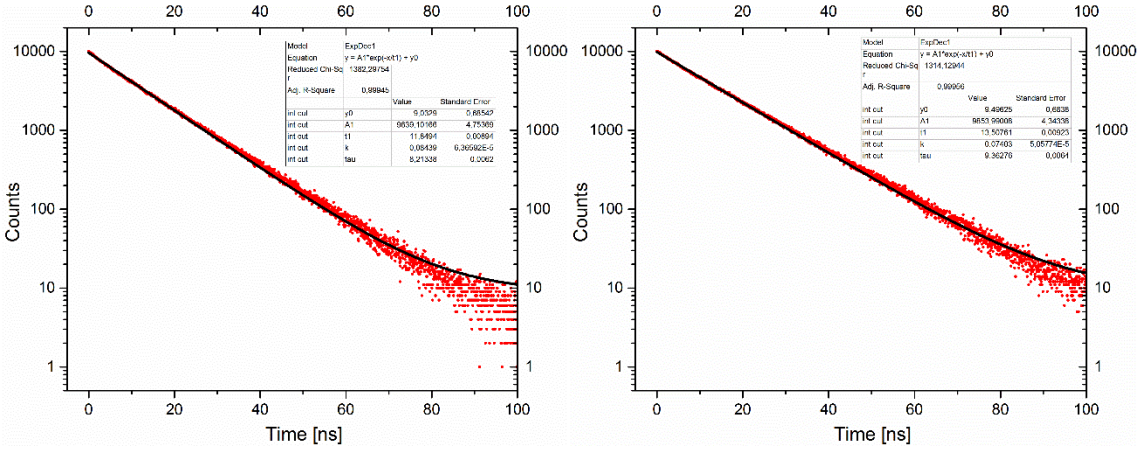

Figure S17. PL decay curves of **BNP** in DCM solution (left: non-degassed, right: degassed) at an emission wavelength of λ_{em} = 530 nm. An exponential fitting gives $\boldsymbol{\tau}$ = 11.8 ns (non-degassed) and $\boldsymbol{\tau}$ = 13.5 ns (degassed).

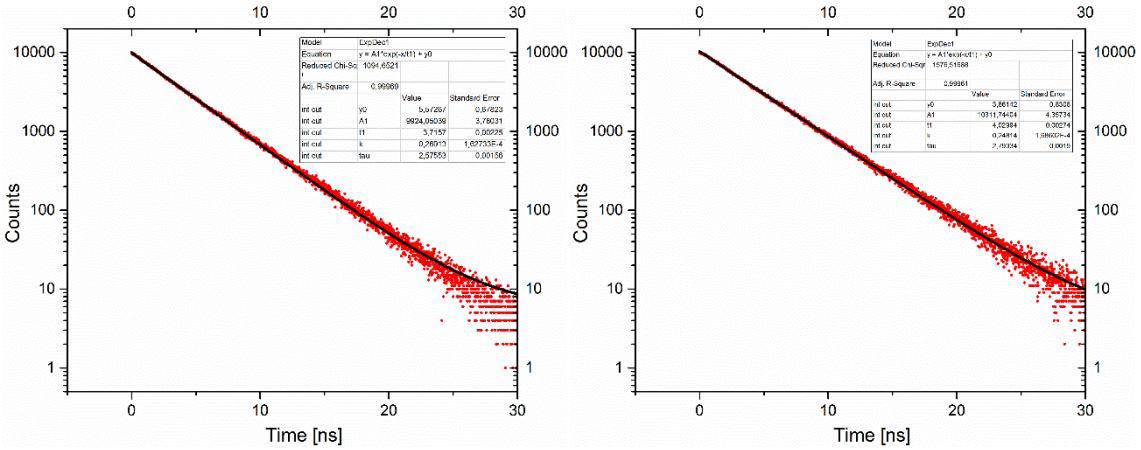

Figure S18. PL decay curves of **CCP** in DCM solution (left: non-degassed, right: degassed) at an emission wavelength of λ_{em} = 420 nm. An exponential fitting gives $\boldsymbol{\tau}$ = 3.7 ns (non-degassed) and $\boldsymbol{\tau}$ = 4.0 ns (degassed).

Figure S19, left shows that the PL lifetimes of **BNP** were almost unchanged ($\boldsymbol{\tau}$ ~ 13 ns) at low to medium concentrations. Only when the concentration was very high (above 10 mg mL^{-1}), it significantly decreased. The PL lifetimes of **BNP** were independent of the fluence, which was tested by setting it to values between 25 µW to 500 µW (Figure S19, right).

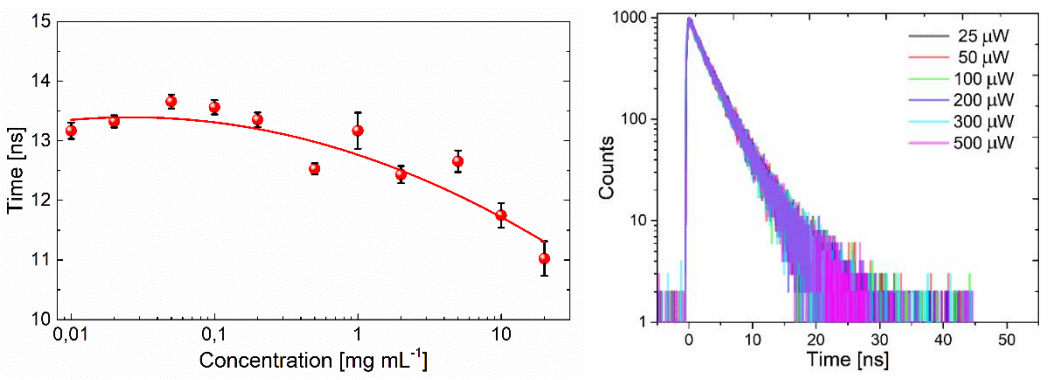

Figure S19. Concentration-dependent PL lifetimes of **BNP** (left) and TCSPC measurements of **BNP** at different fluences (right).

Figure S20 and Figure S21 show the PL lifetimes of **BNP** and **CCP** in solid state at different emission wavelengths.

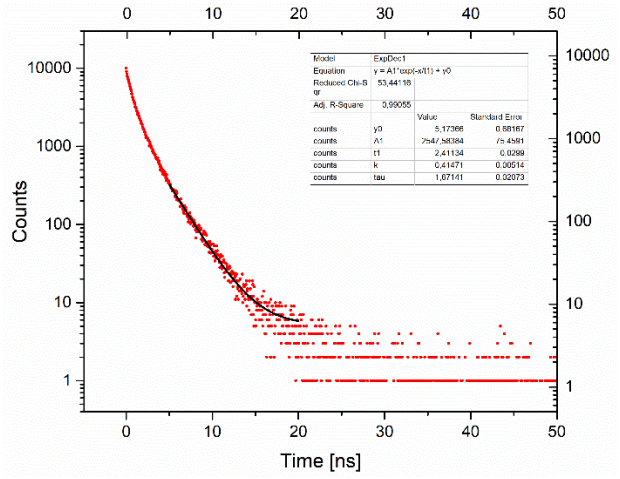

Figure S20. PL decay curve of **BNP** in solid state at an emission wavelength of λ_{em} = 540 nm. An exponential fitting gives $\boldsymbol{\tau}$ = 2.41 ns.

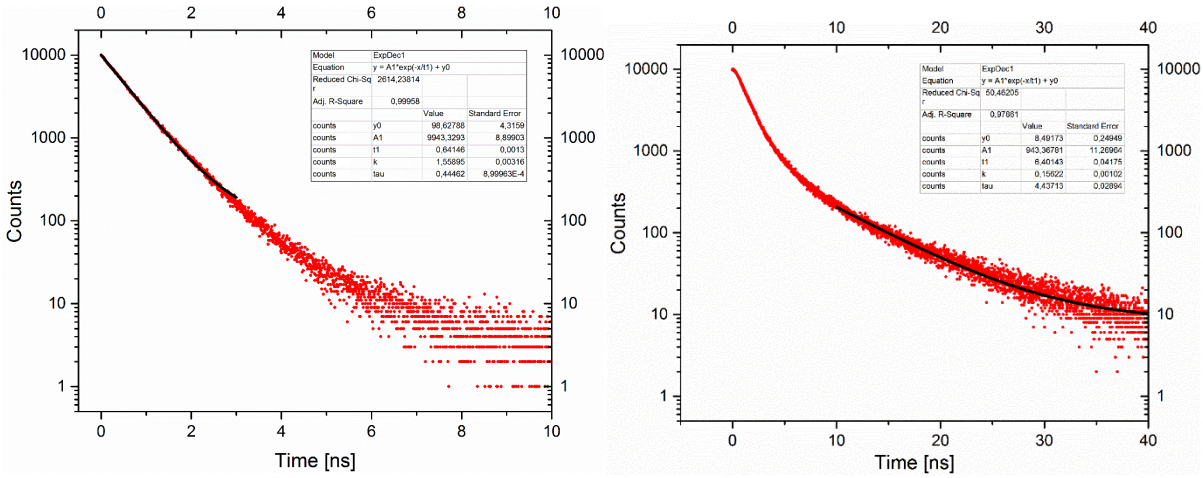

Figure S21. PL decay curves of **CCP** in solid state at emission wavelengths of λ_{em} = 432 nm (left) and λ_{em} = 486 nm (right). An exponential fitting gives $\boldsymbol{\tau}$ = 0.64 ns (λ_{em} = 432 nm) and $\boldsymbol{\tau}$ = 6.40 ns (λ_{em} = 486 nm).

5.4. Solid-State Measurements

Figure S22 shows absorption spectra of **BNP** (red) and **CCP** (blue) in solid / film state. The samples were deposited on a glass slide by dissolving them in DCM and allowing the solvent to evaporate, because absorption measurements of small crumbs of the compounds did not result in reasonable absorption curves. It needs to be considered that this might have caused a rather film-like morphology, different from the excitation and emission measurements as described below, which were performed from small crumbs of the respective compounds.

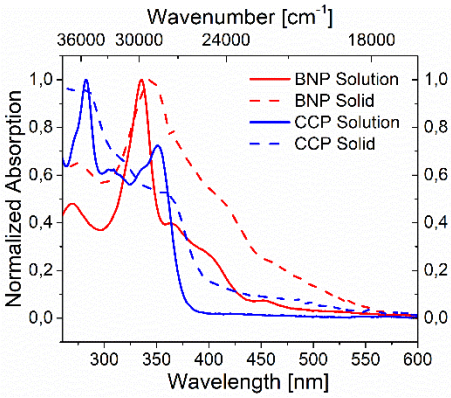

Figure S22. Normalized solid / film state absorption spectra of **BNP** (red) and **CCP** (blue).

Figure S23 shows normalized excitation (dashed) and emission (continuous) spectra of **BNP** (red) and **CCP** (blue) in solid state. The excitation wavelengths were λ_{ex} = 330 nm (**BNP**) and λ_{ex} = 376 nm (**CCP**), while the excitation spectra were obtained at λ_{em} = 540 nm (**BNP**) and λ_{em} = 432 nm (**CCP**).

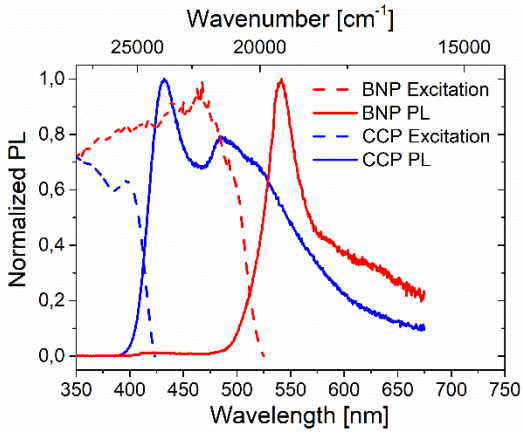

Figure S23. Normalized solid state excitation and emission spectra of **BNP** (red) and **CCP** (blue).

5.5. Additional Measurements

Figure S24 shows the excitation spectra of **BNP** at concentrations between 4.3 E^{-4} mg mL^{-1} and 4.3 E^{-6} mg mL^{-1}, which was close to the detection limit of the spectrometer. No significant changes were observed and the three main bands as they were found in the absorption measurements were present at all concentrations. The intense band at ca. 455 nm is related to the Raman signal of the solvent DCM, which was identified by blank measurements.

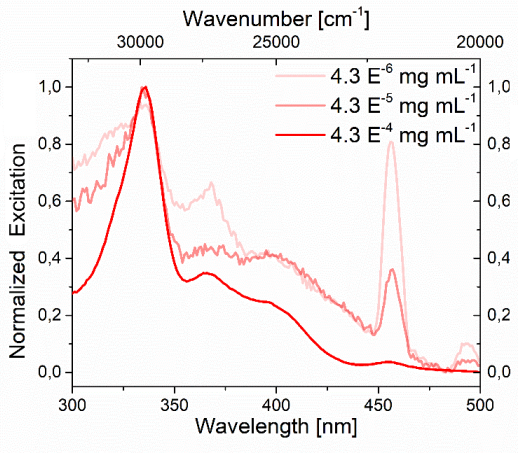

Figure S24. Excitation spectra of **BNP** in DCM solutions at concentrations between 4.3 E^{-6} mg mL^{-1} and 4.3 E^{-4} mg mL^{-1}. The samples were excited at λ_{ex} = 531 nm.

Figure S25 shows the PL spectra of **BNP** at different concentrations (top) and in different solvents (bottom). The variation of the intensity of the highest energy band at λ_{em} ~ 500 nm on these environmental changes indicates that it can be assigned to a different vibronic band and disproves the co-existence of an aggregate species.

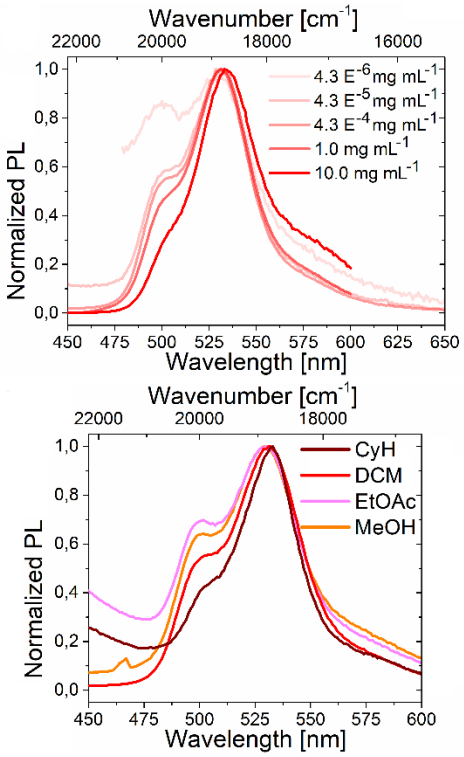

Figure S25. Normalized, concentration-dependent PL spectra of **BNP** (top) and normalized PL spectra of **BNP** in different solvents (bottom).

6. Calculations

6.1. Structure & Optical Properties

The optimized structures of **BNP** and **CCP** in the ground singlet state and in the first electronically excited singlet state were calculated with Orca 4.2.0.[15] The structures were pre-optimized using a universal force field method (UFF).[16] All structural optimizations and calculations of the optical properties were carried out with Density Functional Theory (DFT)[17-18] at the B3LYP[19-21] / cc-pVDZ[22] level of theory using the RIJCOSX[23-24] approximation.

Absorption wavelengths and oscillator strengths were determined by applying time-dependent DFT (TD-DFT)[25] to the optimized structure in the singlet electronic ground state (S_0). Geometry optimizations in the first electronically excited singlet state (S_1) and excited state dynamics calculations were performed in order to obtain the fluorescence spectra.

In all cases, the absence of imaginary frequencies confirmed that the obtained geometries were indeed energetic minima. The coordinates of the optimized structures of **BNP** and **CCP** in S_0 and S_1 are denoted in Table S6 and Table S7.

Table S6. Coordinates of the optimized structure of **BNP** in S_0 (left) and S_1 (right).

Atom	x [Å]	y [Å]	z [Å]	Atom	x [Å]	y [Å]	z [Å]
C	-3.89396825058994	1.24850940095493	-0.28425421847066	C	-3.90114121975847	1.25318203289754	-0.30199253462083
B	-2.54621571827641	1.92814454467687	-0.09903579438829	B	-2.54564453572720	1.93990374536376	-0.10605975343335
C	-3.87178501769502	-0.15663896760767	-0.36722452558562	C	-3.86890152421622	-0.14972028631838	-0.43329844738193
C	-2.67135905717383	-0.87817578870689	-0.26889621218732	C	-2.66282942811212	-0.87483890456151	-0.33861988961309
C	-1.41557527262977	-0.28511089139530	-0.06221845086471	C	-1.40707182496897	-0.28023834433277	-0.09704650196837
C	-1.27379389647250	1.11022373016466	0.05636718203303	C	-1.26802729031096	1.11244309662021	0.06578392331971
H	-4.79015956779776	-0.71972839590840	-0.55103554118152	H	-4.77840570665908	-0.70937867925597	-0.66311071707312
H	-2.71466757608985	-1.96581713420628	-0.37882552504751	H	-2.70086588796586	-1.95812340476446	-0.48042940641929
C	-5.05708080093072	2.09178806473561	-0.41435412224704	C	-5.07493936751351	2.09320405992694	-0.42492417941384
C	-4.88225147631498	3.47024551939502	-0.40066207892695	C	-4.87401774608287	3.48399050583777	-0.44518280245929
C	-3.63312620368335	4.13789779524471	-0.26572192208859	C	-3.63114316198361	4.14930061486644	-0.31916863387511
C	-0.03791194009297	1.82431163757538	0.26504690586289	C	-0.02588460004060	1.82088615375169	0.29665526965607
C	-0.05807448961935	3.21259027633753	0.21321892543141	C	-0.05959354453655	3.22353565861566	0.21563660781879
C	-1.22225913303462	4.00780056256042	0.02134661436709	C	-1.21152957186096	4.01733630424924	-0.00021414534236
H	0.86638551248129	3.76828773559991	0.37787252431722	H	0.86441423251083	3.78179379040659	0.37804887322323
N	-2.46651805049172	3.38425955287441	-0.10991386986483	N	-2.46168673064233	3.39499901199947	-0.13911531188266
C	-3.54481605783021	5.53872717236561	-0.27872258479361	C	-3.53772562708196	5.55938321029247	-0.34933519698302
C	-1.15564861530535	5.40955502714680	-0.00859121978158	C	-1.14154980279330	5.42834936276907	-0.04539519369118
C	-2.31128333864015	6.17317010047151	-0.15403025572608	C	-2.29872880675080	6.19430696809869	-0.21835171494981
H	-5.75457265083918	4.12107259532765	-0.48246416016588	H	-5.74331690026709	4.13822878942045	-0.53697392364666
H	-4.46511053631996	6.11180592926941	-0.39767443695625	H	-4.45374118630106	6.13522526664980	-0.48411283436122
H	-2.24930820663260	7.26359614702625	-0.17132412084466	H	-2.23485732852089	7.28374502830838	-0.25151203629733
H	-0.17729010238254	5.88127574135454	0.09256418441594	H	-0.16473990401509	5.90036755688860	0.06499755649386
H	-0.54084797930879	-0.94002776649480	-0.02734539636352	H	-0.53116006572417	-0.93295448915752	-0.08274846540785
C	1.23574596519629	1.14203447798567	0.56505288105007	C	1.22767082069787	1.14909749629997	0.62231852071870
C	-6.42358688578323	1.55922362912463	-0.57298722579796	C	-6.43174734700566	1.56771378529641	-0.53853876380348
S	-7.55481876494449	2.33411758301580	-1.67756688208781	S	-7.64996294768592	2.41718089424391	-1.50026241002430
S	2.76526951584584	1.73496729762342	-0.07713043437879	S	2.78607229032234	1.82671991242447	0.13018952540423
C	-7.03883318123539	0.49709057599970	0.05958021023797	C	-7.00264437446023	0.44141683670162	0.03854389648731
C	-8.40036992298518	0.31053779376330	-0.32427405185111	C	-8.37947493242523	0.26774081979779	-0.27488048468346
C	-8.82049470628490	1.22609096796967	-1.25553330659334	C	-8.87152654350555	1.25112275360115	-1.09779299499304
C	3.66265508373021	0.52439520641500	0.78485112694979	C	3.66083691272813	0.55577684850958	0.92913286074593
C	2.83910072580233	-0.28717724989437	1.52277217472418	C	2.81186501231467	-0.33870311270328	1.53374094986838
C	1.46150484024619	0.06129775206505	1.39427210172516	C	1.43945977285898	-0.00998135766367	1.35754914817367
H	0.65757588559835	-0.44513111330860	1.92719776113022	H	0.62476222283610	-0.57542982847097	1.80787691869976
H	4.74459105496684	0.46630639248408	0.67655839327326	H	4.74895767323403	0.54069670049404	0.89822159900885
H	3.20409517460732	-1.11024622037547	2.13881674975034	H	3.15892765838061	-1.20803116627577	2.09409626341552
H	-9.79570660884184	1.31052662918868	-1.73137982397800	H	-9.87801915165548	1.35743749590853	-1.49734560768581
H	-9.04391718425996	-0.47132542063526	0.08061162671469	H	-8.98664313859112	-0.55599635455560	0.10273755743240
H	-6.53484256598807	-0.11204089018323	0.80907679818841	H	-6.45471639872062	-0.21325877218043	0.71492247954402

Table S7. Coordinates of the optimized structure of **CCP** in S_0 (left) and S_1 (right).

Atom	x [Å]	y [Å]	z [Å]	Atom	x [Å]	y [Å]	z [Å]
C	-4.54544283136125	-0.68355434310985	-0.45509572531531	C	-4.51807645683816	-0.67908773838043	-0.59188454704841
C	-4.79869869079887	-2.05638952442150	-0.62552142591739	C	-4.72555110202605	-2.04879123329037	-0.89425334010985
C	-3.20579073006746	-0.26349698589448	-0.14775205446462	C	-3.16923074905263	-0.26791100254671	-0.29176838868667
C	-3.77686530461198	-2.99470916278121	-0.49245393289663	C	-3.68887644568350	-2.98132694090167	-0.84900880266071
C	-2.47962971546554	-2.59879811435385	-0.17204477039026	C	-2.40352360073445	-2.60157805491568	-0.47200034590834
C	-2.16582229268021	-1.24094296765182	0.01776938106730	C	-2.12963028380430	-1.24896369637103	-0.15819371143813
C	-2.90027801861315	1.12822113881107	-0.03932245803197	C	-2.85827486881443	1.12443522783862	-0.17796578377127
C	-3.92744867270776	2.10459645902112	-0.21314986208036	C	-3.90025655952817	2.10236810596877	-0.35754005711555

C	-1.56334959173719	1.55124914893565	0.23175498586976	C	-1.51274093903779	1.55978061826466	0.07350453039643
C	-3.60526935286149	3.47032820661493	-0.09617978921835	C	-3.53018638302242	3.47635890652117	-0.27335732800517
C	-2.29605307891136	3.87370827358433	0.17169745789184	C	-2.21630896505984	3.88176660798352	-0.02687832844288
C	-1.28263323862114	2.92724790054615	0.32881448211984	C	-1.20013154384578	2.94291116217952	0.15328289724276
C	-0.81459805244941	-0.79018218221746	0.33626638727960	C	-0.79903595399974	-0.79996323520141	0.22590459368755
C	-0.54976047637235	0.55479046337176	0.41319851476206	C	-0.52122010742498	0.57980724828558	0.27037271599237
C	-5.25894704355997	1.65799051489975	-0.49791029602536	C	-5.22288528482362	1.68010609299361	-0.57162836563682
C	-5.58468749655190	0.32877296677222	-0.61611629618480	C	-5.58814804171494	0.31270795314226	-0.64187632409111
H	-6.04178339498905	2.41224157689617	-0.61144905743835	H	-6.00214591377528	2.44257584859803	-0.62377897753579
H	0.46225195975178	0.88868440861758	0.65418490730076	H	0.48419433221700	0.91401939739996	0.53850839754918
H	-5.80105321902179	-2.38643868247238	-0.89413296566918	H	-5.71063045182555	-2.37168058360224	-1.22440413167879
H	-3.99474325674731	-4.05310763290603	-0.65592633762533	H	-3.88584630555059	-4.01766903604592	-1.13316362701042
H	-1.69064566892813	-3.34541797167537	-0.08562216599289	H	-1.59825752007101	-3.33456375941001	-0.48529271704548
H	-4.39530516567531	4.21515372456292	-0.22281857758827	H	-4.31121025181128	4.23013074729493	-0.40459782213486
H	-2.06196058051627	4.93770564226490	0.26023405557749	H	-1.98685977561547	4.94894678342802	0.02849096221546
H	-0.25911143645978	3.24778468325625	0.53885920373534	H	-0.17298506988888	3.25238434668732	0.35614246239830
C	0.28071648767770	-1.75864241682562	0.57065408952910	C	0.23514610400839	-1.71462154150658	0.65832501747769
C	-6.98230792318800	-0.04926709025487	-0.92152022239671	C	-6.98001536112617	-0.05321856562709	-0.77886958228036
C	0.37012985712596	-2.78873802476568	1.48316863616817	C	0.12167264512579	-2.93187549958772	1.34443515462782
C	1.62513022848156	-3.47034434703114	1.45707650099114	C	1.36057179256284	-3.51977698648722	1.67034351780005
C	2.48708258529781	-2.96425307668211	0.51777497037624	C	2.44168997428349	-2.77458716791075	1.23253783055655
S	1.77465967321227	-1.63898544857234	-0.34814537452267	S	1.95214195912177	-1.32963782101979	0.42173403460863
C	-7.83108571781124	-0.91874038187046	-0.26963725857281	C	-7.68744316145055	-1.19284762329682	-0.37393301452259
C	-9.14203971884389	-0.97263084236522	-0.83303198082777	C	-9.08143756780055	-1.13336941529539	-0.62451333114117
C	-9.28965911820945	-0.14752608862641	-1.91869163641566	C	-9.48428202568058	0.03999614498171	-1.21942437204302
S	-7.81896375245184	0.70588227286000	-2.27129672246611	S	-8.13128256895622	1.10518984883707	-1.49735128600178
H	-0.43880287262365	-3.03636318706094	2.17185345874573	H	-0.84156377649870	-3.34059120939394	1.64349943012553
H	1.87783773089888	-4.30320428418779	2.11472288557407	H	1.46543138676986	-4.45664886584494	2.21708946908405
H	3.49382476299733	-3.29704390680921	0.27261851742645	H	3.49979706078384	-3.00834412989232	1.33943785792735
H	-9.94541727164119	-1.59447355475849	-0.43572467565789	H	-9.77356258122856	-1.93287969917791	-0.35465097438556
H	-10.17233736782613	0.01144516625390	-2.53552690744984	H	-10.48597980201561	0.34303329983238	-1.51587470021849
H	-7.53024223313917	-1.48336232997449	0.61343205873362	H	-7.22216583616704	-2.01739453453119	0.16361098722348

The optimized structures in the electronic ground state and the regarding bond lengths are represented in Figure S26.

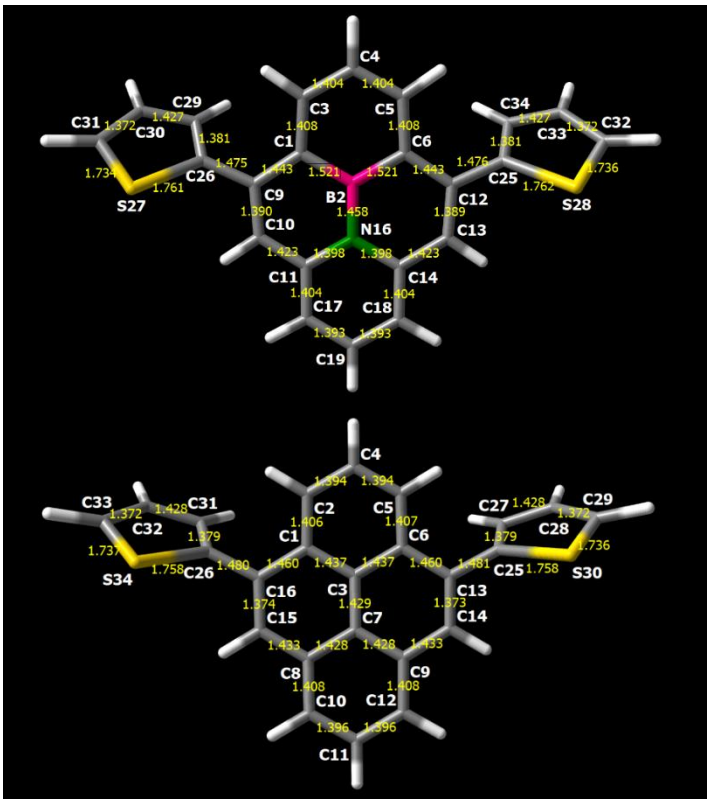

Figure S26. Optimized structures of **BNP** and **CCP** in S_0 and respective bond lengths.

The results indicate that in the lowest energy conformers both thiophene units have the same spatial orientation relative to the pyrene backbone. In **BNP**, the torsion angle between pyrene and thiophene plane (φ = C1-C9-C26-C29: 41.5°, C6-C12-C25-C34: 40.7°) is slightly lower than in **CCP** (φ = C1-C16-C26-C31: 53.9°, C6-C13-C25-C27: 57.0°). As it has been reported for other *BN* systems, the bond length alterations within the boron or nitrogen containing rings in **BNP** are larger than in the all-carbon rings in **CCP**. Generally,

the *B-C* bond lengths are extended, while *N-C* bonds are shortened, compared to *C-C* bonds. Due to these slight distortions in **BNP**, the pyrene scaffold of **CCP** is more planar (φ_{max} = 2.9°) than **BNP** (φ_{max} = 4.7°).

The dipole moments obtained from the geometry optimizations of **BNP** and **CCP** in the ground singlet state (S_0) and the first electronically excited singlet state (S_1) are displayed in Table S8.

Table S8. Dipole moments of **BNP** and **CCP** in S_0 and S_1.

Compound	Dipole moment in S_0 [D]	Dipole moment in S_1 [D]
BNP	4.99	4.87
CCP	1.58	1.71

Both in S_0 and S_1, the dipole moment of **BNP** is largely increased compared to **CCP**, reflecting the strong influence of the *BN* unit on the polarity. Due to the rigid aromatic systems, both molecules do not undergo great structural reorientations during the excitation into S_1, as it becomes obvious by the small changes in dipole moments.

The calculated absorption wavelengths and respective oscillator strengths of **BNP** and **CCP** are denoted in Table S9, the respective plots of the calculated states and the measured values are depicted in Figure S27.

Table S9. Calculated absorption wavelengths and oscillator strengths of **BNP** and **CCP**.

	BNP				**CCP**		
State	Wavelength [nm]	Wavenumber [cm^{-1}]	Oscillator Strength	State	Wavelength [nm]	Wavenumber [cm^{-1}]	Oscillator Strength
1	444.5	22499.3	0.00131	1	348.2	28721.0	0.05209
2	403.5	24783.7	0.06002	2	347.9	28747.3	0.22844
3	371.8	26895.3	0.42667	3	324.8	30787.9	0.13720
4	335.9	29772.3	0.35648	4	321.1	31144.1	0.21800
5	322.4	31020.2	0.07828	5	300.9	33233.5	0.01199
6	308.1	32458.2	0.09943	6	282.6	35385.5	0.00057
7	302.7	33039.9	0.10923	7	275.8	36258.5	0.33097
8	297.5	33612.8	0.16945	8	274.7	36406.6	0.00358
9	291.8	34266.0	0.02051	9	274.2	36469.3	0.02305
10	284.0	35213.9	0.00719	10	270.7	36945.6	0.00398
11	254.3	39327.1	0.57947				

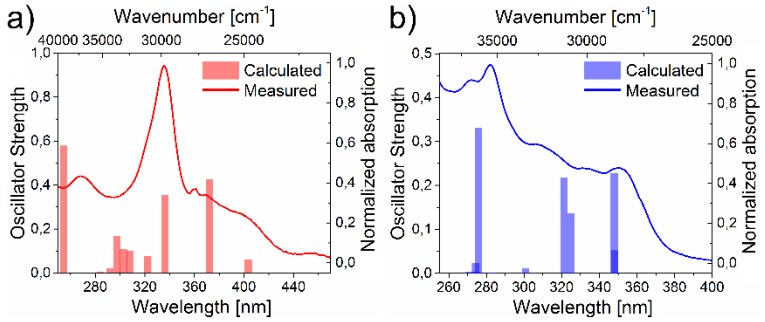

Figure S27. Measured, normalized absorption bands and calculated absorption sticks of **BNP** (a) and **CCP** (b).

The theoretical values match well with the experimental data, as all local maxima are mapped by the calculated states. The most significant maximum band of **BNP** (λ_{exp} = 336 nm) is exactly mirrored by the calculated state, the maxima of **CCP** (λ_{exp} = 351, 283 nm) are just slightly shifted bathochromically, compared to the calculated values (λ_{calc} = 348, 276 nm). All other local maxima were mapped by calculation by deviations of less than 15 nm. Comparing both spectra, it becomes clear that the *B-N* unit in **BNP** induces a large change in the absorption characteristics compared to **CCP**, as the band positions as well as the respective oscillator strengths deviate significantly. The results prove that the main contributor to the bathochromic shift in **BNP** is the difference of the electronic structure and not any kind of aggregation.

The calculated PL spectra of **BNP** and **CCP** and the respective measured spectra are depicted in Figure S28. The calculated emission maximum of **BNP** was shifted hypsochromically by 25 nm ($\lambda_{em\ calc}$ = 506 nm), compared to the experimental value ($\lambda_{em\ exp}$ = 531 nm). The calculated emission maximum of **CCP** was shifted bathochromically by 17 nm ($\lambda_{em\ calc}$ = 417 nm), compared to the experimental value ($\lambda_{em\ exp}$ = 400 nm). Although the calculated curve of **BNP** exhibits a vibronic fine structuring in contrast to

the experimental curve, both calculated curves mirror the trends of the measurements. On the one hand, the full width half maximum of **CCP** appears to be narrower than for **BNP**. On the other hand, the shoulder signal of **CCP** towards lower energies and the shoulder signal of **BNP** towards higher energies (band I) are represented.

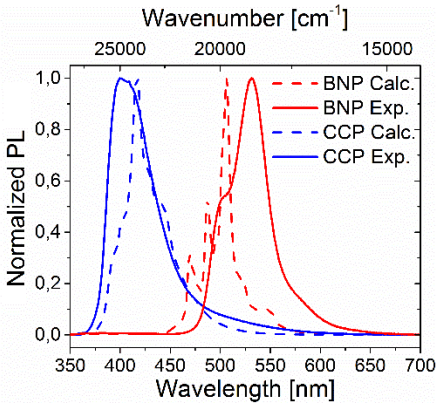

Figure S28. Measured (continuous, c = 2.0 mg mL^{-1}) and calculated (dashed), normalized PL spectra of **BNP** (red) and **CCP** (blue).

6.2. Natural Transition Orbitals (NTOs)

To describe the nature of the S_1 state, which accounts for the transition that is related to fluorescence, we plotted the highest occupied Natural Transition Orbitals (HONTOs) and the lowest unoccupied Natural Transition Orbitals (LUNTOs) as well as the regarding HONTO-1 and LUNTO+1 (Figure S29). For both **BNP** and **CCP**, these were the main contributors to the S_1 states. The given percentages describe the share to which the displayed NTOs contribute to the transition.

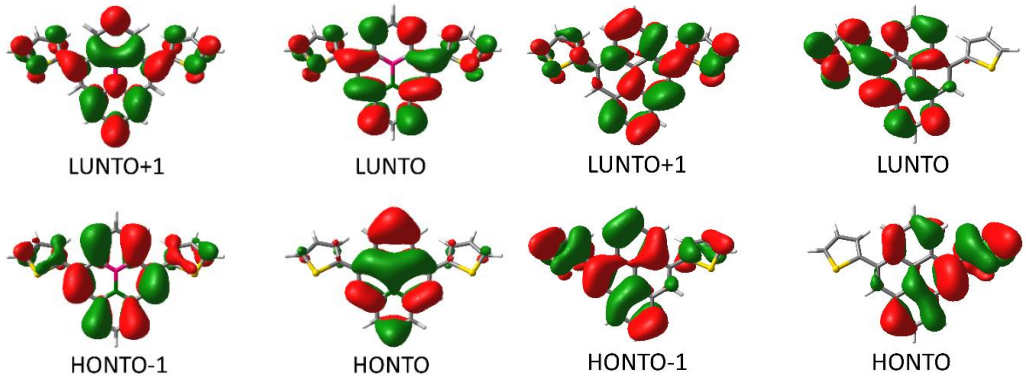

Figure S29. NTO analysis of **BNP** (four structures on the left) and **CCP** (four structures on the right).

Detailed contributions to the S_1 states:

BNP: 50.7% (HONTO → LUNTO), 48.9% (HONTO-1 → LUNTO+1).

CCP: 85.3% (HONTO → LUNTO), 13.9% (HONTO-1 → LUNTO+1).

Figure S30 shows the calculated orbital energies and surfaces of the described NTOs that contribute most to the S_1 states.

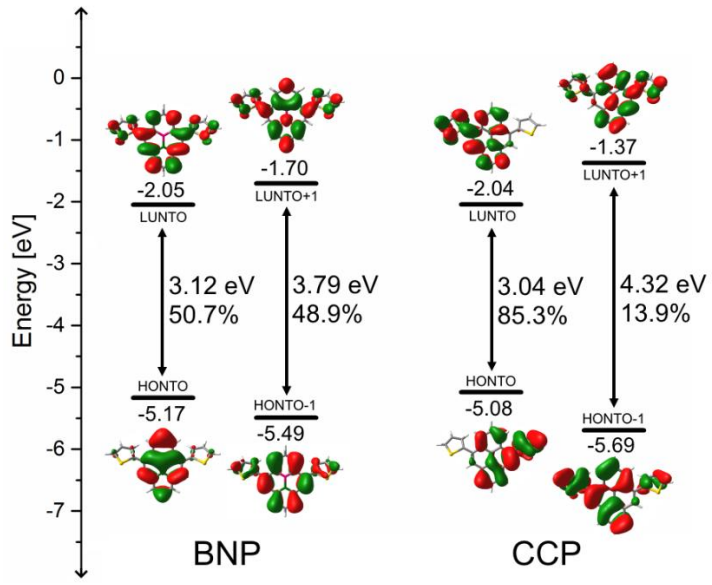

Figure S30. Molecular orbital diagram of **BNP** (left) and **CCP** (right) including orbital shapes, energy levels, orbital gaps and the respective percentage of the transition in the S_1 states.

In **BNP**, all displayed NTOs spread symmetrically over the pyrene and thiophene units. The HONTO-1 and the LUNTO exhibit a nodal plane through the center of the molecule, involving the boron and nitrogen heteroatoms, which are consequently uninvolved in these orbitals. Concluding, the observed transitions are clearly local π-π* transitions. **CCP** does not exhibit this high symmetry, the HONTO and LUNTO display an accumulation of orbitals at opposite sides of the molecule, especially involving the thiophene units. This indicates that the occurring transition has an increased charge transfer character. Notwithstanding, both the experimental absorption and PL spectra are well reproduced by the calculations. This rendered the application of long-range corrected functionals or wavefunction-based methods unnecessary.

6.3. Nucleus-Independent Chemical Shifts

Calculations of the NICS(0)[26] (in plane nucleus-independent chemical shift) values were run with Q-Chem 5.2,[27] using the coordinates of optimized ground state structures as inputs. The isotropic shielding tensors were calculated at the MP2[28] / cc-pVDZ[22] level of theory (Figure S31).

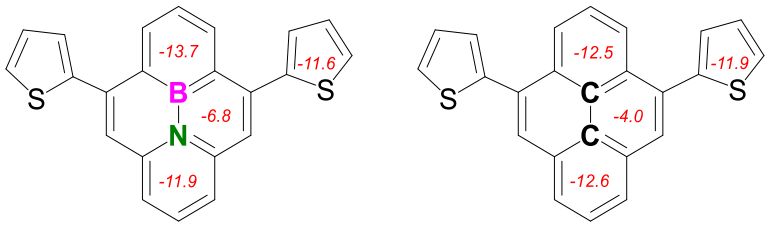

Figure S31. Calculated NICS(0) values of **BNP** and **CCP**.

The results for **CCP** are in good agreement with reported values for unsubstituted pyrene,[29] pointing out the increased aromaticity of the phenyl rings at the long end of the molecule. These findings also account for **BNP**, where the boron containing ring was slightly more aromatic than the nitrogen containing ring. Compared to **CCP**, the short end rings were even more aromatic in **BNP**, which is in contrast to PAHs with peripheral *BN*-units, exhibiting decreased aromaticities.[30]

7. References

1. Ashe, A. J.; Chan, W. T.; Smith, T. W.; Taba, K. M. Electrophilic Aromatic-Substitution Reactions of Arsabenzene. *J. Org. Chem.* **1981,** *46*, 881-885.

2. Hernán, A. G.; Horton, P. N.; Hursthouse, M. B.; Kilburn, J. D. New and Efficient Synthesis of Solid-Supported Organotin Reagents and Their Use in Organic Synthesis. *J. Organomet. Chem.* **2006,** *691*, 1466-1475.

3. Hoic, D. A.; Wolf, J. R.; Davis, W. M.; Fu, G. C. Chemistry of Borabenzene: Efficient and General Synthesis of New Neutral Borabenzene−Ligand Complexes. *Organometallics* **1996,** *15*, 1315-1318.

4. Awuah, E.; Capretta, A. Access to Flavones via a Microwave-Assisted, One-Pot Sonogashira−Carbonylation−Annulation Reaction. *Org. Lett.* **2009,** *11*, 3210-3213.

5. Uttiya, S.; Miozzo, L.; Fumagalli, E. M.; Bergantin, S.; Ruffo, R.; Parravicini, M.; Papagni, A.; Moret, M.; Sassella, A. Connecting Molecule Oxidation to Single Crystal Structural and Charge Transport Properties in Rubrene Derivatives. *J. Mat. Chem. C* **2014,** *2*, 4147-4155.

6. Leroux, F. R.; Berthelot, A.; Bonnafoux, L.; Panossian, A.; Colobert, F. Transition-Metal-Free Atropo-Selective Synthesis of Biaryl Compounds Based on Arynes. *Chem. Eur. J.* **2012,** *18*, 14232-14236.

7. Machuy, M. M.; Wuertele, C.; Schreiner, P. R. 2,6-Bis(phenylethynyl)biphenyls and Their Cyclization to Pyrenes. *Synthesis* **2012,** *44*, 1405-1409.

8. Stille, J. K.; Simpson, J. H. Stereospecific Palladium-Catalyzed Coupling Reactions of Vinyl Iodides with Acetylenic Tin Reagents. *J. Am. Chem. Soc.* **1987,** *109*, 2138-2152.

9. Dolomanov, O. V.; Bourhis, L. J.; Gildea, R. J.; Howard, J. A. K.; Puschmann, H. OLEX2: A Complete Structure Solution, Refinement and Analysis Program. *J. Appl. Cryst.* **2009,** *42*, 339-341.

10. Sheldrick, G. M. SHELXT - Integrated Space-Group and Crystal-Structure Determination. *Acta Cryst.* **2015,** *A71*, 3-8.

11. Sheldrick, G. M. Crystal Structure Refinement with SHELXL. *Acta Cryst.* **2008,** *A64*, 112-122.

12. Spackman, P. R.; Turner, M. J.; McKinnon, J. J.; Wolff, S. K.; Grimwood, D. J.; Jayatilaka, D.; Spackman, M. A. CrystalExplorer: A Program for Hirshfeld Surface Analysis, Visualization and Quantitative Analysis of Molecular Crystals. *J. Appl. Crystallogr.* **2021,** *54*, 1006-1011.

13. Frisch, M. J.; Trucks, G. W.; Schlegel, H. B.; Scuseria, G. E.; Robb, M. A.; Cheeseman, J. R.; Scalmani, G.; Barone, V.; Petersson, G. A.; Nakatsuji, H., et al. *Gaussian 16 Rev. C.01*, Wallingford, CT, 2016.

14. Turner, M. J.; Grabowsky, S.; Jayatilaka, D.; Spackman, M. A. Accurate and Efficient Model Energies for Exploring Intermolecular Interactions in Molecular Crystals. *J. Phys. Chem. Lett.* **2014,** *5*, 4249-4255.

15. Neese, F. The ORCA Program System. *Wiley Interdiscip. Rev.: Comput. Mol. Sci.* **2012,** *2*, 73-78.

16. Rappe, A. K.; Casewit, C. J.; Colwell, K. S.; Goddard, W. A.; Skiff, W. M. UFF, A Full Periodic Table Force Field for Molecular Mechanics and Molecular Dynamics Simulations. *J. Am. Chem. Soc.* **1992,** *114*, 10024-10035.

17. Hohenberg, P.; Kohn, W. Inhomogeneous Electron Gas. *Phys. Rev. B* **1964,** *136*, 864-871.

18. Kohn, W.; Sham, L. J. Self-Consistent Equations Including Exchange and Correlation Effects. *Phys. Rev. A* **1965,** *140*, 1133-1138.

19. Becke, A. D. Density-Functional Exchange-Energy Approximation with Correct Asymptotic Behavior. *Phys. Rev. A* **1988,** *38*, 3098-3100.

20. Becke, A. D. A New Mixing of Hartree–Fock and Local Density-Functional Theories. *J. Chem. Phys.* **1993,** *98*, 1372-1377.

21. Lee, C.; Yang, W.; Parr, R. G. Development of the Colle-Salvetti Correlation-Energy Formula into a Functional of the Electron Density. *Phys. Rev. B* **1988,** *37*, 785-789.

22. Dunning Jr., T. H. Gaussian Basis Sets for Use in Correlated Molecular Calculations. I. The Atoms Boron Through Neon and Hydrogen. *J. Chem. Phys.* **1989,** *90*, 1007-1023.

23. Weigend, F. A Fully Direct RI-HF Algorithm: Implementation, Optimised Auxiliary Basis Sets, Demonstration of Accuracy and Efficiency. *Phys. Chem. Chem. Phys.* **2002,** *4*, 4285-4291.

24. Neese, F.; Wennmohs, F.; Hansen, A.; Becker, U. Efficient, Approximate and Parallel Hartree-Fock and Hybrid DFT Calculations. A 'Chain-of-Spheres' Algorithm for the Hartree-Fock Exchange. *Chem. Phys.* **2009,** *356*, 98.
25. Bauernschmitt, R.; Ahlrichs, R. Treatment of Electronic Excitations within the Adiabatic Approximation of Time Dependent Density Functional Theory. *Chem. Phys. Lett.* **1996,** *256*, 454-464.
26. Schleyer, P. v. R.; Maerker, C.; Dransfeld, A.; Jiao, H.; van Eikema Hommes, N. J. R. Nucleus-Independent Chemical Shifts: A Simple and Efficient Aromaticity Probe. *J. Am. Chem. Soc.* **1996,** *118*, 6317-6318.
27. Shao, Y.; Gan, Z.; Epifanovsky, E.; Gilbert, A. T. B.; Wormit, M.; Kussmann, J.; Lange, A. W.; Behn, A.; Deng, J.; Feng, X., et al. Advances in Molecular Quantum Chemistry Contained in the Q-Chem 4 Program Package. *Mol. Phys.* **2015,** *113*, 184-215.
28. Møller, C.; Plesset, M. S. Note on an Approximation Treatment for Many-Electron Systems. *Phys. Rev.* **1934,** *46*, 618-622.
29. Havenith, R. W. A.; van Lenthe, J. H.; Dijkstra, F.; Jenneskens, L. W. Aromaticity of Pyrene and Its Cyclopentafused Congeners - Resonance and NICS Criteria. An Ab Initio Valence Bond Analysis in Terms of Kekulé Resonance Structures. *J. Phys. Chem. A* **2001,** *105*, 3838-3845.
30. Appiarius, Y.; Stauch, T.; Lork, E.; Rusch, P.; Bigall, N. C.; Staubitz, A. From a 1,2-Azaborinine to Large BN-PAHs via Electrophilic Cyclization: Synthesis, Characterization and Promising Optical Properties. *Org. Chem. Front.* **2021,** *8*, 10-17.

8. ORCID IDs

- Yannik Appiarius: https://orcid.org/0000-0002-9849-6950.
- Philipp J. Gliese: https://orcid.org/0000-0001-6779-8529.
- Stephan A. W. Segler: n.a.
- Pascal Rusch: https://orcid.org/0000-0001-5088-4447.
- Jiangbin Zhang: https://orcid.org/0000-0001-6565-5962.
- Paul J. Gates: https://orcid.org/0000-0001-8619-7745.
- Rumpa Pal: https://orcid.org/0000-0003-3080-3333.
- Lorraine A. Malaspina: https://orcid.org/0000-0002-8281-4264.
- Kunihisa Sugimoto: https://orcid.org/0000-0002-0103-8153.
- Tim Neudecker: https://orcid.org/0000-0001-7599-3578.
- Nadja C. Bigall: https://orcid.org/0000-0003-0171-1106.
- Simon Grabowsky: https://orcid.org/0000-0002-3377-9474.
- Artem A. Bakulin: https://orcid.org/0000-0002-3998-2000.
- Anne Staubitz: https://orcid.org/0000-0002-9040-3297.